Laboratory of Biotechnology
University of Ioannina

ΙΑΤΡΙΚΗ ΧΗΜΕΙΑ

UNIVERSITY OF IOANNINA

SCHOOL OF HEALTH SCIENCES

DEPARTMENT OF BIOLOGICAL APPLICATIONS AND TECHNOLOGIES

LABORATORY OF BIOTECHNOLOGY

Postgraduate program: “Medicinal Chemistry”

Master's thesis:

"Study of the structure and function of enzymes in carbon nanomaterials."

STEFANIA ZAMPARA

Biologist, MSCi

IOANNINA, FEBRUARY 2026

Acknowledgments

This master's thesis was completed as part of the master's program in “Medical Chemistry”, offered by the departments of Chemistry, Medicine, and Biological Applications and Technology. The laboratory component was carried out in the Biotechnology Laboratory of the Department of Biological Applications and Technology during the academic year 2024-2025.

I would like to express my sincere gratitude to my supervisor, Professor of the Department of Biological Applications and Technologies, Haralambos Stamatis, for trusting me once again and giving me the opportunity to work under his guidance for my postgraduate studies, following the completion of my undergraduate thesis. His continuous support, valuable advice, and confidence in my abilities have played a crucial role in the successful completion of this work. I am especially thankful for his encouragement and the knowledge he shared with me throughout this academic journey.

I would also like to thank the other two members of my examination committee, Assistant Professor Petros Katapodis and Dr. Angeliki Polydera, a member of the Laboratory Teaching Staff. I thank them both for their participation in the examination committee and for their help and friendly attitude throughout the years that I have been a member of the Biotechnology Laboratory.

Of course, I would like to express my heartfelt gratitude to Dr. Vasiliki-Michaela Patila, for her invaluable support throughout this journey. She has always been there to offer her knowledge, encouragement, and understanding. I am especially thankful for the trust she has shown in me and for the meaningful relationship we have developed over the years, which goes far beyond a typical academic collaboration. Her presence, both as a mentor and as a person, has made this experience truly meaningful, and I am deeply grateful for everything she has offered me.

Additionally, I would like to thank all the members of the laboratory, including the postdoctoral researchers, PhD candidates, postgraduate and undergraduate students, for the wonderful environment we shared throughout this period. The supportive and friendly atmosphere in the lab made this journey not only productive but also truly enjoyable. I am grateful for all the moments we experienced together, the collaboration, the discussions, and the mutual support. Being part of such a positive team has been a valuable and memorable experience.

Finally, I would like to express my deepest gratitude to my family and friends for their unconditional support, understanding, and encouragement throughout this journey. I am truly grateful to have them by my side.

Abstract

Enzymes are essential biological macromolecules whose activity and stability are strongly influenced by their structural integrity and their interaction with the surrounding environments. In recent years, carbon-based nanomaterials have attracted significant attention as promising platforms for enzyme immobilization due to their unique physicochemical properties, high surface area, and potential to enhance enzyme performance. The present study focuses on the investigation of the structure and function of two important enzymes, lysozyme and α-amylase, following their immobilization on graphene oxide and two environmentally friendly nanomaterials, bio-graphene and magnetic bio-graphene.

The primary objective of this work was to examine how the interaction between these enzymes and carbon nanomaterials affects their functional characteristics. Enzyme immobilization on nanomaterial surfaces can influence protein folding, stability, and activity through physicochemical interactions such as electrostatic forces, hydrogen bonding, and surface adsorption. Understanding these interactions is essential for the development of advanced nanobiotechnological applications, including biosensors, biocatalytic systems, and biomedical devices.

To further investigate these effects, spectroscopic techniques were employed to monitor potential structural and conformational changes in the enzymes' molecules. Ultraviolet–visible (UV–Vis) absorption spectroscopy was used to evaluate changes in the electronic environment of the enzymes and to confirm their interaction with the nanomaterials. Fluorescence spectroscopy provided valuable information regarding alterations in the tertiary structure and the microenvironment of aromatic amino acid residues, allowing the detection of conformational modifications. Additionally, Circular Dichroism (CD) spectroscopy was utilized to analyze changes in the secondary structure of the enzymes, offering insight into variations in α-helix and β-sheet content induced by their interaction with graphene oxide, bio-graphene, and magnetic bio-graphene.

The use of green nanomaterials such as bio-graphene and magnetic bio-graphene represents an important step toward more sustainable and biocompatible nanobiotechnological systems. These materials provide potential advantages, including enzyme stabilization, reusability, and environmentally friendly synthesis routes. The results of this study contribute to a better understanding of enzyme–nanomaterial interactions at the molecular level and highlight the potential of carbon-based nanomaterials as effective platforms for enzyme immobilization.

Overall, this work provides valuable insight into the structural behavior of lysozyme and α-amylase in the presence of graphene-based nanomaterials, contributing to the broader field of nanobiotechnology and supporting the development of advanced functional nanomaterial–enzyme systems for future applications.

Contents

1. Introduction

1.1. Biotechnology

The term "*Biotechnology"* was first used by Károly Ereky in 1919 to refer to the production of products from raw materials with the aid of living organisms. Nowadays, the term *Biotechnology* refers to the use of biological systems or their components to produce useful or commercially exploitable products, as well as to provide services. Biotechnology has now become one of the leading-edge technologies, with a wide range of applications in fields such as pharmaceuticals, medicine, environmental protection, and bioremediation.

Biotechnology is divided into four main categories, which are characterized for symbolic reasons by a different color (KAFARSKI, 2012):

- **Blue Biotechnology,** also known as marine biotechnology, refers to the exploitation of aquatic ecosystems to create products for applications of industrial interest (Maldonado-Ruiz et al., 2024)
- **Green Biotechnology** refers to the use of living organisms, biological systems, or their derivatives to develop sustainable, environmentally friendly processes and products—particularly in agriculture, industry, and ecological remediation—aimed at reducing environmental impact while enhancing resource efficiency (Eskandar, 2025)
- **Red Biotechnology,** also known as medical or pharmaceutical biotechnology, involves the production of vaccines and antibiotics, the discovery of new drugs and therapies, the development of artificial organs, and the creation of novel diagnostic methods (V. Gupta et al., 2017).
- **White Biotechnology,** also known as industrial biotechnology, primarily focuses on the application of biocatalysis in industrial processes. White biotechnology is considered the largest sector of biotechnology and is associated with:
  - the replacement of traditional industrial processes with biocatalytic processes aimed at the production of pharmaceuticals, cosmetics, chemicals, and food additives,
  - the production of biodegradable polymers,
  - the generation of fuels and energy from renewable sources or through photosynthetic microorganisms.

Although the four-color classification system is the most widely used in biotechnology, alternative classification schemes featuring a broader spectrum of colors also exist (Figure 1).

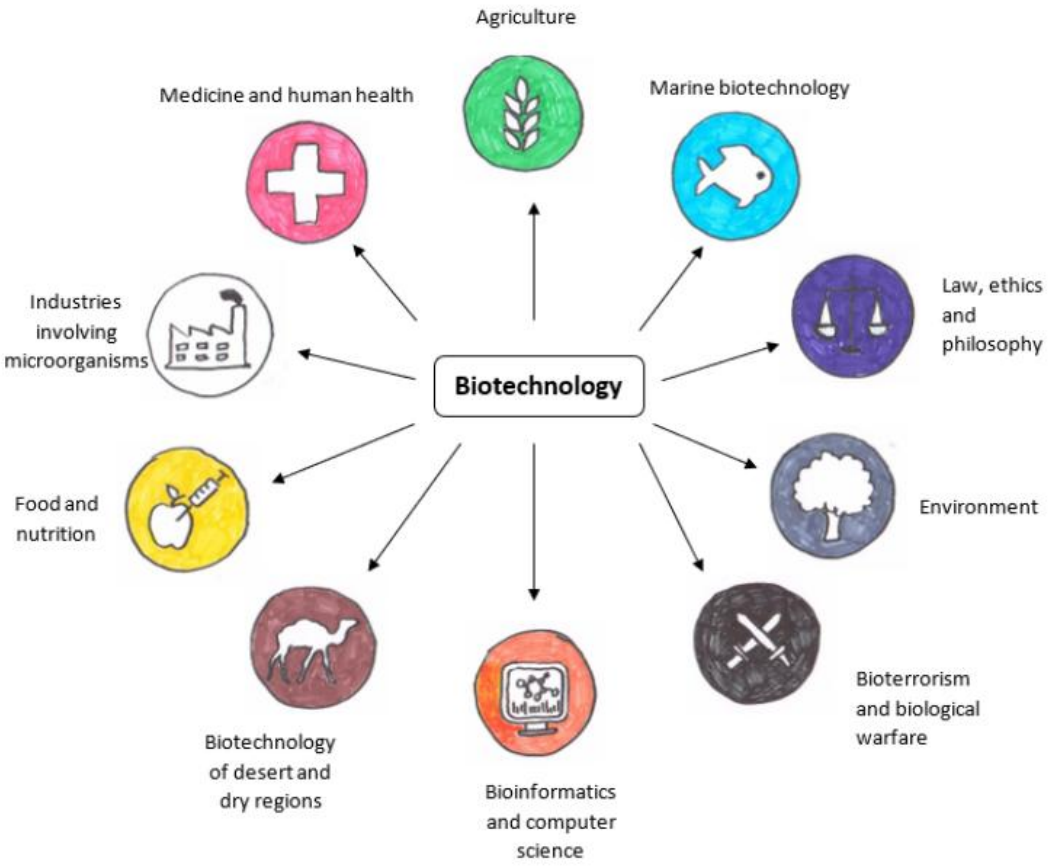

***Figure 1**: The Colors of Biotechnology (Source: weacademia.com)*

1.2. Enzymes in biocatalysis

Enzymes, which are involved in biocatalysis, have emerged as indispensable tools in modern industrial biotechnology due to their capacity to catalyze chemical reactions with remarkable specificity, efficiency, and environmental compatibility (Sheldon & Woodley, 2018). Unlike conventional chemical catalysts, enzymes operate under mild, aqueous conditions, thereby reducing energy demands, limiting the use of hazardous solvents, and ensuring safer production environments. Their high substrate selectivity not only minimizes the formation of undesired by-products but also decreases purification requirements and overall material waste, making enzymatic processes both economically and ecologically advantageous (Tawfik, 2014). These properties have facilitated their adoption across diverse industrial sectors, including pharmaceuticals, food processing, textiles, and biofuels, where enzymes are employed to transform raw materials into high-value products under sustainable processing conditions. Furthermore, advances in protein engineering have expanded the operational stability of enzymes, enabling them to function under challenging industrial environments such as extreme pH or temperature, and thereby broadening their applicability within large-scale biomanufacturing (Farhan et al., 2025).

Enzymes act as biocatalysts, accelerating chemical reactions to produce desired end products efficiently. Advances in biotechnology have significantly expanded the application of enzymes beyond their traditional uses, enabling their integration into a wide range of industries. Given the rapid and ongoing growth of enzyme utilization in the biotechnology field, it is essential to examine recent developments and assess the broader impact of enzyme technology across these industries (Fasim et al., 2021).

1.3. Categories of enzymes

Enzymes are classified into seven major families according to the guidelines of the Nomenclature Committee of the International Union of Biochemistry and Molecular Biology (IUBMB). Initially, six categories were established in 1961 based on the type of reaction catalyzed, each enzyme being assigned a four-digit Enzyme Commission (EC) number indicating class, subclass, sub-subclass, and substrate specificity (McDonald & Tipton, 2023). In 2018, a seventh class was added to include enzymes responsible for transporting ions or molecules across membranes (Concu & Cordeiro, 2019). The seven enzyme families are:

- **Oxidoreductases (E.C.1)**, which catalyze oxidation–reduction reactions and are subdivided into 22 groups. These enzymes have important technological applications.
- **Transferases (E.C.2)**, which mediate the transfer of functional groups such as methyl or acyl groups. These enzymes play a crucial role in cellular metabolism.
- **Hydrolases (E.C.3)**, which hydrolyze chemical bonds, and include many enzymes of industrial interest such as esterases, proteases, and glycosidases. These enzymes are crucial for catabolism, as they provide the cell with digestible nutrients.
- **Lyases (E.C.4)**, which catalyze non-hydrolytic bond cleavage, and are often relevant in metabolic pathways. They are divided into seven subgroups, according to the type of bond they cleave (C-C, C-O, C-N).
- **Isomerases (E.C.5)**, which enable structural rearrangements within molecules.
- **Ligases (E.C.6)**, which create covalent bonds between two molecules. These enzymes are responsible for the anabolism of cells and therefore play a key role in the synthetic reactions that occur within the cell. There are six subgroups of ligases based on the type of bond formed (C-O, C-S, C-N, C-C).
- **Translocases (E.C.7)**, which facilitate the transport of ions or molecules across membranes. This classification underscores the

functional diversity of enzymes and their essential roles in both metabolism and biotechnology.

This thesis focuses on the study of enzymes that belong to the class of Hydrolases, namely lysozyme and alpha-amylase.

1.4. Hydrolases

Hydrolases are a class of enzymes that catalyze the cleavage of chemical bonds by adding water. Their primary biological role is digestive, breaking down complex nutrients into simpler units. For instance, proteases degrade proteins into peptides and subsequently into amino acids, while lipases hydrolyze triglycerides into glycerol and free fatty acids. Due to the diversity of substrates encountered in biological systems, hydrolases typically exhibit broad substrate specificity (Shukla et al., 2022).

Several key features make hydrolases particularly valuable in organic synthesis:

- They possess wide substrate versatility.
- They often demonstrate high stereoselectivity, even with non-natural substrates.
- Beyond hydrolysis, many of them can catalyze related reactions such as condensation (reverse of hydrolysis) and alcoholysis (using alcohol instead of water).
- Many hydrolases are inexpensive, commercially available, and easy to obtain.
- They do not require cofactors and are generally compatible with water-miscible organic solvents like Dimethyl sulfoxide (DMSO) or Dimethylformamide (DMF); some, such as lipases and certain proteases, remain stable and active even in pure organic solvents.
- Most hydrolases are extracellular, facilitating straightforward purification.

The study of various hydrolase types, including lipases, proteases, esterases, epoxide hydrolases, nitrile hydrolases, and glycosidases, focuses on their synthetic applications, particularly where regioselectivity and stereoselectivity are critical (Alcántara et al., 2011)

1.4.1. Lysozyme

Lysozyme was first identified by Alexander Fleming, who observed that a nasal mucus accidentally dropped onto a bacterial culture caused bacterial cell

lysis. He referred to this as a *"remarkable bacteriolytic element"*, later named lysozyme (Alexander Flemming, 1922). Since then, lysozymes are widely distributed across nature, occurring in significant amounts in human tissues and secretions—such as tears, saliva, skin, milk, and serum—as well as in various animals, plants, and microorganisms, highlighting their universal biological presence (Wu et al., 2019).

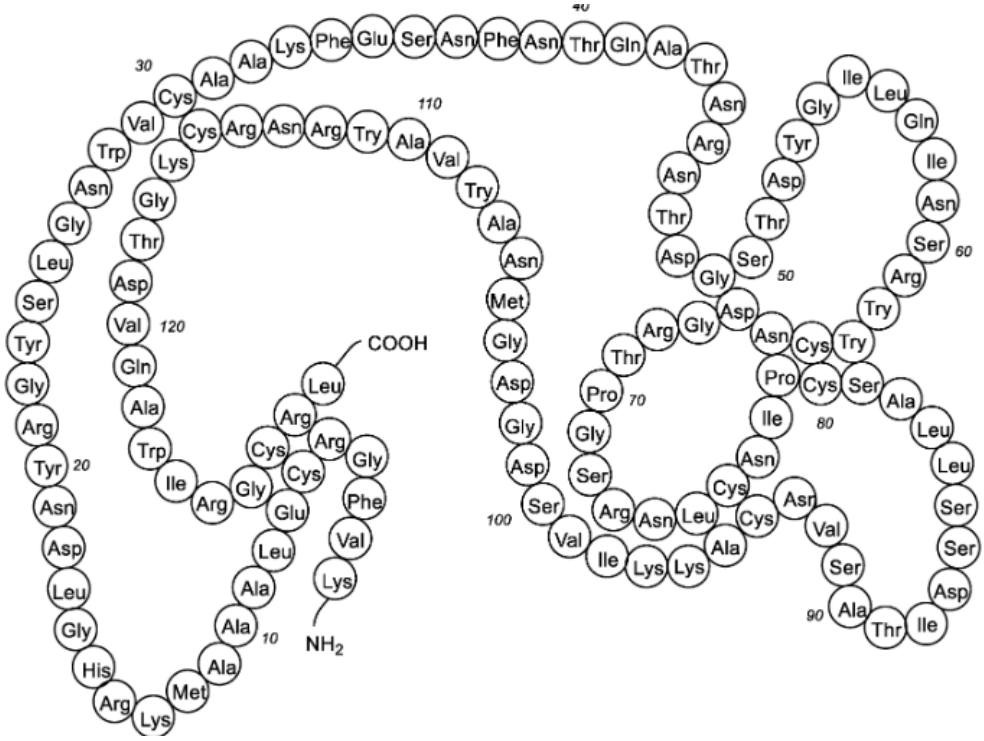

***Figure 2**: Structure of lysozyme (Wu et al., 2019).*

Lysozyme (Figure 2), also known as muramidase or N-acetylmuramide glycanohydrolase, is a naturally occurring enzyme with strong antimicrobial activity (Khorshidian et al., 2022). This enzyme catalyzes the hydrolysis of the β-1,4-glycosidic linkages between N-acetylmuramic acid (NAM) and N-acetyl-D-glucosamine (NAG) in the peptidoglycan layer of bacterial cell walls, a crucial structural matrix surrounding most bacteria (Saurabh & Sahoo, 2008). This enzymatic cleavage disturbs cell wall integrity, causing osmotic imbalance and, ultimately, cell lysis, especially in Gram-positive bacteria, which lack a protective outer membrane (Ferraboschi et al., 2021). For this reason, lysozyme plays a central role in the innate immune defense of animals and plants. Beyond its antibacterial function, lysozyme has also been shown to interact with some viral particles, exerting antiviral effects. Moreover, it appears to regulate immune responses by suppressing pro-inflammatory cytokines, suggesting additional anti-inflammatory potential (Leśnierowski & Yang, 2021). These diverse biological activities may operate synergistically to enhance lysozyme's overall protective role in host systems.

Lysozymes are broadly classified into three main types: chicken-type (c-type), goose-type (g-type), and invertebrate-type (i-type) (Figure 3), based on their amino acid sequences, catalytic mechanisms, and evolutionary lineage. More detailed:

- **C-type lysozymes** are the most extensively studied and widely distributed across vertebrates and some invertebrates. Hen egg-white lysozyme (HEWL), a well-characterized example, has a compact α/β structure stabilized by disulfide bridges and exhibits high enzymatic activity against Gram-positive bacteria (W. Zhang & Rhim, 2022). Its structural and biochemical properties have made it a model system in enzymology.
- **G-type lysozymes**, first found in goose eggs (Nawaz et al., 2022), are generally larger and less thermally stable, with fewer cysteine and tryptophan residues. However, some variants exhibit improved activity against Gram-negative bacteria and play roles in mucosal immunity, especially in aquatic species.
- **I-type lysozymes** are mostly found in invertebrates and often display broader functionality. Some of them, like destabilase-lysozyme from leeches, not only hydrolyze peptidoglycan but also exhibit thrombolytic or isopeptidase activity (Kurdyumov et al., 2015). This multifunctionality makes i-type lysozymes promising in therapeutic contexts (Tarahi et al., 2025).

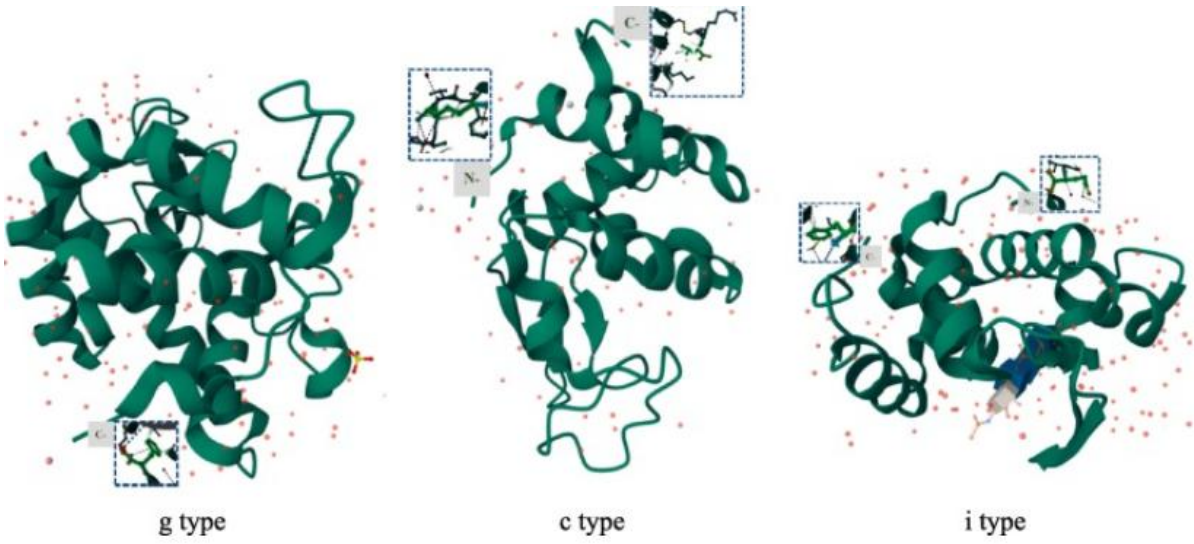

***Figure 3**: Three-dimensional structure of three types of lysozymes (Footage from UniProt) (Q. Zhang et al., 2024).*

1.4.1.1. Hen Egg White Lysozyme (HEWL)

C-type lysozyme has attracted significant interest due to its widespread availability and favorable functional characteristics. Hen egg-white lysozyme (HEWL) was the first c-type lysozyme whose three-dimensional structure was

resolved through X-ray crystallography, laying the groundwork for structural enzymology. Compared to g-type lysozymes, which typically range from 20 to 22 kDa, c-type lysozymes are smaller in molecular size, generally falling within the 11–15 kDa range (Q. Zhang et al., 2024)

HEWL is a polypeptide composed of 129 amino acid residues and exhibits an isoelectric point between 10.0 and 11.0. The primary structure of lysozyme is stabilized by four disulfide bonds formed by eight cysteine residues; these bonds are critical for maintaining its structural integrity (Wu et al., 2019). Its secondary structure is predominantly made up of α-helices and β-sheets, while the tertiary structure consists of two distinct domains connected by a long α-helix. This configuration forms a deep catalytic cleft, where the active site, spanning from Glu-35 to Asp-52, is located (Figure 4). A notable structural feature of HEWL is the interaction between Lys97 and Phe38, which brings the two domains closer. This interaction contributes to a compact monomeric structure characterized by an internal hydrophobic core and an external hydrophilic surface (Yang & Yan, 2025).This structural organization not only supports the enzyme's high solubility but also contributes to its exceptional stability. HEWL can be stored at 5 °C for extended periods without loss of catalytic activity, even in dry conditions. It also exhibits considerable thermal stability, retaining activity after exposure to 100 °C for 3 minutes at pH 4.5, or for 30 minutes at pH 5.0. These features make c-type lysozymes, particularly HEWL, highly suitable for a range of industrial and scientific applications (Masschalck & Michiels, 2003).

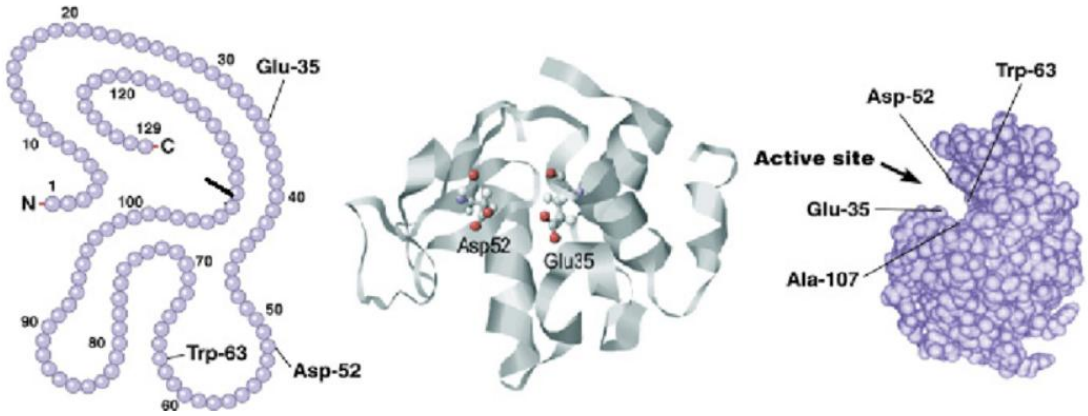

***Figure 4**: (left) HEWL primary structure (unfolded), (middle) tertiary structure (folded), (right) active site with the amino acids responsible for the lysozyme activity (folded) (Gálvez-Iriqui et al., 2020).*

1.4.1.2. Applications for HEWL

HEWL is widely studied for its potent antibacterial activity, high stability, and well-characterized structure. Its natural abundance and safety have made it a valuable component in a variety of fields:

- **In the food industry**, HEWL is the only lysozyme approved for use as a natural preservative (Khorshidian et al., 2022). It inhibits several foodborne pathogens and spoilage bacteria, such as *Listeria monocytogenes*, *Clostridium butyricum*, and various *Lactobacillus* species (Lesnierowski & Kijowski, 2007). Its use extends to dairy products, meats, wine, and fresh produce, where it helps prolong shelf life. HEWL is also incorporated into antimicrobial food packaging. Recent studies have explored its chemical modification to improve thermal stability and antioxidant properties. However, such changes may reduce its enzymatic activity.
- Beyond preservation, HEWL plays a growing role in **animal agriculture as an alternative to antibiotics**. When incorporated into feed, it supports gut health, strengthens immune function, and promotes growth in poultry, fish, and farm animals. Studies demonstrate dose-dependent benefits; for instance, dietary supplementation in tilapia and broiler chickens has been shown to enhance disease resistance and performance, highlighting HEWL's potential in antibiotic-free farming systems (Oliver & Wells, 2015).
- HEWL also has a crucial role **in scientific research**, particularly as a model protein for studies in crystallography, protein folding, and drug interactions. As mentioned before, its structure was one of the first to be solved by X-ray crystallography, and it remains widely used in proteomics and biophysics. HEWL is employed to study protein aggregation and misfolding, processes linked to diseases such as Alzheimer's and Parkinson's. Its versatility, stability, and ease of handling make it ideal for use in biochemical and biophysical experiments (Chen et al., 2024).
- **In the medical field**, HEWL is available in pharmaceutical products such as tablets, lozenges, and sprays for treating throat infections, ulcers, and skin wounds. It exhibits antimicrobial, anti-inflammatory, and wound-healing properties (Bergamo & Sava, 2023). Recent work focuses on incorporating HEWL into biomaterials like hydrogels, nanofibers, and microneedles to enhance drug delivery and healing. Some modified HEWL systems have even shown promising anticancer activity *in vitro*, further expanding their therapeutic potential.
- **In materials science**, HEWL acts as a natural surfactant for dispersing hydrophobic nanomaterials in aqueous systems. This eco-friendly method stabilizes particles through non-covalent interactions, enabling the creation of functional nanocomposites for use in packaging, drug delivery, and biosensors (Chen et al., 2024).

1.4.2. Amylases

Amylases represent a significant class of industrial enzymes, accounting for approximately 30% of global enzyme production (Calik & Ozdamar, 2001). These enzymes are employed across a broad range of industries, including food

processing, fermentation, textiles, paper, detergents, and sugar manufacturing. Additionally, amylases have found increasing utility in various biotechnology-related applications, such as the biodegradation of environmental pollutants, microbial conversion of starch into valuable substrates, treatment of starch-containing waste, and the biosynthesis of biochemical compounds using starch as a substrate (MOTTA et al., 2023). With ongoing advancements in biotechnology, the scope of amylase applications has expanded to encompass fields such as clinical diagnostics, medicinal research, and analytical chemistry. Notably, the first enzyme to be produced on an industrial scale was a fungal-derived amylase in 1894, which was utilized as a pharmaceutical agent for the treatment of digestive disorders (Mobini-Dehkordi M. & Javan F., 2012)

Enzymes belonging to amylases, such as endoamylases and exoamylases, can hydrolyze starch. The enzymes are classified according to the way the glycosidic bond is attacked (Figure 5) (Castro et al., 2018):

- α-amylases (EC 3.2.1.1): endoamylases that can cleave α,1-4 glycosidic bonds in the inner part of the amylose or amylopectin chain. They are found in a wide variety of microorganisms, such as Archaea and Bacteria (Tiwari SP et al., 2015).
- β-amylases (EC 3.2.1.2): exoamylases that exclusively cleave the α,1-4 glycosidic bond. They act on the external glucose residues of amylose or amylopectin, and they are key enzymes in the production of maltose, which is utilized by yeast during fermentation.
- γ-amylases (EC 3.2.1.3): they cleave the α,1-6 glycosidic linkages, in addition to cleaving the α,1-4 glycosidic linkages at the non-reducing end of amylose and amylopectin, yielding glucose. They are most effective in acidic environments and have an optimum pH of 3.0 (Sivaramakrishnan et al., 2006).

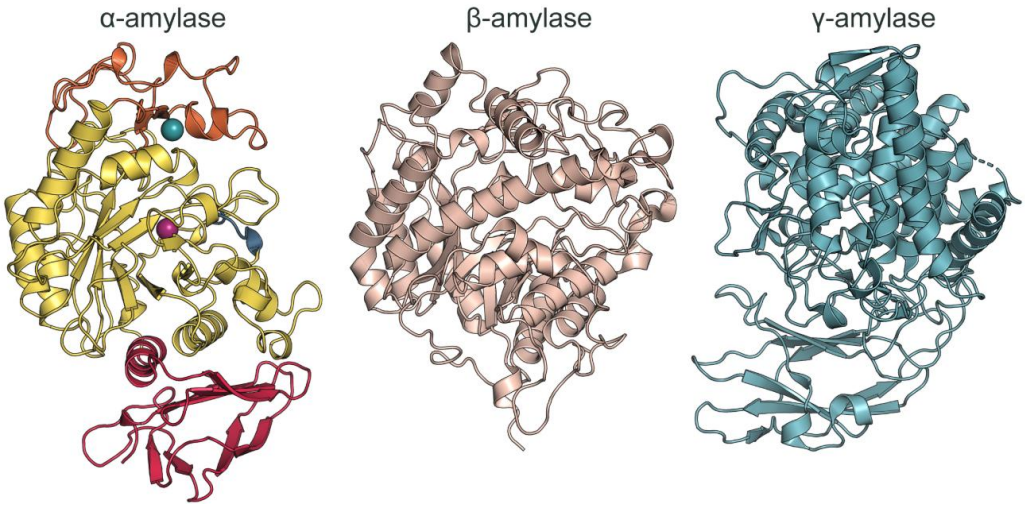

***Figure 5**: (Left) structure of human alpha-amylase (PDB 1SMD), (Middle) structure of barley beta-amylase (PDB 2XFR), (Right) Structure of Penicillium oxalicum's gamma-amylase (PDB 6FHV) (source: Protein Data Bank in Europe)*

1.4.2.1. α-amylase

α-Amylase (EC 3.2.1.1) is a hydrolase enzyme that catalyzes the hydrolysis of internal α-1,4-glycosidic bonds in starch, resulting in the formation of smaller sugars, such as glucose and maltose. It is classified as a calcium metalloenzyme, meaning its catalytic activity requires the presence of a metal cofactor, specifically calcium ions. As previously discussed, hydrolases can be divided into two main categories: endo-hydrolases and exo-hydrolases. Endo-hydrolases cleave internal bonds within the substrate molecule, whereas exo-hydrolases act on the terminal, non-reducing ends. Consequently, α-amylase, as an endo-hydrolase, is unable to cleave terminal glucose residues or α-1,6-glycosidic linkages (Movahedpour et al., 2022).

The primary substrate for α-amylase is starch, a polysaccharide composed of two polymeric components: amylose and amylopectin. Amylose constitutes approximately 20–25% of the starch structure and consists of linear chains of glucose units linked by α-1,4-glycosidic bonds. Amylopectin, which makes up 75–80% of starch, is a highly branched molecule. The linear portions of amylopectin are also linked via α-1,4-glycosidic bonds, while branching occurs at intervals of every 15–45 glucose units through α-1,6-glycosidic linkages (Klonis, 2018). The composition of the hydrolysates resulting from starch degradation by α-amylase is significantly influenced by factors such as temperature, hydrolysis conditions, and the origin of the enzyme. The enzyme exhibits optimal catalytic activity at a pH of approximately 7.0.

Due to its ability to hydrolyze starch efficiently, α-amylase has gained considerable industrial significance. One notable application is in the production of glucose and high-fructose syrups. α-Amylase catalyzes the initial step of starch breakdown in this process. Historically, starch hydrolysis was achieved via acid hydrolysis, which required harsh conditions, including highly acidic environments and elevated temperatures. Enzymatic hydrolysis, utilizing α-amylase, offers a more favorable alternative by operating under milder conditions and yielding higher-quality fructose syrup (R. Gupta et al., 2003; Sundarram A. et al., 2014)

1.4.2.2. Sources of α-amylase

α-Amylases can be derived from plants, animals, or microorganisms. Plant sources include cereals such as barley and rice, while cassava wastewater has also been identified as a potential source. Animal-derived α-amylase, such as salivary ptyalin, is well-known for initiating starch digestion. However, these sources are not suitable for large-scale applications.

Microorganisms are the preferred source of industrial α-amylase due to their rapid growth, cost-effectiveness, and ease of cultivation. In addition, microbial strains can be genetically modified or subjected to strain improvement techniques to enhance production and optimize enzyme properties, such as

thermostability or halotolerance, making them highly adaptable to industrial requirements (KONSOULA & LIAKOPOULOU KYRIAKIDES, 2007). Among bacteria, *Bacillus* species are the most important producers, with *B. amyloliquefaciens*, *B. licheniformis*, *B. subtilis*, and *B. stearothermophilus* widely used in commercial processes. Fungal species, particularly *Aspergillus oryzae*, *A. niger*, and *A. awamori*, also serve as common production hosts. In recent years, genetically engineered microorganisms have further expanded the possibilities for efficient and tailored α-amylase production (Sundarram A. et al., 2014)

1.4.2.3. Molecular structure

α-Amylases are members of the glycosyl hydrolase family 13 (GH-13) and share about 30% amino acid sequence identity across different organisms. These enzymes are typically monomeric, calcium-dependent proteins composed of a single polypeptide chain organized into three structural domains (A–C) (Figure 6) (Gopinath et al., 2017; Prakash & Jaiswal, 2010):

- The A-domain is the most conserved and consists of a characteristic fold of eight parallel β-strands arranged in a barrel encircled by eight α-helices. Within this domain, several highly conserved residues are in loop regions at the C-termini of β-strands, forming the catalytic site. These residues are critical for substrate recognition and hydrolysis, a feature common to the α/β-barrel protein family.
- The B-domain protrudes between the third β-strand and the third α-helix of the A-domain. Its sequence and size vary significantly among different α-amylases, ranging from short, irregular structures to complex β-strand folds, such as those observed in *Bacillus* enzymes. This domain plays an important role in substrate interaction and calcium binding, with the Ca^{2+} binding site typically located at the interface between domains A and B. In some bacterial α-amylases, additional anion-binding sites, such as chloride-binding pockets, have been identified. These contribute to catalytic efficiency by stabilizing the ionization state of residues in the active site (Muralikrishna & Nirmala, 2005).
- The C-domain is structurally more conserved and folds into an antiparallel β-barrel. While its exact function is not fully understood, it is thought to contribute to overall stability and may influence substrate binding in some cases. The spatial orientation of domain C relative to domain A varies depending on the source of the enzyme (van der Maarel et al., 2002)

The active site is positioned in a cleft between domains A and B. Substrate binding is facilitated by aromatic residues such as phenylalanine, tryptophan, and tyrosine, which interact with sugar rings through hydrophobic stacking, as well as by residues that form hydrogen bonds directly or via water molecules. Structural and mutational studies have demonstrated the importance of three conserved

acidic residues: one glutamic acid that serves as a proton donor, one aspartic acid acting as a nucleophile, and a second aspartic acid stabilizing the transition state and maintaining the catalytic proton donor in its active form. Together, these features explain the versatility and efficiency of α-amylases across diverse organisms (Tiwari SP et al., 2015).

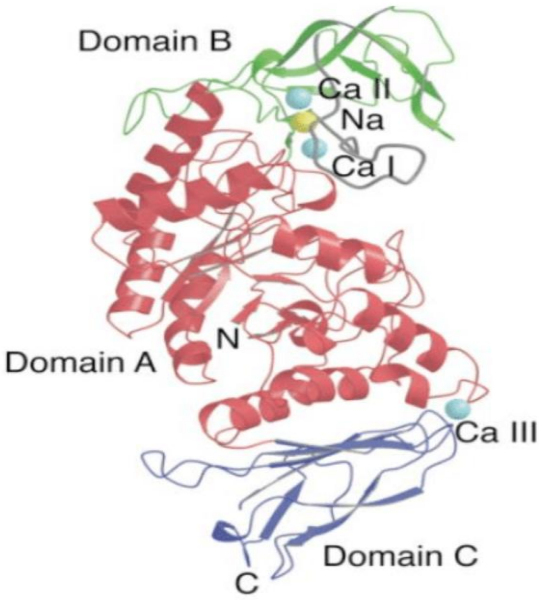

***Figure 6**: Structure of alpha-amylase found in Bacillus licheniformis (Machius et al., 1998)*

1.4.2.4. Applications

α-Amylase is one of the most widely applied industrial enzymes due to its ability to hydrolyze starch into smaller sugars:

- In the **food industry**, it plays a crucial role in baking, where it improves dough handling, enhances loaf volume, and contributes to the aroma, flavor, and crust color of bread. It also delays stalling by generating fermentable sugars that support yeast activity during proofing and baking. In addition, α-amylase is extensively employed in the production of sweeteners such as glucose, maltose, and high-fructose syrups, as well as in confectionery processes where it stabilizes chocolate syrups and improves texture (Couto & Sanromán, 2006).
- In the **beverage and fermentation sector**, α-amylase is indispensable for the liquefaction and saccharification of starch-based raw materials. By converting starch from grains into fermentable sugars, the enzymes enable the production of alcoholic beverages such as beer and whisky, as well as bioethanol. The use of microbial α-amylases in brewing also reduces the

dependence on malt, thus lowering production costs (Mobini-Dehkordi M & Javan F., 2012).

The enzyme also has significant applications in **non-food industries**.

- In the **textile sector**, α-amylase is applied during the desizing process to remove starch-based coatings from fabrics, thereby improving subsequent dyeing and finishing (de Souza & de Oliveira Magalhães, 2010).
- In the **paper industry**, it is used to modify starch for coating and sizing, enhancing paper strength, surface smoothness, and printability, while also finding use in conservation practices for the removal of starch adhesives from historical documents (Porfirif et al., 2016).
- In the **detergent industry**, α-amylase is incorporated into laundry and dishwashing formulations to efficiently remove starchy stains. Its stability across a wide range of pH and temperatures makes it particularly suitable for modern detergent applications (Hmidet et al., 2008).

Beyond these uses, α-amylase contributes to:

- The **animal feed industry** can improve the digestibility of starch-rich feed components, thereby enhancing the nutritional value of livestock diets.
- In the **biofuel sector**, the enzyme is a key catalyst in bioethanol production, facilitating the conversion of starch into fermentable sugars that can be further processed by yeas (Sanchez & Cardona, 2008).
- In the **pharmaceutical and medical fields** as digestive aid and in diagnostic assays, while also finding roles in the **cosmetic and fine chemicals industries**, where it is used in the synthesis of syrups, sweeteners, and other starch derivatives incorporated into personal care and specialty products (Paul et al., 2021).

1.5. Nanotechnology and nanobiotechnology

Nanotechnology refers to the manipulation, design, characterization, and application of materials at the nanoscale, typically between 1 and 100 nanometers, where size-dependent phenomena (e.g., quantum effects, increased surface-area-to-volume ratio) begin to dominate properties and behavior. At this scale, materials often exhibit novel optical, electronic, magnetic, mechanical, and chemical properties that differ significantly from those observed in the same material in its bulk form. Therefore, nanotechnology has applications across diverse fields such as electronics, energy storage, catalysis, sensors, materials science, and more (Kintzios 2016; Stamatis 2016).

Nanobiotechnology is the intersection of nanotechnology and the biological sciences (Figure 7). It involves applying nanoscale tools, materials, and devices to study biological systems and to develop new biotechnological

solutions (Jun, 2021). Examples include nano-biosensors, nanocarriers for drug or gene delivery, nano-diagnostics, and artificial scaffolds for tissue engineering. Nanobiotechnology leverages specific interactions of nanoscale structures with biomolecules (proteins, nucleic acids, lipids, cells) to achieve functions such as targeted therapy, improved diagnostics, controlled release, and novel imaging modalities. Its potential lies in improving selectivity, reducing side effects, enabling earlier detection, and creating therapeutic and diagnostic methods that are not possible with larger-scale materials (Hossein Hosseinkhani, 2022; Kaur & Thombre, 2021).

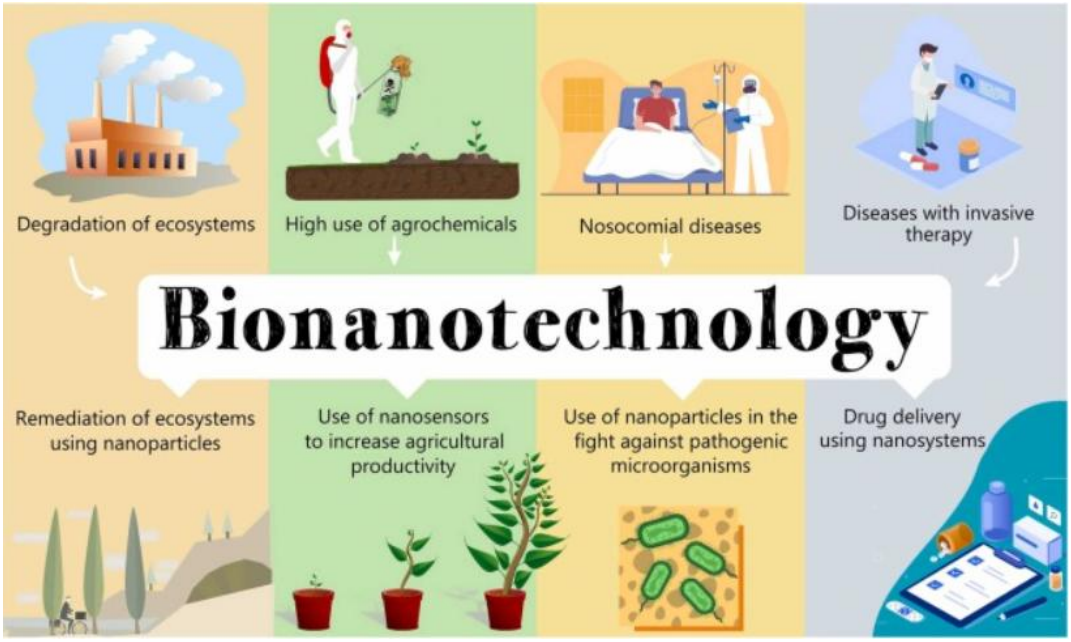

***Figure 7**: Bionanotechnology is a multidisciplinary science that aims to solve emerging social, environmental, and medical issues of a sustainable, biocompatible, and regenerative nature (dos Santos et al., 2024).*

1.5.1. Nanomaterials

Nanomaterials are defined as materials smaller than 100 nm (Laurent et al., 2008). The classification of nanomaterials into broader categories includes nanofibers, carbon nanomaterials, nanofilms, nanoblocks, nanocrystalline alloys, nanocomposites, nanocrystalline solids, and nanoparticles. Nanoparticles are typically composed of multiple layers with distinct functions: a functional core (often with optical or magnetic properties such as fluorescence), a protective shell that prevents chemical degradation and reduces toxicity, and an outer layer that ensures biocompatibility (W.-K. Shin et al., 2016). This last layer usually may be functionalized with a variety of small molecules, metal ions, surfactants, and polymers. These provide water solubility and enable specific binding to biomolecules or cells (I. Khan et al., 2019). Due to these properties, nanoparticles are increasingly applied in biology and biotechnology. They are

used in fluorescent labeling and biomolecular analysis, pathogen and protein detection, purification and manipulation of biomolecules, and as carriers for drug and gene delivery. Additionally, they are explored in cancer therapy (through chemical or thermal methods), biosensor and nanodevice development, and as contrast enhancers in imaging techniques such as MRI (Stamatis, 2016).

In this thesis, the nanomaterials that were used belong to the carbon-based nanomaterials category, namely graphene oxide, biographene, and magnetic biographene.

1.5.2. Carbon-based nanomaterials

Carbon, a well-known element with six electrons, possesses four outer shell orbitals (2s, 2px, 2py, and 2pz), which allow it to undergo hybridization into sp, sp^2, and sp^3 states. This versatility makes carbon one of the most remarkable elements in nature. Its ability to exist in multiple forms gives rise to compounds with highly diverse properties, depending on the spatial arrangement of carbon atoms. Among its natural allotropes, diamond and graphite are the most notable; diamond is characterized by sp^3 hybridization with a bond length of approximately 1.56 Å (Onyancha et al., 2022).

Carbon-based nanomaterials (Figure 8) represent a highly promising class of nanomaterials composed entirely of carbon atoms arranged in unique nanoscale architectures. Their unique geometry and atomic configuration impart exceptional electrical, mechanical, and optical properties. Among them, carbon nanotubes (CNTs), graphene, graphene oxide (GO), and carbon dots (CDs) have been extensively investigated for biomedical applications due to their notable conductivity, biocompatibility, and adjustable optical characteristics (M. Shin et al., 2024) . Since they are composed of pure carbon, they exhibit high stability, good conductivity, low toxicity, and environmental friendliness. The good electrical conductivity, high surface area, and linear geometry make their surface highly accessible to the electrolytic solution. Carbon-based nanomaterials also have strong anisotropic thermal conductivity. This property allows the carbon-based nanomaterials to be used in advanced computing electronics where the temperature of uncooled chips can reach over 100℃ (Q.-L. Yan et al., 2016)

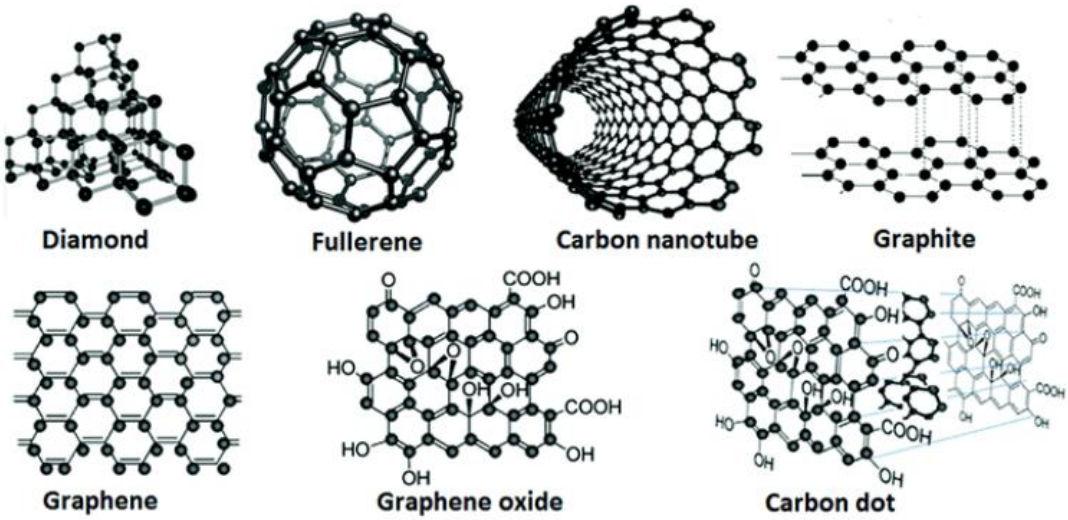

***Figure 8**: The schematics of the representative carbon-based nanomaterials (Yan et al.,2016).*

1.5.2.1. Graphene

Graphene is a single two-dimensional layer of carbon atoms bound in a hexagonal lattice structure. Although it was first isolated in 2004, it has since become one of the most extensively studied nanomaterials. In recognition of their pioneering work, Andre Geim and Konstantin Novoselov were awarded the 2010 Nobel Prize in Physics for the discovery of graphene (Geim & Novoselov, 2007). The rapid surge of interest in this material stems from its remarkable and diverse set of properties (Cooper et al., 2012).

Graphene is known for its exceptional strength, flexibility, electrical and thermal conductivity, and large surface area. Graphene is also transparent and impermeable to most gases and liquids. These properties make graphene suitable for use in bioelectronic devices, supercapacitors, and as a reinforcing agent in nanocomposite materials (M. Shin et al., 2024).

Although the term “graphene” strictly refers to a single atomic layer of carbon atoms, it is often broadly used to describe materials composed of multiple stacked layers. Various synthesis methodologies have been established, producing graphene materials with distinct characteristics such as the number of layers, lateral size, residual chemical groups, surface charge, and functionalization. These methods are generally classified into two main categories (Figure 9): bottom-up and top-down approaches (Speranza, 2021).

Top-down methods start from bulk graphite and work by breaking it down into thin graphene layers, for example, by mechanical exfoliation, chemical or liquid-phase exfoliation, ball milling, or electrochemical peeling. By contrast, bottom-up methods build graphene up from molecular or atomic carbon sources, often via processes such as chemical vapor deposition (CVD), epitaxial growth on

substrates like silicon carbide, or organic synthesis of graphene nanoribbons (Figure 9) (Gutiérrez-Cruz et al., 2022). While top-down approaches tend to be more scalable and lower cost, they often introduce defects and have less control over the structure. Bottom-up methods yield higher structural quality and more precise control over layers, but are usually more complex and costly (Madurani et al., 2020)

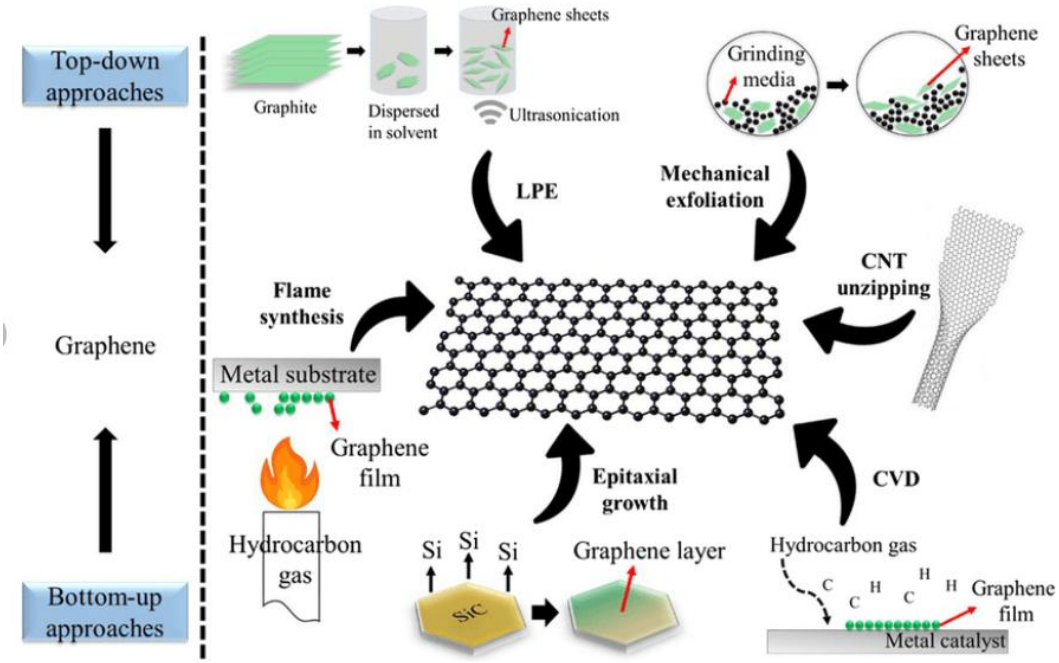

***Figure 9**: Examples of conventional bottom-up and top-down approaches for the synthesis of graphene (Pang et al., 2021).*

1.5.2.2. Graphene oxide (GO)

Graphene oxide (GO) is derived from graphene through chemical modification with oxygen-containing functional groups, including hydroxyl, epoxide, and carboxyl groups (Figure 10). The presence of these groups enhances the hydrophilicity and dispersibility of GO in aqueous solutions, though it simultaneously disrupts the sp^2 lattice and reduces electrical conductivity relative to pristine graphene. Owing to its versatile properties, GO has been explored in water treatment, drug delivery systems, and as an intermediate material for producing other graphene-based structures (M. Shin et al., 2024). The most widely adopted synthesis route is the Hummers' method, in which graphite is oxidized using strong oxidizing agents such as potassium permanganate in concentrated sulfuric acid, leading to the incorporation of oxygen functionalities and facilitating exfoliation (Chung et al., 2013). Due to the similarities of GO and graphene, as well as the fact that it is more cost-effective, it is the most used and considered the representative graphene nanomaterial (Gladwin Alex et al., 2022)

***Figure 10**: Chemical structure of graphene and graphene oxide (Ricci et al., 2022).*

1.5.3. Green approaches for nanomaterials

Over the past years, nanotechnology has made significant progress and has transformed the development and application of innovative functional materials. Although nanomaterials hold immense promise, those produced through conventional synthesis methods encounter significant drawbacks. These include poor stability under harsh conditions, potential risks of toxicity and bioaccumulation, difficulties in device integration, and dependence on harmful reagents. Such issues not only limit their extension but also raise serious concerns regarding the long-term safety and sustainability of existing fabrication techniques. As a result, increasing attention has shifted toward eco-conscious production strategies grounded in green chemistry (Dhaffouli, 2025; Oliveira et al., 2024).

Green methods for nanoparticle synthesis have emerged as sustainable alternatives to conventional chemical routes. Green synthesis utilizes natural or renewable resources such as plant extracts, microorganisms (bacteria, fungi), enzymes, and even agricultural or food wastes as reducing and capping agents (Dikshit et al., 2021). These biologically derived routes are environmentally friendly, cost-effective, and inherently safer, while also enabling the production of nanoparticles with diverse morphologies and tunable properties (Alqarni et al., 2022). The resulting products, often referred to as *biogenic nanomaterials*, are generated through biological constituents such as proteins, phenolic compounds, or enzymes, which mediate reduction and stabilization mechanisms. This approach not only minimizes ecological harm but also aligns with the principles of green chemistry, emphasizing safety, economic viability, and long-term sustainability (D. Gupta et al., 2023)

1.5.3.1. Biographene

A material can be defined as *biographene* when it is produced through a "green" synthetic process that employs environmentally friendly solvents as well as biological stabilizing agents (Celina Selvakumari et al., 2020).

Initially, exfoliation of graphite into graphene is primarily governed by the disruption of the strong van der Waals forces holding adjacent carbon layers together. This disruption is achieved through the intercalation of molecules that can bind within or between the graphene layers, thereby expanding the interlayer spacing and reducing binding energy. The effectiveness of exfoliation depends on several interrelated factors: the chemical nature and polarity of the intercalating agent, its molecular size and charge, the dielectric constant of the solvent, and the mechanical energy applied through sonication, shear, or milling (Coleman, 2013). Molecules capable of π–π stacking or hydrophobic interactions—such as aromatic surfactants, polymers, or proteins—can insert between graphite layers and stabilize the exfoliated sheets by preventing restacking (Guardia et al., 2011).

The exfoliation of graphite using organic solvents, ionic liquids, or surfactant-based aqueous solutions—whether through ultrasonication or shear mixing—generally does not result in materials with high biocompatibility, limiting their suitability for biological applications such as cell culture or drug delivery. Graphene obtained through these conventional approaches is typically not inherently biocompatible (Pinto et al., 2013). To improve both the biocompatibility and hydrophilicity of graphene, exfoliation can instead be performed using environmentally benign solvents, such as water, coupled with biological molecules that act as stabilizing agents for the graphene sheets (Losada-Garcia et al., 2019). Stabilization in aqueous media can be achieved either through electrostatic interactions or by applying mechanical energy to produce homogeneous dispersions (Pattammattel & Kumar, 2015). Among the biomolecules explored, proteins have demonstrated significant potential, as their amphiphilic nature—comprising both hydrophilic and hydrophobic amino acid residues—facilitates strong interactions with the graphene surface. These interactions promote exfoliation while preventing sheet aggregation. Experimental studies have shown that hydrophobins, small surface-active proteins, adsorb onto one side of the graphene surface via hydrophobic interactions, exposing their hydrophilic residues outward. This amphiphilic behavior renders them particularly suitable for stabilizing two-dimensional nanomaterials such as biographene (Paredes & Villar-Rodil, 2016). In addition to hydrophobins, other proteins such as lysozyme and bovine serum albumin (BSA) have also been identified as highly effective stabilizing agents for biographene (Kumar & Pattammattel, 2016).

1.5.3.2. Bovine Serum Albumin (BSA) as a stabilizer for Biographene production

Unlike conventional chemical or mechanical exfoliation, which often relies on harsh reagents or energy-intensive conditions, BSA offers a sustainable and biocompatible route for graphene production. As a naturally occurring protein, BSA is amphiphilic and rich in functional groups that can interact with the surface of graphite layers through hydrophobic, electrostatic, and π–π interactions. These interactions stabilize the delaminated graphene sheets (Figure 11) and prevent their restacking, yielding dispersions that are more environmentally friendly and potentially safer for biomedical and environmental applications (Pattammattel & Kumar, 2015).

From a theoretical perspective, the use of BSA in graphite exfoliation illustrates how biomolecules can serve a dual role as both exfoliating and stabilizing agents, reducing the need for toxic surfactants or synthetic polymers. The protein not only aids in the separation of graphene layers but also provides a biocompatible coating that enhances dispersion stability in aqueous media. This makes BSA-based biographene particularly attractive for applications in biosensing, drug delivery, tissue engineering, and enzymatic immobilization, where both material performance and biological safety are critical. By aligning with the principles of green chemistry and nanotechnology, biographene demonstrates how biologically derived methods can bridge the gap between advanced material performance and ecological responsibility (Thomas et al., 2021)

In the context of the present master's thesis, the biographene used was produced at the Laboratory of Biotechnology of the Department of Biological Applications and Technologies at the University of Ioannina. Its production was part of the research work of Alatzoglou et al., 2022.

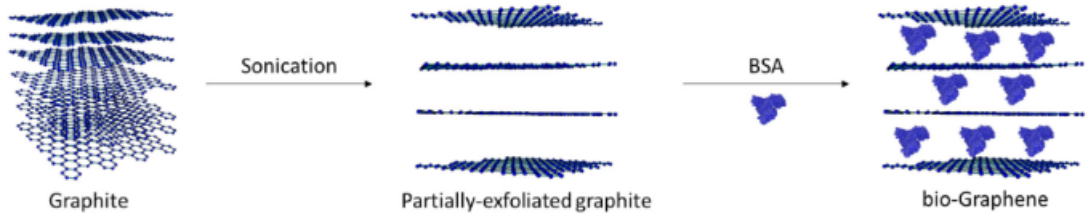

***Figure 11**: Schematic presentation of the production of bio-Graphene (Alatzoglou et al., 2022).*

1.5.4. Magnetic Nanoparticles

Magnetic nanoparticles (MNPs) are nanomaterials that exhibit strong magnetic properties due to their small size, which often makes them super-

paramagnetic. This unique behavior allows them to be magnetized under an external magnetic field while minimizing aggregation when the field is removed. MNPs have versatile applications in biomedicine, catalysis, environmental remediation, and sensing, where their magnetic responsiveness, high surface area, and tunable surface chemistry are particularly advantageous (Rezaei et al., 2024)

Among MNPs, iron oxide nanoparticles (IONPs), such as magnetite (Fe_3O_4) and maghemite (γ-Fe_2O_3), are the most widely studied due to their biocompatibility, chemical stability, and strong magnetic behavior. They are extensively used in magnetic resonance imaging (MRI) as contrast agents, in targeted drug delivery guided by external magnetic fields, and in hyperthermia-based cancer treatments. Functionalization of IONPs with polymers, proteins, or other coatings further enhances their stability, dispersibility, and suitability for biomedical applications (A. K. Gupta & Gupta, 2005).

One of the most widely employed techniques for the synthesis of IONPs is the co-precipitation method, originally introduced by Massart in 1981. This approach is based on the reaction of ferric (Fe^{3+}) and ferrous (Fe^{2+}) ions, typically in a 2:1 molar ratio, within a basic medium. Ammonia is frequently used as the precipitating agent, providing hydroxide ions that promote the nucleation and growth of magnetite (Fe_3O_4) nanoparticles while simultaneously acting as a stabilizing medium by ensuring a non-oxidizing environment. Control over reaction parameters such as pH (ideally 9.0–14.0), temperature, and oxygen concentration is crucial for obtaining nanoparticles with uniform size, shape, and magnetic properties. The method is favored for its simplicity, high yield, and reproducibility, and it also allows for the incorporation of surfactants or organic molecules during synthesis to fine-tune surface properties and enable in situ functionalization. Nevertheless, precise regulation of the reaction conditions is necessary to achieve narrow size distributions and to prevent the loss of desirable magnetic behavior (Popescu et al., 2019)

The method described above was used to produce magnetic nanoparticles. The molecule that was added during the synthesis was biographene. Attaching MNPs onto carbon allotropes such as graphene through in situ co-precipitation represents a promising strategy for numerous applications. The resulting composites demonstrate outstanding properties, including a high surface-to-volume ratio, excellent mechanical strength, and superparamagnetic behavior (Mehta, 2017). The combination of these has attracted considerable interest because of their broad application potential across multiple fields. Overall green approaches can lead to more biocompatible nanosupports, making them well-suited for enzyme immobilization and enhancing catalytic performance through non-denaturing interactions between the support and the biocatalyst (Alatzoglou et al., 2025). It is worth noting that magnetic nanobiocatalytic systems enable straightforward separation from

reaction mixtures using an external magnetic field, facilitating their reuse in a wide range of applications (Ashwini John et al., 2023).

1.6. Immobilization of enzymes on nanoparticles

Enzymes, often referred to as *biocatalysts*, represent a groundbreaking advancement in bioprocess technology. Their widespread adoption across multiple industries is largely due to their ease of production, substrate specificity, and alignment with green chemistry principles. However, for large-scale commercialization, ensuring enzyme reusability is essential. Without it, their application becomes economically unviable. A major challenge lies in preserving their structural stability during biochemical reactions.

To address this, immobilized enzymes are employed as effective alternatives, offering enhanced functional efficiency and reproducibility despite their relatively high cost. Enzyme immobilization involves confining the enzyme to a distinct phase (matrix or support) separate from that of the substrates and products. Beyond affordability, an ideal matrix should provide inertness, mechanical strength, stability, reusability, improved enzyme specificity or activity, and reduced issues such as product inhibition, nonspecific adsorption, and microbial contamination. Nanoparticles are widely used as nanocarriers for enzyme immobilization. A variety of immobilization techniques exist, and the performance of immobilized enzymes is influenced by multiple factors (Datta et al., 2013).

This thesis focuses on the use of physical adsorption; other techniques are presented in Figure 12.

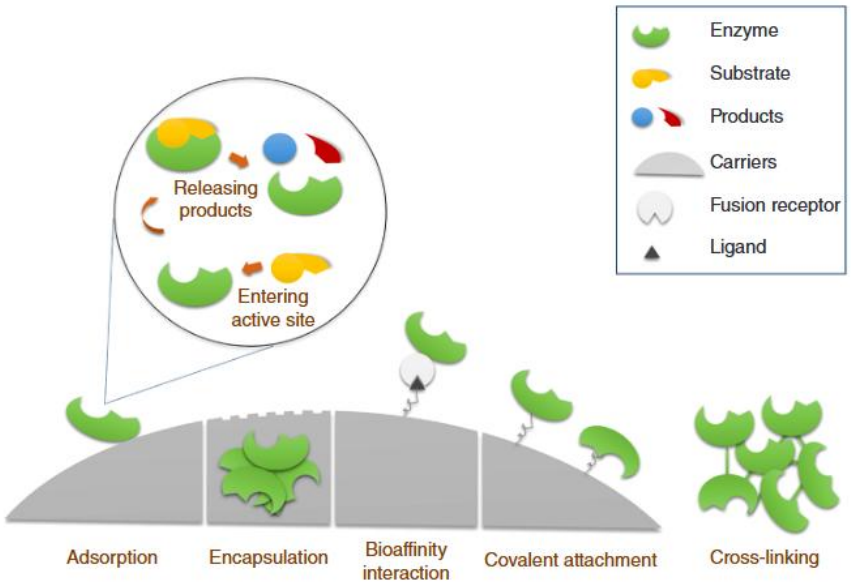

***Figure 12**: Illustration of general enzyme immobilization methods and reaction of immobilized enzyme (Lee & Au-Duong,2018).*

1.6.1. Physical adsorption (non-covalent bonding)

Physical adsorption primarily depends on van der Waals forces, hydrogen bonding, hydrophobic interactions, and electrostatic attractions between enzyme molecules and the surface of insoluble carriers. This method helps protect enzymes from deactivation, which is often observed in techniques involving chemical modifications of the enzyme structure, such as covalent attachment and cross-linking (Lee & Au-Duong, 2018). Also, the enzyme remains insoluble in the aqueous medium or is retained on the insoluble surface support. Compared to other techniques, it is simple, inexpensive, does not require activation, and allows the enzyme to be reused. In addition, it can alleviate enzyme inhibition. However, a disadvantage is that pH variations can lead to enzyme desorption, complicating other process steps. The effectiveness of this technique depends on many factors, including support surface area, porosity, pore size, enzyme concentration, and the amount of enzyme adsorbed per unit of support (Silva Almeida et al., 2024).

The approach typically followed is largely the same across applications. It begins with dispersing the nanomaterial in the immobilization medium, followed by the addition of the enzyme and incubation of the mixture for a pre-defined period. Finally, the biocatalyst is recovered through successive washing steps (Patila, 2016). The hydrophobic interactions formed between the hydrophobic surface of the nanomaterial and the hydrophobic amino acids on the enzyme surface can also play an important role during the process of non-covalent immobilization. In addition, attractive forces (π–π interactions) may arise during physical adsorption, occurring between the aromatic rings of the nanomaterial surface and the aromatic amino acids exposed on the enzyme surface (Stamatis, 2016).

1.7. Spectroscopic Techniques

Spectroscopy is the measurement and interpretation of electromagnetic radiation (EMR) absorbed and emitted when the molecules, atoms, or ions of a sample move from one energy state to another (Gandhimathi R., 2012). Spectroscopy involves the examination of how electromagnetic radiation EMR interacts with matter. Spectroscopic techniques are based on various phenomena, including emission, absorption, fluorescence, and scattering. These methods are widely employed in the analysis and characterization of diverse samples. Spectroscopy serves both qualitative and quantitative analytical purposes: qualitative analysis aims to identify a substance, while quantitative analysis focuses on measuring the concentration of an analyte within a sample.

Certain spectroscopic techniques, such as Ultraviolet-Visible (UV–Vis) spectrophotometry, are commonly utilized as preliminary screening tools. These

methods provide tentative identification and are generally non-specific. In contrast, techniques like infrared (IR) spectroscopy and mass spectrometry are regarded as confirmatory methods due to their high specificity and ability to provide definitive identification of compounds (Bumbrah & Sharma, 2016).

1.7.1. UV-Vis spectroscopy

UV-Vis spectroscopy refers to an analytical technique used to evaluate various solvents and chemical substances based on their interaction with ultraviolet and visible light. This method is particularly favored by small-scale industries due to its relatively low cost and minimal maintenance requirements. The analytical principle involves measuring the absorption of monochromatic light by typically colorless compounds within the near-ultraviolet region of the electromagnetic spectrum, specifically between 200 and 400 nm (Govinda Verma, 2018).

The fundamental principle of UV-Vis spectroscopy is that a molecule or an ion absorbs electromagnetic radiation in the ultraviolet or visible region when the energy of the radiation induces an electronic transition within its structure. In other words, the absorption of light in these regions results in a change in the electronic state of the molecules in the sample. The energy from the incident light promotes electrons from a ground-state orbital to a higher-energy excited orbital, often referred to as an anti-bonding orbital. Generally, three types of ground-state orbitals can participate in these transitions, depending on the molecular structure and the nature of the electronic configuration (Tom J., 2023).

UV-Vis spectroscopy has a wide range of applications across various fields like the pharmaceutical industries, microbiology, and quality control for food and beverages. Apart from these, UV–Vis spectroscopy is a valuable and widely used technique for investigating the structural characteristics of proteins. The absorbance spectrum of proteins arises primarily from aromatic amino acid residues such as tryptophan, tyrosine, and phenylalanine, as well as from peptide bonds and prosthetic groups, all of which exhibit characteristic electronic transitions in the UV region (Figure 13). Variations in spectral features, including peak positions and intensities, can provide insight into conformational changes, tertiary structure, and the local environment of chromophore residues (Hansen et al., 2013; Zobel-Roos et al., 2017)

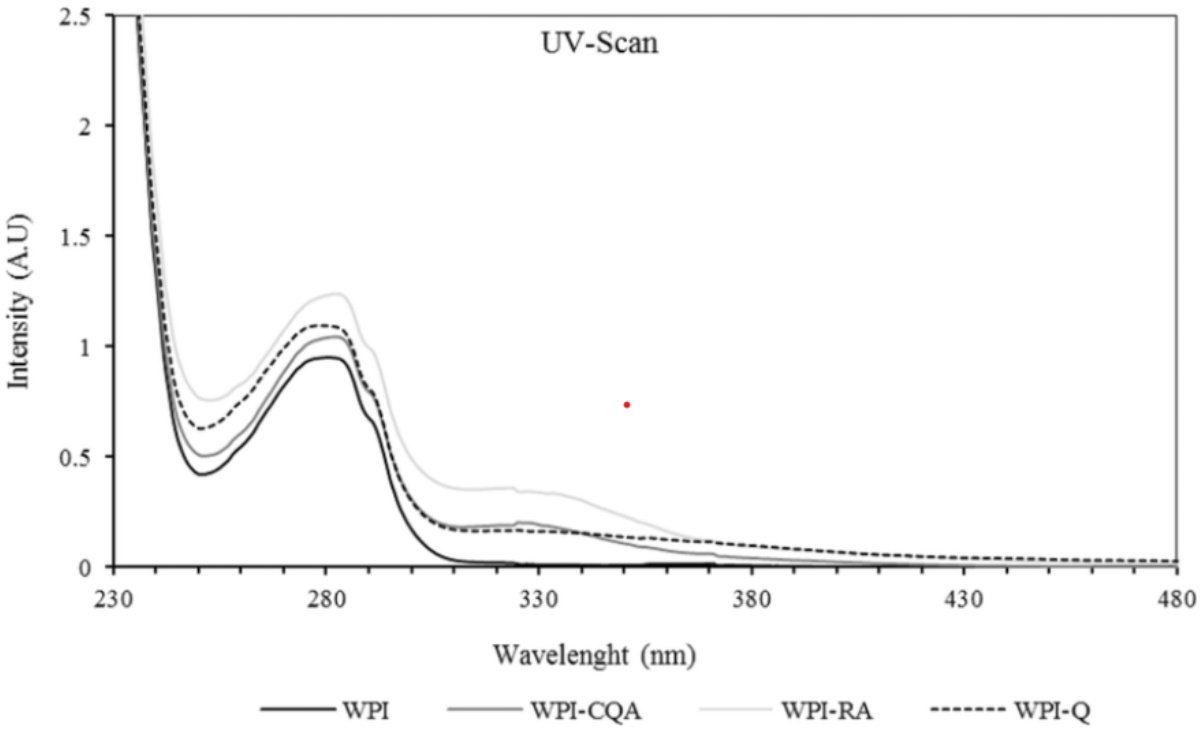

***Figure 13**: The change in the UV–Vis spectra of proteins. WPI: unmodified whey protein isolate (control), WPI-CQA: modified WPI with chlorogenic acid (CQA), WPI-RA: modified WPI with rosmarinic acid (RA) and WPI-Q: modified WPI with quercetin (Q) (Ali, 2019).*

1.7.2. Fluorescence spectroscopy

Fluorescence is defined as the emission of light by a substance that has absorbed light or other electromagnetic radiation, typically occurring almost instantaneously upon excitation. It is an optical technique used to detect fluorescent analytes (Liao et al., 2025). The fundamental principle of fluorescence involves the excitation of a molecule from its electronic ground state (S_0) to a higher energy singlet state (S_1 or S_2) upon absorption of light at a specific wavelength. Once in the excited state, the molecule is energetically unstable. It undergoes internal conversion and vibrational relaxation, dissipating part of the absorbed energy as heat to the surrounding environment. Eventually, the molecule returns to the ground state by emitting a photon, typically from the lowest excited singlet state (S_1), resulting in fluorescence (El Masry et al., 2015).

The fluorophores are typically fluorescent molecules that consist of multiple conjugated aromatic rings or linear and cyclic molecules with one or more conjugated bonds. They can be hydrophilic, hydrophobic, or even amphiphilic. Fluorescence studies of proteins are essential due to their wide range of biochemical applications in cellular systems. The intrinsic fluorescence

of proteins arises primarily from three aromatic amino acids: phenylalanine (Phe), tryptophan (Trp), and tyrosine (Tyr). Among them, tryptophan exhibits the highest sensitivity to changes in the local environment (Ghosh et al., 2016). Both tryptophan and tyrosine can be excited at a wavelength of 280 nm; however, for more selective excitation of tryptophan, a wavelength of 295 nm is often preferred. The main fluorescence parameters include the maximum fluorescence intensity (I_{max}) at specific excitation and emission wavelengths, as well as the maximum emission wavelength (λ_{max}), where the emission intensity reaches its maximum value. The emission spectra of these amino acids (Figure 14) can provide valuable insights into protein structural changes, particularly during denaturation processes (Turoverov & Kuznetsova, 1998).

Fluorescence spectroscopy is a fast and highly sensitive technique used to analyze molecular environments and interactions within various samples. It is favored for its exceptional sensitivity, strong specificity, simplicity, and relatively low cost compared to other analytical methods. Widely recognized as a powerful and versatile tool, fluorescence spectroscopy is applied across numerous fields, including environmental monitoring, industrial processes, medical diagnostics, DNA sequencing, forensic science, genetic analysis, and biotechnology. It serves as an important method for both qualitative and quantitative analysis. Despite all the advantages, the method has several limitations, including sensitivity to pH and buffer conditions, photobleaching from UV excitation, and interference from oxygen, iodide, or nitrogen oxides acting as quenchers. Additionally, it is not suitable for analyzing major sample components due to reduced accuracy at high concentrations, and its applicability is limited since not all compounds exhibit fluorescence (Bose Aswathy, 2018).

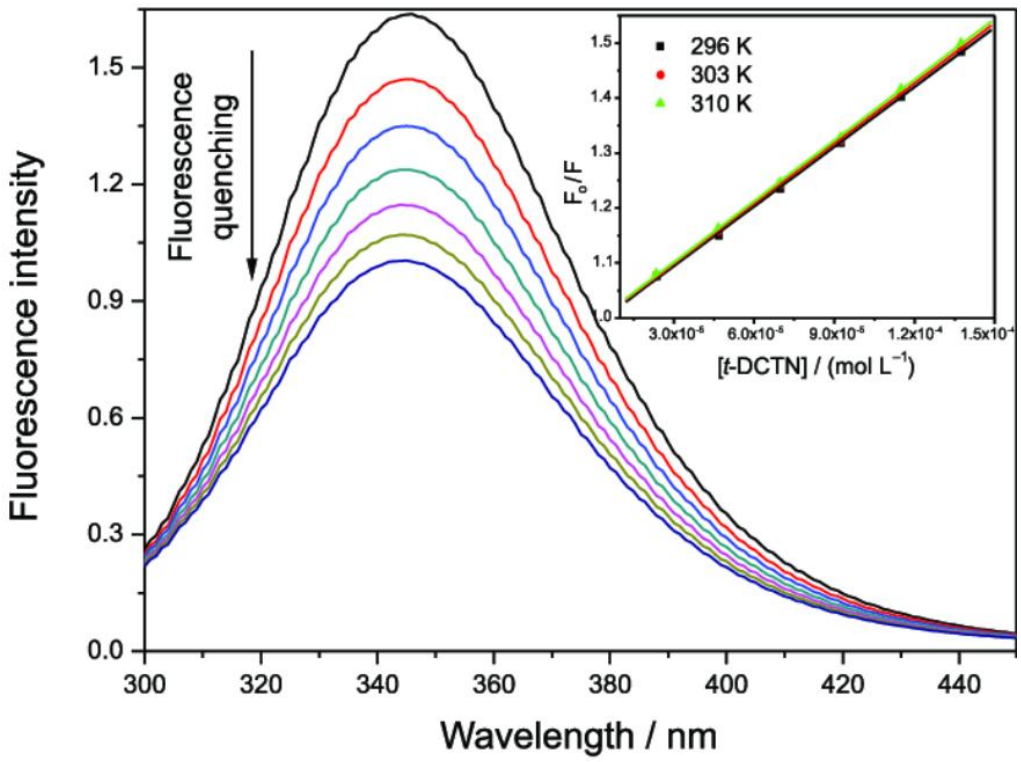

***Figure 14**: Fluorescence emission spectra of free bovine serum albumin (BSA) and its fluorescence quenching by addition of successive aliquots of 19-nor-clerodane diterpene (t-DCTN) (Chaves et al., 2016)*

1.7.3. Circular Dichroism

Circular dichroism (CD) spectroscopy is an optical technique that measures the differential absorption of left- and right-circularly polarized light by chiral chromophores, providing valuable insight into protein structure. It is extensively employed to assess protein secondary structure through electronic transitions in the far-UV region (approximately 170–240 nm), and to investigate tertiary structural features by analyzing the environment of aromatic residues in the near-UV region (approximately 260–300 nm). These measurements reflect changes in the protein's physical or chemical environment, amino acid sequence (including mutations), and intermolecular interactions.

Circular dichroism is an excellent method for determining the secondary structure of proteins. All amino acids, except glycine, are optically active due to their asymmetry. The peptide bond of the protein, its aromatic amino acids, as well as prosthetic groups in their structure, produce characteristic CD spectra in different regions. When the chromophores of the peptide backbone amides are aligned in arrays, their optical transitions shift or split into multiple transitions because of interactions. Consequently, different structural elements yield distinct CD spectra. For example, proteins with α-helices display negative bands

at 222 nm and 208 nm and a positive band at 193 nm, while proteins with well-defined antiparallel β-sheets show negative bands at 218 nm and positive bands at 195 nm (Figure 15). In contrast, disordered proteins exhibit very low ellipticity above 210 nm and negative bands near 195 nm (Greenfield, 2006).

Circular dichroism (CD) offers several advantages compared to high-resolution structural techniques such as X-ray crystallography, electron microscopy, and NMR spectroscopy. Notably, it requires relatively small amounts of sample and can be performed under experimental conditions—such as temperature, concentration, and buffer composition—that closely resemble those found in biological systems. These practical benefits have led to their widespread adoption in both the biochemical and structural biology fields, where they are used to complement data obtained from other biophysical methods. Additionally, CD spectroscopy is frequently employed in the pharmaceutical industry to evaluate proper protein folding, to monitor conformational changes resulting from ligand or protein interactions, and to assess protein stability in response to environmental factors such as pH or temperature shifts (Miles et al., 2021).

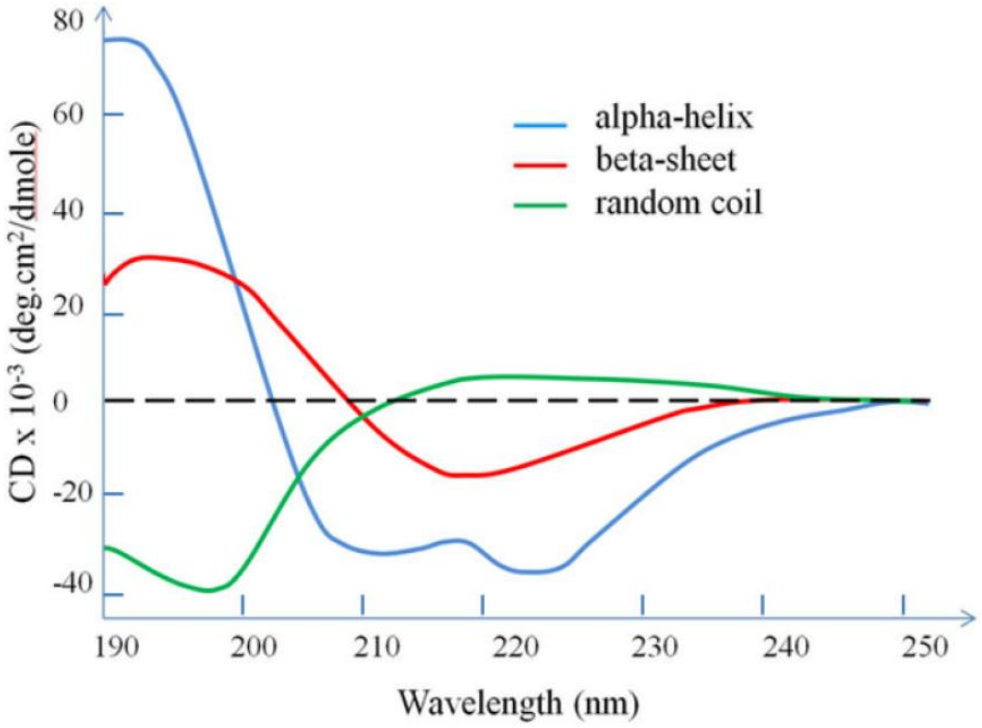

***Figure 15**: Standard CD spectra. Each of the three basic secondary structures of a polypeptide chain (α-helix, β-sheet and random coil) show a distinctly different characteristic CD spectrum* (Corrêa & Ramos, 2009)

2. Materials and methods

2.1. Materials

2.1.1. Enzymes-Proteins

- Lysozyme from chicken egg white (HEWL, SIGMA, 40,000 units/mg protein)
- α-Amylase from *Bacillus Licheniformis* (SIGMA, 500 units/mg protein)
- Bovine serum albumin (BSA Fraction V, SIGMA)

2.1.2. Substrates

- *Micrococcus lysodeikticus* (ATCC, SIGMA)
- Starch (Riedel)

2.1.3. Solvents and Aqueous Solutions

- Phosphate buffer solution, 50 mM
- Phosphate buffer solution 10 mM
- Acetone (MERCK)
- Double-distilled water (ddH_2O)

2.1.4. Other reagents

- Ammonia solution 25% (NH_3, MERCK)
- Coomassie brilliant blue (G250, SIGMA)
- Potassium Bromide (KBr, SIGMA)
- 3,5-Dinitrosalicylic acid (DNSA, SIGMA)
- Iron (II) chloride tetrahydrate 99+% ($FeCl_2$, Thermo Scientific)
- Iron (III) chloride hydrate >=97% ($FeCl_3$, Fisher Scientific)
- D-(+)-Maltose monohydrate 95% (Alfa Aesar)
- Graphite powder (<20 μg synthetic, Sigma-Aldrich)

2.1.5. Nanomaterials

The nanomaterials used in the present thesis were prepared at the Biotechnology laboratory of the Department of Biological Applications and Technologies and at the laboratories of the Department of Materials Science and Engineering of the University of Ioannina:

- Graphene oxide (GO)
- Biographene (bG)
- Magnetic biographene (bG-MNPs)

2.2. Methods

2.2.1. Synthesis of bio-graphene (bG)

Liquid exfoliation of graphite to produce bG was based on previous work (Alatzoglou et al., 2022). Briefly, 100 mg of graphite were added to 20 mL of ddH_2O. The suspension was ultrasonicated for 1 h (200 W, 10 kHz, pulse 50%). The process was stopped every 10 minutes, and the sample was placed on ice for a minute. The graphite flakes were partially exfoliated. In the next step, 96 mg of BSA were dissolved in 4 mL of ddH_2O, and then the protein solution was transferred to the graphite suspension. The graphite–protein mixture was stirred for 1 hour at room temperature. The unexfoliated graphite was separated by centrifugation at 500 rpm for 2 min, and the supernatant was collected carefully. In the following step, the supernatant was subjected to another centrifugation at 4,000 rpm for 10 minutes to remove excess BSA. After the centrifugation, the supernatant was discarded. Then, 1 mL of acetone was added to the precipitate, and the solution was left to dry at 50 °C.

2.2.2. Synthesis of magnetic bio-graphene (bG-MNPs)

The synthesis of bG-MNPs with ammonia was based on a previous work (Sun et al., 2015). Briefly, 25 mg of bG were suspended in 15 mL of ddH_2O, and 12.5 mg $FeCl_3$ and 75 mg $FeCl_2$ were dissolved in 10 mL of ddH_2O. Then, the bG suspension was transferred to a conical flask and heated to 50◦C. When the solution reached the desired temperature (50 °C), the iron salt solutions were added dropwise, under continuous magnetic stirring (final volume 25 mL). The pH of the mixture was adjusted to 10.0 by adding ammonia dropwise. After adjusting the pH, the mixture was left under continuous stirring at 50 °C for 30 minutes with

a continuous supply of nitrogen gas and sealed with parafilm. The suspension was centrifuged at 9,500 rpm for 15 minutes. The process was repeated 5 times. Finally, the precipitant dried at 37 °C.

2.2.3. Immobilization of enzymes on nanomaterials

2.2.3.1. Non-covalent immobilization of lysozyme on GO, bG, and bG-MNPs

Firstly, GO, bG, and bG-MNPs were dispersed in 4 mL of phosphate buffer (50 mM, pH 7.5, and final concentration of nanomaterial of 0.73 mg/mL) by ultrasound for 10 minutes. Then, 1 mL of lysozyme aqueous solution (15 mg/ml) was added to the nanomaterial suspension. The mixtures were incubated in a rotary shaking incubator at 180 rpm/min at 4 °C overnight for GO and bG, and at room temperature overnight for bG-MNPs suspension. The nanomaterial-enzyme conjugates were centrifuged at 9,000 rpm/min for 10 min, and the precipitates were dried at a speed vacuum concentrator.

2.2.3.2. Non-covalent immobilization of α-amylase in GO, bG, and bG-MNPs

Firstly, GO, bG, and bG-MNPs were dispersed in 4 mL in phosphate buffer (50 mM, pH 7.0, and final concentration of nanomaterial of 0.73 mg/mL) by ultrasound for 10 minutes. Then, 1 mL of α-amylase aqueous solution (3 mg/ml) was added to the nanomaterial suspension. The mixtures were incubated in a rotary shaking incubator at 180 rpm/min at 4 °C overnight for GO and bG, and at room temperature overnight for bG-MNPs suspension. The nanomaterial-enzyme conjugates were centrifuged at 9,000 rpm/min for 10 min, and the precipitates were dried at a speed vacuum concentrator.

2.2.4. Determination of enzyme immobilization efficiency on nanomaterials

The immobilization yield (%) was determined by analyzing the supernatants collected at the end of the immobilization process using the Bradford assay (Bradford, 1976). This colorimetric method quantifies protein concentration through the binding of Coomassie Brilliant Blue G-250 dye to amino acid residues of proteins. Upon binding, the dye undergoes a shift in its absorption maximum from 465 nm to 595 nm, enabling quantification of protein in the supernatant at 595 nm. In this way, the fraction of protein that remained un-immobilized was determined, allowing the calculation of the amount of immobilized enzyme. Protein quantification was performed using a standard calibration curve prepared with bovine serum albumin (BSA).

For the determination of enzyme immobilization yield on nanomaterials, the preserved supernatants from non-covalent immobilization experiments were analyzed. In 1.5 mL Eppendorf tubes, 200 μL of sample was mixed with 800 μL of Bradford reagent, resulting in a final reaction volume of 1 mL. Following a 10-minute incubation in the dark, the absorbance of each sample was recorded at 595 nm. All measurements were carried out in duplicate, and in each case, the corresponding blank samples (prepared without protein) were included.

Knowing the initial enzyme concentration in the final immobilization volume and the enzyme concentration in the supernatant determined by the Bradford assay, the immobilization yield (%) was calculated as:

$$\text{Immobilization yield (\%)} = \frac{\textit{Concentration before immobilization} - \textit{Supernatant concentration} * 100}{\textit{Concentration before immobilization}} \quad (1)$$

2.2.5. Determination of enzyme activity

2.2.5.1. Determination of enzyme activity of free lysozyme

The determination of the activity of free lysozyme was based on the hydrolysis of *Micrococcus Lysodeikticus*. In a 1 cm cuvette, phosphate buffer solution (50 mM, pH 7.5) and an appropriate aliquot of an aqueous solution of the substrate (final concentration of 0.06 mg/mL) were added. The reaction was initiated by the addition of free lysozyme (final concentration of 1 μg/mL). The enzymatic activity was monitored by recording the decrease in absorbance at 450 nm for a total amount of time of 5 min, at room temperature.

The effect of the presence of GO, bG, and bG-MNPs on the activity of lysozyme was also investigated. The experimental procedure was the same as that described above, with the difference that in the reaction medium, the nanomaterials were added at various final concentrations (2.5-100 μg/mL).

2.2.5.2. Determination of enzyme activity of immobilized lysozyme

The determination of the activity of immobilized lysozyme was based on the hydrolysis of *Micrococcus lysodeikticus*. The experimental procedure was the same as described in Section 2.5.1, with the difference that the final enzyme concentration was 25 μg/ml.

2.2.5.3. Determination of enzyme activity of free α-amylase

The determination of the activity of free a-amylase was based on the hydrolysis of starch. Firstly, a starch solution (2% w/v) was prepared using

phosphate buffer solution (50 mM, pH 7.0). The solution was transferred to a conical flask and heated to 100◦C, though not boiling, wrapped in aluminum foil, and under continuous magnetic stirring. After that, when the solution was completely dissolved, it was centrifuged at 4,000 rpm for 10 minutes. After centrifugation, only the supernatant was kept. Then an aqueous solution of α-amylase (10 μg/ml) was prepared. Continuing with the reaction, Eppendorf tubes of 1.5 mL and a final volume of 500 μL, were prepared, containing 450 μL of the starch solution. The reaction was initiated by the addition of free α-amylase (final concentration 1 μg/mL). The reaction time was 10 minutes, and the temperature was 50 °C. The reaction took place in a thermomixer. Then, 250 μl of DNSA reagent and 250 μl from the reaction solution were added to glass tubes. The samples were stirred and then boiled for 5 min. After boiling, the samples were left for a few minutes to come to room temperature, and then 2 mL of distilled water were added to each tube, stirred again and the absorbance was measured at 540nm.

The effect of the presence of GO, bG, and bG-MNPs on the activity of α-amylase was also investigated. The experimental procedure was the same as that described above, with the difference that in the reaction medium, the nanomaterials were added at various final concentrations (2.5-25 μg/mL).

2.2.5.4. Determination of enzyme activity of immobilized α-amylase

The determination of the activity of α-amylase was based on the hydrolysis of starch. Firstly, an amount of 0.5-1 mg of the immobilized enzyme was weighed into a 1.5 mL Eppendorf tube. Then, a stock solution of starch substrate was prepared as described in Section 2.5.3. One mL from the starch solution (2% w/v) was added to the Eppendorf tube containing the immobilized enzyme. The mixture was incubated in a thermomixer at 50 °C for 10 min and subsequently centrifuged at 12,000 rpm for 2 min. Afterward, 250 μL of DNSA reagent and 250 μL of the reaction supernatant were transferred into glass tubes. The samples were mixed and boiled for 5 min. Following boiling, the tubes were allowed to cool to room temperature, and next, 2 mL of distilled water were added to each tube. The mixtures were stirred again, and the absorbance was measured at 540 nm.

2.2.6. Determination of the Kinetic Parameters (Km and Vmax) of Free and Immobilized Lysozyme

For the determination of the kinetic parameters of lysozyme, hydrolysis reactions were carried out using different substrate concentrations. Specifically, the reaction medium consisted of phosphate buffer (50 mM, pH 7.5) and the substrate at various concentrations, ranging from 0.015 to 0.18 mg/mL. The reaction was initialized by the addition of lysozyme (at a final concentration of 1 μg/mL). The enzymatic activity was monitored by recording the decrease in

absorbance at 450 nm for a total amount of time of 5 min, at room temperature. One Unit (U) of lysozyme was defined as the reduction of the absorbance by 0.001 per minute.

The same process was performed for the immobilized lysozyme. The final concentration of the enzyme in these experiments was 25 μg/mL.

2.2.7. Study of the effect of pH and temperature on the activity of Free and Immobilized Lysozyme

To investigate the effect of pH on enzyme activity, hydrolysis reactions were carried out in reaction media with varying pH values (6.0-8.0). The procedure followed was the same as described above. The final substrate concentration was 0.06 mg/mL, while the final concentrations of free and immobilized enzymes were 1 μg/mL and 25 mg/mL, respectively.

To investigate the effect of temperature on enzyme activity, hydrolysis reactions were carried out in reaction media with varying temperature values (25-80 °C). The procedure followed was the same as described above. The final substrate concentration was 0.06 mg/mL, while the final concentrations of free and immobilized enzyme were 1 μg/mL and 25 mg/mL, respectively. The reaction medium was phosphate buffer (50 mM, pH 7.5).

2.2.8. Study of the Thermal Stability of Free and Immobilized Lysozyme

The thermal stability of free lysozyme was investigated at various temperatures (50, 60 °C) by measuring the remaining enzyme activity at pre-defined time intervals. Aqueous solutions of free lysozyme (final concentration of 0.1 mg/mL) in phosphate buffer (50 mM, pH 7.5) were incubated at the specified temperatures. At regular time intervals, an amount of the enzyme solution was transferred into quartz cuvettes containing the reaction buffer (phosphate buffer 50 mM, pH 7.5) and the substrate (final concentration of 0.06 mg/mL). The reaction volume was 1mL and the final enzyme concentration was 1 μg/mL. The reaction was monitored as described above. The stability of free lysozyme is expressed as the remaining activity (%) at each temperature, calculated according to the following equation (2):

$$\text{Remaining activity (\%)} = \frac{\textit{Activity at } t=i * 100\%}{\textit{Initial activity}} \quad (2)$$

The same procedure was performed for immobilized lysozyme, though the concentration of the enzyme solution was 1 mg/mL, and the final concentration was 25 μg/mL.

2.2.9. Spectroscopic techniques for determining the structure of enzymes

2.2.9.1. UV-Vis Spectroscopy

UV-Vis spectra of lysozyme (25 μg/mL) were recorded in phosphate buffer (50 mM, pH 7.5) on a UV-Vis spectrophotometer (Shimadzu, Tokyo, Japan) in the presence of GO, bG, and bG-MNPs (at a concentration range of 5–40 μg/mL). The spectra were recorded in the range of 200–350 nm at room temperature. For each sample, a baseline was recorded, whereas two full wavelength scans were averaged for each sample.

For α-amylase, the same procedure was performed, but the spectra were recorded in phosphate buffer, 50 mM, pH 7.0, and the enzyme concentration was 100 μg/mL.

2.2.9.2. Fluorescence spectroscopy

Fluorescence measurements were recorded on a luminescence spectrofluorometer Jasco-8300 (Tokyo, Japan), using a 1 cm path-length quartz cuvette. A nominal bandpass of 5 nm was used for both the excitation and emission rays. The fluorescence emission spectra of the enzymes were recorded from 300 to 400 nm after excitation at 280 nm, associated with the tryptophan residue. Both enzymes were added at a concentration of 10 μg/mL. The emission spectra were recorded in the presence of GO, bG, and bG-MNPs (at a concentration range of 2.5–100 μg/mL). All emission measurements were taken in 50 mM phosphate buffer, pH 7.5 for lysozyme and 50 mM phosphate buffer, pH 7.0, for α-amylase, at room temperature. For every scanned sample, a baseline was recorded and subtracted from the sample spectrum. Each spectrum was recorded twice.

2.2.9.3. Circular Dichroism (CD)

Circular dichroism (CD) measurements were performed at a Jasco J-1500 Circular Dichroism Spectrometer (Tokyo, Japan). The far-UV CD spectra (200–260 nm) of lysozyme were recorded by the addition of lysozyme (10 μg/mL) and GO or bG or bG-MNPS (at concentrations of 5 and 25 μg/mL) to the phosphate buffer (10 mM, pH 7.5). All spectra were obtained in a 1 cm quartz cuvette, with a 2 nm bandwidth and a scan rate of 50 nm/min. For every sample, a baseline was recorded and subtracted from the protein spectrum, whereas at least two scans were averaged for each sample. The secondary structure content of lysozyme was

estimated by implementing the K2D algorithm on the DichroWeb server (Whitmore & Wallace, 2004).

For α-amylase, the same procedure was performed, but the spectra were recorded in 10 mM phosphate buffer, pH 7.0.

2.2.10. Reuse of immobilized enzymes

2.2.10.1. Reuse of immobilized α-amylase

For the reuse of α-amylase, an amount of 0.5-1 mg of the immobilized enzyme was weighed into a 1.5 mL Eppendorf tube. Then, a stock solution of starch substrate was prepared as described in Section 2.5.2. One mL from the starch solution (2% w/v) was added to the Eppendorf tube containing the immobilized enzyme. The mixture was incubated in a thermomixer at 50 °C for 10 min and subsequently centrifuged at 12,000 rpm for 2 min. Afterward, 250 µL of DNSA reagent and 250 µL of the reaction supernatant were transferred into glass tubes. The samples were mixed and boiled for 5 min. Following boiling, the tubes were allowed to cool to room temperature, and next, 2 mL of distilled water were added to each tube. The mixtures were stirred again, and the absorbance was measured at 540 nm.

3. Results and Discussion

3.1. Lysozyme

3.1.1. Effect of the presence of nanomaterials on the activity of free lysozyme

The effect of nanomaterials on the activity of free lysozyme was studied as described in Section 2.2.5, for material concentrations ranging from 2.5 to 100 μg/ml. The nanomaterials used were graphene oxide (GO), biographene (bG), and biographene magnetic nanoparticles (bG-MNPs). The results are presented in Graph 3.1. In each case, 100% corresponds to the maximum activity exhibited by the enzyme in the absence of nanomaterials.

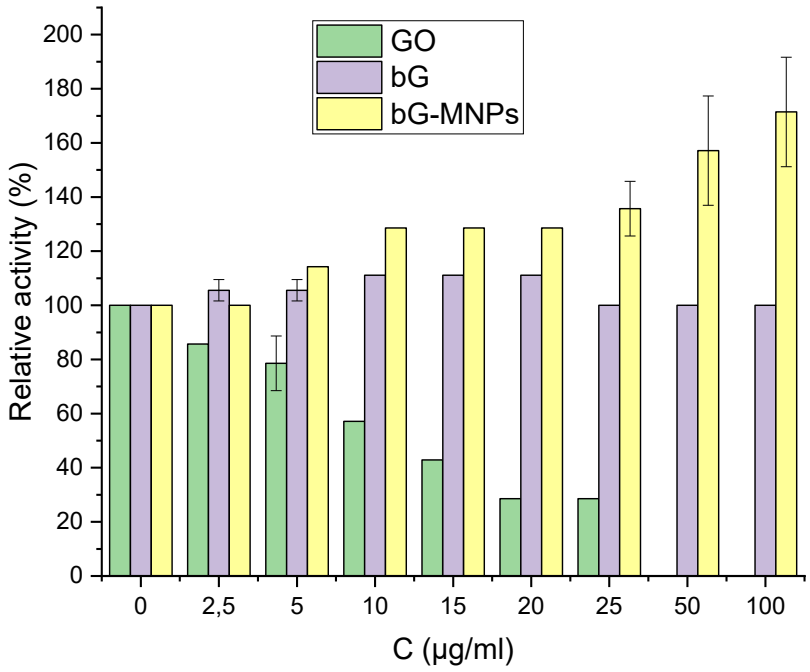

Graph 3.1. *Effect of the presence of nanomaterials on the activity of free lysozyme.*

From Graph 3.1, regarding the effect of GO on lysozyme activity, it is observed that this specific nanomaterial negatively affects the enzyme's activity. Moreover, this effect is dose-dependent; as the concentration of GO increases, the activity of lysozyme decreases. According to the literature, in a similar experiment investigating the interaction between lysozyme and GO, Bai et al., 2017 showed that lysozyme activity is significantly reduced in the presence of GO due to strong adsorption and direct interactions between the enzyme and the GO surface. GO exhibits high adsorption capacity for lysozyme, driven by multiple interactions, including π–π stacking, electrostatic forces, hydrogen bonding,

hydrophobic interactions, and van der Waals forces. These interactions can induce structural changes in lysozyme or block its active site, leading to the formation of lysozyme-GO complexes. Furthermore, the oxidized nature of GO allows it to bind near or at the catalytic site of lysozyme, directly inhibiting enzymatic activity. However, another factor that should be considered is the strong cytotoxicity of GO. This could lead to the destruction of the substrate's cells and, consequently, to a decrease in the reaction rate (B. Li et al., 2022).

In the case of bG, no decrease in lysozyme activity was observed. This is likely because bG is modified with the biological molecule albumin (BSA), which makes it more biocompatible and less cytotoxic than chemically modified GO (Papanikolaou et al., 2023). The interactions between the nanomaterial surface and lysozyme may be influenced by the presence of albumin, reducing both the negative interactions between the graphene sheets and the enzyme, as well as the interactions between bG and the cells of the substrate.

Last, the observed increase in lysozyme activity in the presence of magnetic biographene (bG-MNPs) is consistent with previous studies reporting that Fe_2O_3 nanoparticles enhance the enzyme's structural stability (Shareghi et al., 2015). Specifically, the nanoparticles were found to change the structure of lysozyme, and the enzyme appears to have a structural arrangement that enhances enzymatic efficiency, leading to higher activity compared to free enzyme.

3.1.2. Lysozyme immobilization efficiency on nanomaterials

The immobilization of lysozyme on the nanomaterials was achieved through physical adsorption, and in each case, the immobilization efficiency was calculated as described in Section 2.2.4. The results are presented in Table 3.1.

Table 3.1. *Immobilization efficiency of lysozyme on nanomaterials*.

Nanomaterial	Immobilization yield
GO	96.9% ± 1.6%
bG	98.3% ± 0.1%
bG-MNPs	94.0% ± 0.9%

The high immobilization efficiency of lysozyme on GO can be attributed to the strong and specific interactions between the protein and the oxygen-containing functional groups of GO. As reported by S. Li et al., (2014), GO exhibits remarkable affinity toward lysozyme, achieving adsorption efficiencies of around 96%. This strong binding is driven by a combination of electrostatic interactions

between the positively charged lysozyme (isoelectric point ≈ 11) and the negatively charged GO surface, as well as hydrogen bonding and hydrophobic interactions. Similarly, Tiwari et al., 2023 demonstrated that lysozyme forms stable complexes with GO sheets, with adsorption strength increasing in GO samples with high oxygen content, suggesting that surface chemistry plays a critical role in protein binding. These findings corroborate the high immobilization efficiency observed herein, attributable to the abundant active sites provided by the functional groups and large surface area of GO, which facilitate stable lysozyme attachment.

The high immobilization efficiency of lysozyme on bG, observed in this work, can be explained by the unique surface properties imparted by the green synthesis process. During exfoliation, BSA not only facilitates the dispersion of graphene sheets in water but also functionalizes their surfaces with protein-derived groups such as carboxyl, amine, and hydroxyl moieties (Pattammattel & Kumar, 2015b); Thomas et al., 2018). These functionalities enhance the hydrophilicity and biocompatibility of the graphene surface, promoting strong electrostatic and hydrogen-bond interactions with lysozyme, which carries a net positive charge near neutral pH. Furthermore, the large surface area of few-layer bG provides numerous adsorption sites, leading to efficient enzyme attachment. As demonstrated in related studies (Alatzoglou et al., 2022), enzymes such as glucose oxidase, horseradish peroxidase, and β-glucosidase have beem successfully immobilized onto few-layer bG.

As for the immobilization efficiency on bG-MNPs, this may be due to the synergistic effect between the magnetic core of the formed iron oxide nanoparticles and the bioactive graphene coating. MNPs synthesized by chemical co-precipitation with ammonia provide abundant hydroxyl and iron oxide sites that promote strong attachment of the graphene layer (W. Wu et al., 2008). Also, in their recent work, Alatzoglou et al. (2025), used a similar magnetic bio-graphene for the co-immobilization of cellulase and β-glucosidase, which was found to serve as an excellent immobilization matrix. Last, as mentioned before, bG contributes reactive and biocompatible surface groups that favor enzyme adsorption. Together, these features enable multiple interactions with lysozyme and facilitate stable, high-capacity binding.

3.1.3. Determination of lysozyme activity

Having determined the immobilization rate of lysozyme, the enzymatic activity was subsequently calculated, as described in Section 2.2.5. According to the literature, 1 Unit corresponds to a decrease of 0.001 in absorbance at 450 nm per minute (Cerón et al., 2023). Based on the above data, the results obtained are presented in Table 3.2.

Table 3.2. *Specific activity of free and immobilized lysozyme.*

Enzyme	Enzyme activity *10^4 (U/mg)
Free lysozyme	4.20 ± 0.00
Lysozyme - GO	0.22 ± 0.03
Lysozyme- bG	0.18 ± 0.01
Lysozyme- bG-MNPs	0.12 ± 0.00

As can be observed from Table 3.2, the specific enzyme activity decreases upon immobilization, regardless of the nanomaterial used as a matrix. Immobilization through physical adsorption relies on non-specific interactions between the enzyme and the nanomaterial surface and occurs through weak forces that depend on the surface chemistry of the nanocarrier and the type of amino acids that are present on the surface of the enzymes. These interactions can induce conformational changes in the enzyme structure, potentially affecting the integrity of the active site and leading to partial unfolding or denaturation. Consequently, such structural alterations often result in reduced catalytic activity, with the extent of activity loss depending on the compatibility between the enzyme and the nanocarrier (Gkantzou et al., 2021).

For GO, enzymatic activity decreased by 19-fold compared to the free enzyme. According to Bai et al. (2017), the decrease in lysozyme activity after immobilization on GO is mainly caused by strong electrostatic and hydrogen-bonding interactions between the enzyme and the oxygen-containing groups on the GO surface. These interactions can induce conformational alterations and partial unfolding of the lysozyme structure, particularly around the active site, which reduces substrate accessibility and catalytic efficiency. Also, fluorescence microscopy experiments demonstrated that GO binds near the active site of lysozyme, specifically near the residues Trp62 and Trp108, which play an important role in enzyme–substrate binding (Bera et al., 2018). A similar decrease in enzyme-specific activity was observed when the other two nanomaterials were used. However, previous studies have shown that, although immobilization often leads to reduced bioactivity when the enzyme interacts too strongly with the support material, it usually enhances enzyme stability and allows for repeated use (Anastas et al., 2021).

3.1.4. Kinetic Parameters (K_m and V_{max}) of free and immobilized lysozyme

The Michaelis constant (K_m) represents the substrate concentration at which the reaction rate reaches half of its maximum velocity, indicating the enzyme's affinity for its substrate, while the maximum velocity (V_{max}) corresponds to the rate achieved when the enzyme is fully saturated with substrate. These kinetic parameters are fundamental for characterizing enzyme activity and

efficiency under various conditions (McDonald & Tipton, 2022). The results showing the apparent K_m and V_{max} for free and immobilized lysozyme are presented in Table 3.3, while the respective Michaelis-Menten Graphs are presented in Graphs A1-A4 in the Appendix.

Table 3.3. *Apparent Kinetic parameters of free and immobilized lysozyme.*

Enzyme	K_m (µg/ml)	V_{max} *10^4 (U/mg)
Free Lysozyme	59.32±15.01	7.70 ±0.87
Lysozyme-GO	85.31±20.32	0.47±0.05
Lysozyme-bG	58.83±7.23	0.34 ±0.01
Lysozyme-bG-MNPs	23.53±7.98	0.15±0.01

As expected, the apparent K_m and V_{max} were significantly affected after immobilization of lysozyme. For lysozyme immobilized on GO, a higher K_m value was observed in comparison with that of the free form of the enzyme. This indicates that the immobilized enzyme has a lower affinity for the substrate. This effect may result from limitations in mass transfer or substrate diffusion, or from reduced enzyme flexibility that is required for effective substrate binding (W. Li et al., 2016). Many common nanomaterials, such as GO or inorganic carriers, exhibit increased K_m values due to steric hindrance, restricted enzyme conformations, or diffusion limitations (M. R. Khan, 2021).

In the case of bG, the apparent K_m was not affected after immobilization. This observation indicates that the enzyme's apparent affinity for its substrate has not changed due to immobilization. The immobilization process probably did not alter the active site structure or intrinsic catalytic mechanism.

Interestingly, in the case of bG-MNPs, it was observed that lysozyme exhibited a decrease in apparent K_m compared to the free enzyme. This behavior suggests enhanced substrate accessibility or increased local substrate concentration near the immobilized enzyme, likely due to favorable enzyme orientation and biofunctionalized surface chemistry (Singh et al., 2025). Although many studies report increased K_m for immobilized enzymes, few previous studies have shown a decrease in K_m when enzymes are immobilized on bio-functionalized or nanocomposite supports that promote favorable substrate interaction or enzyme orientation. For example, Monajati et al. (2024), showed lower K_m for L-asparaginase immobilized on biofunctionalized magnetic graphene oxide nanocomposites and Shokoohizadeh et al. (2022), showed similar results after immobilizing IMP-1 metallo-beta-lactamase on magnetic silica nanoparticles.

In all three cases, the apparent V_{max} for the immobilized enzymes was lower than that of the free form, attributed to several factors such as enzyme conformational change induced by the support and diffusional limitation imposed

on the flow of substrate (J.-F. Liu et al., 2012). V_{max} often decreases because fewer active sites are available or because there is mass transfer resistance. The restricted substrate diffusion limit's reaction rates while conformational shifts induced by support materials stabilize favorable active site geometries for binding but hinder product release or enzyme flexibility. (Cerón et al., 2023).

Finally, it is worth noting that in the case of bG-MNPs, there was a decrease in both apparent constants (K_m and V_{max}). Due to the slower diffusion of the substrate to the active site of the enzyme, the apparent V_{max} is decreased, while at the same time the local concentration of the substrate is increased, resulting in the observed decrease in the apparent K_m. Moreover, it could be possible that although immobilization stabilizes the active sites of the enzymes, the support could hinder product release or enzyme flexibility.

3.1.5. Effect of pH on the activity of free and immobilized lysozyme

The effect of pH in the activity of free and immobilized lysozyme was investigated through the hydrolysis of the substrate *Micrococcus lysodeikticus*, as described in Section 2.2.7. In each case, 100% corresponds to the maximum activity exhibited by the enzyme. The results are presented in Graph 3.2.

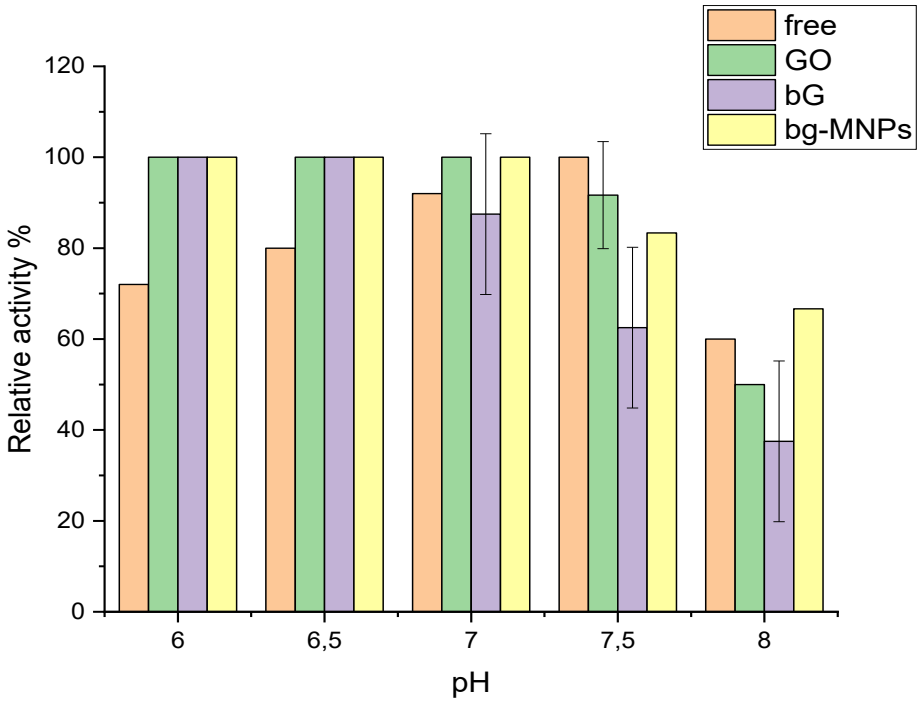

Graph 3.2. *Relative activity of free and immobilized lysozyme at different pH values.*

As observed in Graph 3.2, the optimal activity of free lysozyme occurs at pH 7.5. It is also evident that free lysozyme retains a significant portion of its activity at acidic pH values, whereas under more alkaline conditions, the enzyme's rate decreases. This finding is supported by the literature, which reports that lysozyme remains more stable near pH 7.0, while its activity decreases at more acidic or alkaline values (Li et al., 2022).

When lysozyme is immobilized on GO, the pH effect is different compared to free lysozyme. Specifically, lysozyme retains a greater proportion of its activity at acidic pH values after immobilization compared to the free enzyme. In general, immobilization can often lead to modifications in enzymatic activity that depend on pH. According to the literature, this is likely due to the reduction of the positive charge of lysozyme upon interaction with GO, which is negatively charged. Consequently, the dependence of enzyme activity on pH is altered (Bera et al., 2018).

The pH activity of immobilized lysozyme on bG is similar to that of GO. The enzyme has greater activity in more acidic pH values. At pH 6–6.5, the enzyme retains a strong net positive charge (pI~ 11.0) and the bG surface carries a net negative charge (BSA pI~ 5.3) (Alatzoglou et al., 2023). Thus, the electrostatic attractive forces are moderate and stabilize the enzyme in a favorable conformation with good substrate access. At higher pH values (7.0–8.0), although the enzyme remains positively charged, its net charge magnitude decreases and at the same time, the negative charge density on the support may increase, strengthening the enzyme-surface interaction. This stronger binding may restrict conformational flexibility or obstruct substrate access, thereby reducing catalytic activity (Li et al.,2014). Moreover, molecular dynamics and adsorption studies show that lysozyme binding to graphene–type surfaces can induce changes in enzyme mobility and binding free energy (Anastas et al., 2021).

For the bG-MMPs, similar results are observed. In their work, Shareghi et al. (2015) mentioned that the adsorption of lysozyme on MNPs offers several advantages, but the stability of the adsorbed layer is typically much weaker than in covalently bound systems, and detachment of the ligand resulting from changes in temperature, pH, or ionic strength is often observed. Lysozyme immobilized in bG-MNPs, has higher relative activity under more alkaline conditions (pH 8.0), than any other case. This is probably because the free lysozyme reacts directly with the substrate in a soluble manner, while the groups of the immobilized carrier affect the proton microenvironment near lysozyme. Similar results have been observed by Yu et al., (2022), who studied the immobilization of lipase on magnetic GO.

3.1.6. Effect of Temperature on the activity of free and immobilized lysozyme

The effect of temperature on the activity of free and immobilized lysozyme was investigated through the hydrolysis of the substrate *Micrococcus lysodeikticus*, as described in Section 2.2.7. In each case, 100% corresponds to the maximum activity exhibited by the enzyme. The results are presented in Graph 3.3, and the individual graphs for better clarity are presented in Graphs B1-B4 in Appendix.

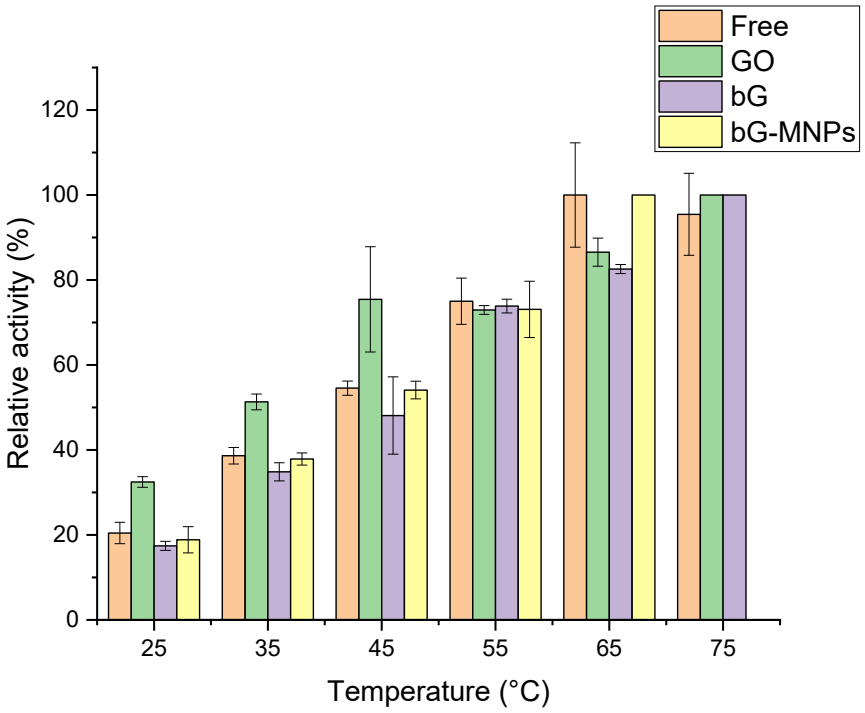

Graph 3.3. *Relative activity of free and immobilized lysozyme at different temperatures.*

As shown in Graph 3.3, the reaction rate of free lysozyme increases with rising temperature, reaching its maximum at 65 °C. However, a further increase in temperature leads to a decline in the reaction rate. According to literature, at temperatures over 65°C, lysozyme loses its catalytic activity primarily due to thermal denaturation, which disrupts its native α-helical structure and alters the geometry of the active site. The breakdown of intramolecular hydrogen bonds and disulfide bridges leads to protein unfolding and aggregation, preventing the enzyme from properly binding to its substrate and thereby eliminating its biological function (Kundu et al., 2016; Meersman et al., 2010).

The reaction rate of immobilized lysozyme on GO reaches its maximum activity at 75 °C. That can be attributed to the combined effects of enhanced substrate accessibility and favorable interfacial interactions. The elevated

temperature facilitates molecular diffusion and reaction kinetics, while the GO support helps preserve the enzyme's active conformation by restricting large-scale unfolding. These synergistic effects result in higher apparent catalytic activity compared to the free enzyme under the same conditions (Bolibok et al., 2017; Hermanová et al., 2015).

For immobilized lysozyme on bG and bG-MNPs the highest activity of the enzyme occurs at 75°C and 70°C, respectively. It can be mentioned that immobilization can alter the optimal temperature and broaden the temperature activity profile, due to changes in the enzyme microenvironment and support interactions (Khan et al., 2021).

3.1.7. Thermal Stability of free and immobilized lysozyme

The thermal stability of free and immobilized lysozyme was investigated through the hydrolysis of the substrate *Micrococcus lysodeikticus*, as described in Section 2.2.8. In each case, 100% corresponds to the activity at t=0. The results are presented in Graphs 3.4 and 3.5.

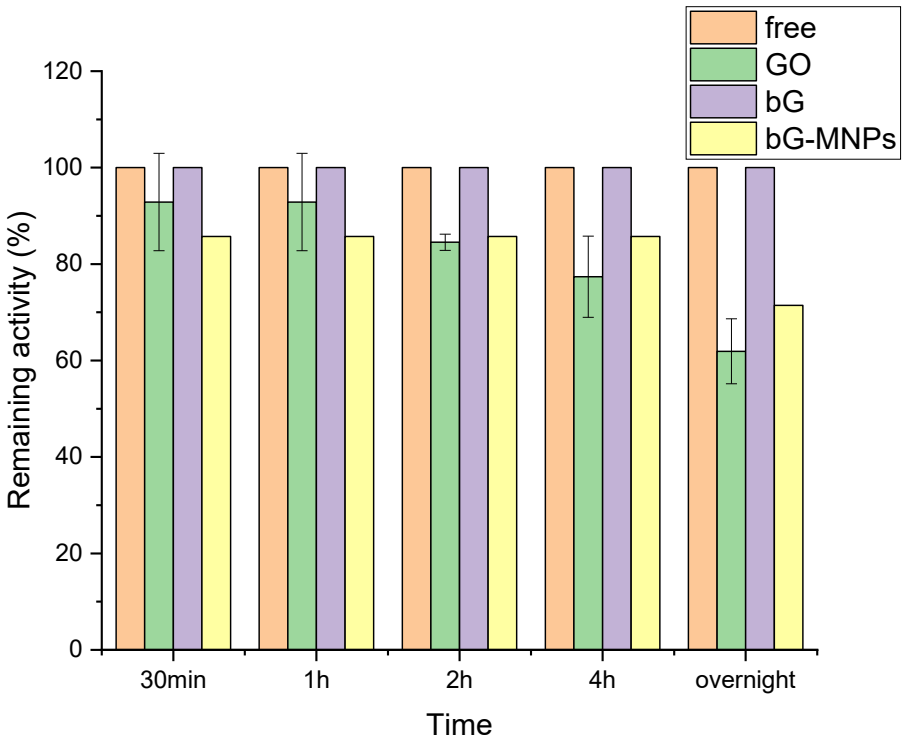

Graph 3.4. *Stability of free and immobilized lysozyme after incubation at 50 °C.*

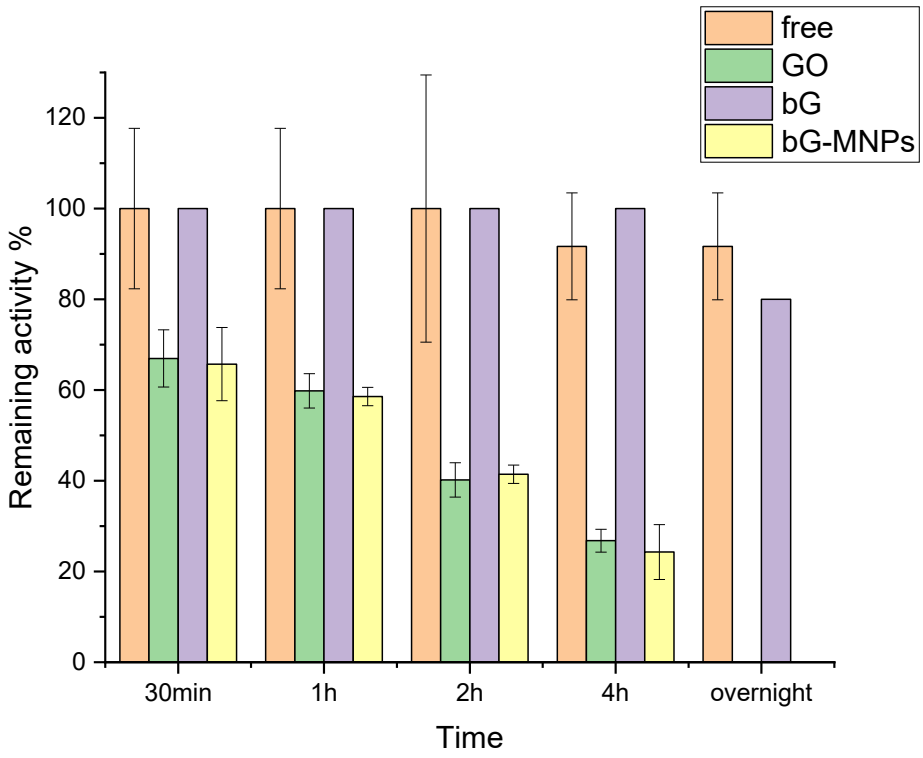

Graph 3.5. *Stability of free and immobilized lysozyme after incubation at 60 °C.*

According to the results, free lysozyme presents overall better thermal stability than the immobilized formed. After overnight incubation at 50 °C, immobilized lysozyme on GO retains 65% of its initial activity. Several studies have shown that immobilization of lysozyme on GO can alter its structural stability due to interactions between the enzyme and the oxygen-containing surface groups of GO, which may partially disrupt the native conformation (Li et al., 2014; Bai et al., 2017). Consistent with these findings, Bera et al. (2018) observed a decrease in Tm for the lysozyme-GO complex (46.2 ± 0.2 °C) compared to the free enzyme (71.2 ± 0.2 °C), suggesting reduced thermostability.

On the contrary, when lysozyme is immobilized on bG, it preserves its initial activity after overnight incubation at 50 °C and it retains 80% of its initial activity after overnight incubation at 60 °C. A possible explanation is that the BSA layer likely acts as a biocompatible interface, minimizing direct disruptive interactions between lysozyme and the graphene surface, thereby preserving enzyme structure at moderate temperatures.

Lastly, immobilized lysozyme on bG-MNPs presents a similar result to immobilized lysozyme on GO. Although the immobilized enzymes lose some of their initial activity after 24 hours of incubation, it still preserves its catalytic capacity up to 72% after overnight incubation at 50 °C.

3.1.8. Spectroscopic techniques for determining the structure of lysozyme

3.1.8.1. UV-Vis Spectroscopy

UV–Vis spectroscopy was employed to investigate the absorbance characteristics of the enzyme, with particular attention to the peak observed around 280 nm. This wavelength is characteristic of the aromatic amino acid residues, mainly tryptophan and tyrosine, and is commonly used to evaluate protein concentration and structural integrity. The UV-Vis spectra of lysozyme, were studied in the absence and in the presence of different concentrations of nanomaterials (5-40 μg/mL), as described in Section 2.2.9.1. The results are presented in Graphs 3.6-3.8.

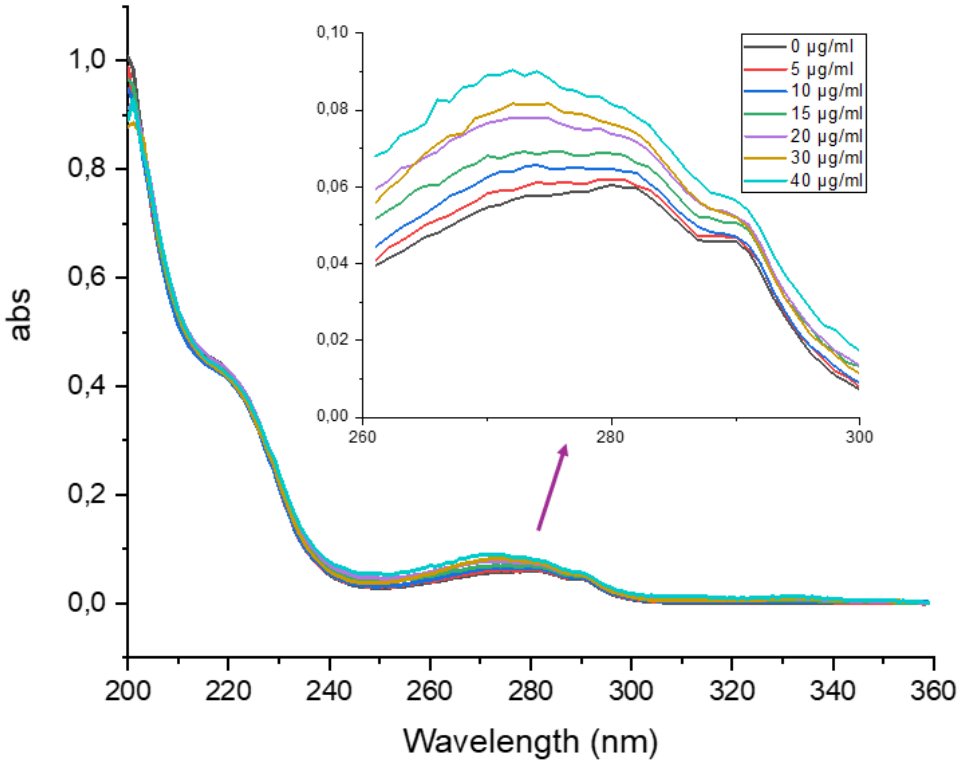

Graph 3.6. *UV-Vis spectra of Lysozyme (25 μg/ml) in the presence of GO.*

As observed from Graph 3.6, the absorbance at 280 nm increases with the increase of GO concentration. GO contains abundant oxygen-based functional groups that interact strongly with proteins through electrostatic attraction. These interactions partially unfold lysozyme, exposing aromatic residues like tryptophan and tyrosine, which increases absorbance at 280 nm. This increase indicates that GO interacted with the aromatic amino acids and changed the structure of lysozyme. Moreover, these interactions between GO and lysozyme can increase the transition energy of aromatic residues, causing a shift of the adsorption band

to lower wavelengths, as depicted in the inserted graph. In their studies, Bai et al. (2017) and Li et al. (2022) have presented similar results.

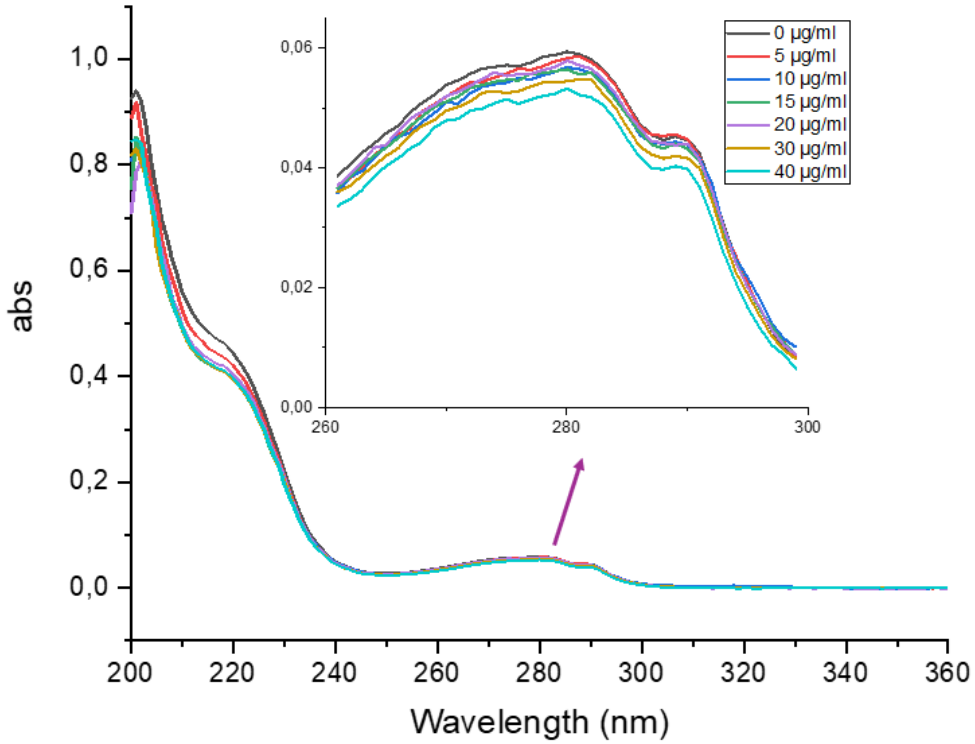

Graph 3.7. *UV-Vis spectra of lysozyme (25 μg/ml) in the presence of bG.*

As observed from Graph 3.7, in the case of bG, the absorbance at 280 nm decreased in the presence of this nanomaterial. An explanation for this might be that, since the graphene sheets are coated with BSA, the direct interaction with lysozyme is reduced. As a result, lysozyme experiences only mild adsorption and partial shielding of its aromatic residues, leading to a decrease in its absorbance.

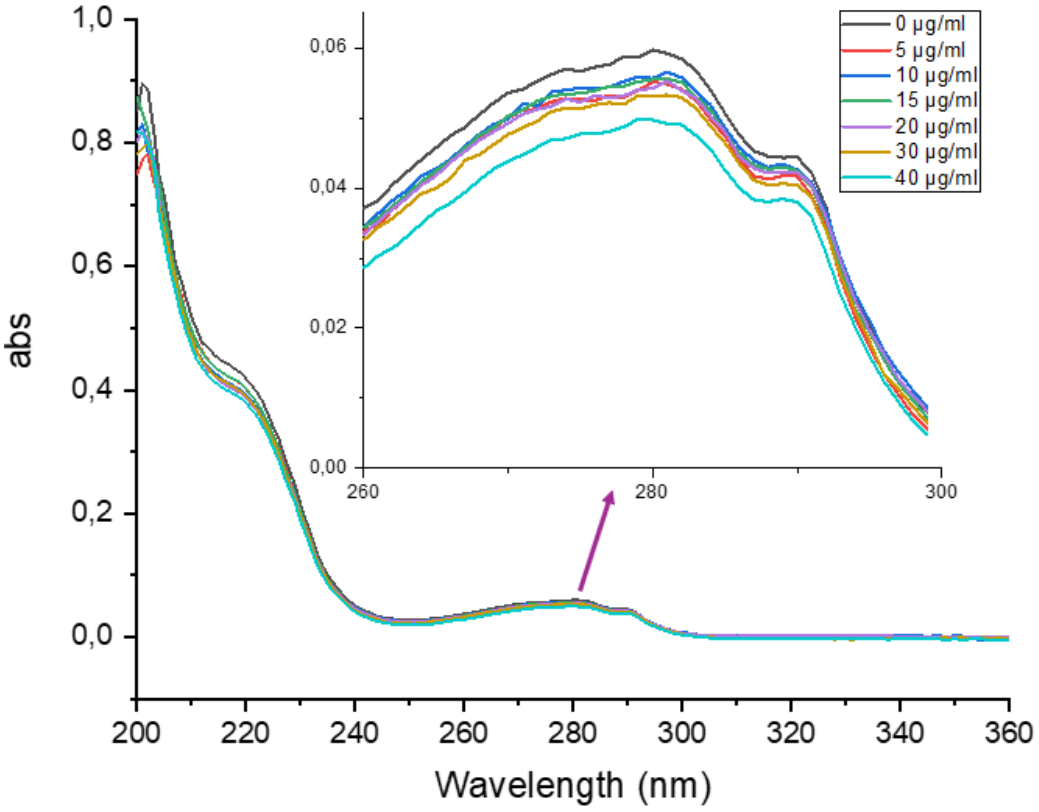

Graph 3.8. *UV-Vis spectra of lysozyme (25 µg/ml) in the presence of bG-MNPs.*

According to Graph 3.8, the absorbance of lysozyme slightly decreases in the presence of bG-MNPs. These results contrast with literature reports, where the absorbance of lysozyme near 280 nm increases in the presence of Fe_2O_3 NPs due to strong electrostatic attraction and formation of a ground-state complex with a higher extinction coefficient (Shareghi et al., 2016). In our case, the surface of bG likely reduces the direct interaction between positively charged lysozyme and negatively charged MNPs. This shielding effect prevents the strong adsorption and partial unfolding observed for uncoated metal oxides, resulting instead in a mild hypochromic shift rather than the hyperchromic response reported for bare Fe_2O_3 NPs.

3.1.8.2. Fluorescence spectroscopy

Fluorescence spectroscopy provides sensitive insight into protein–nanoparticle interactions. In this thesis, the technique is applied to examine the photophysical behavior of lysozyme, with emphasis on changes in emission intensity, spectral shifts, and quenching effects. The results outline how nanomaterials influence the fluorescent properties of lysozyme and contribute to a clearer understanding of protein–nanomaterial interactions. The fluorescence spectrum of lysozyme was recorded in the absence and presence of different

concentrations of nanomaterials (5-50 μg/mL), as described in Section 2.2.9.2. The results are presented in Graphs 3.9-3.11.

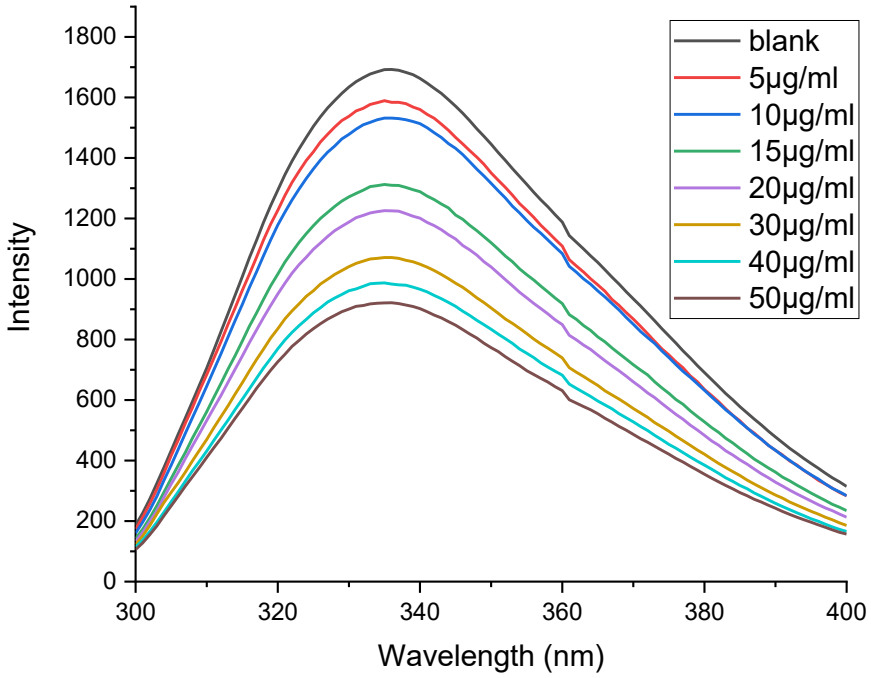

Graph 3.9. *Fluorescence emission spectra of lysozyme (10 μg/ml) in the presence of GO.*

As observed from Graph 3.9, the fluorescence intensity of lysozyme gradually decreases with the increase of GO concentration, while no shift in the emission wavelength is observed. In the work of Bai et al. (2017), it is mentioned that GO only influences the Trp residues. The intrinsic fluorescence quenching suggests that incubation with GO causes partial unfolding of the protein, which increases the exposure of Trp residues to the aqueous environment. Because Trp62 and Trp63 are located near the active site, changes in their local environment may alter the structure of the active site and ultimately reduce the enzyme's activity. These results support that GO induces conformational changes to lysozyme, in agreement with results obtained from the UV-Vis analysis. These results agree with other similar studies in literature (Bera et al., 2018; Li et al., 2022).

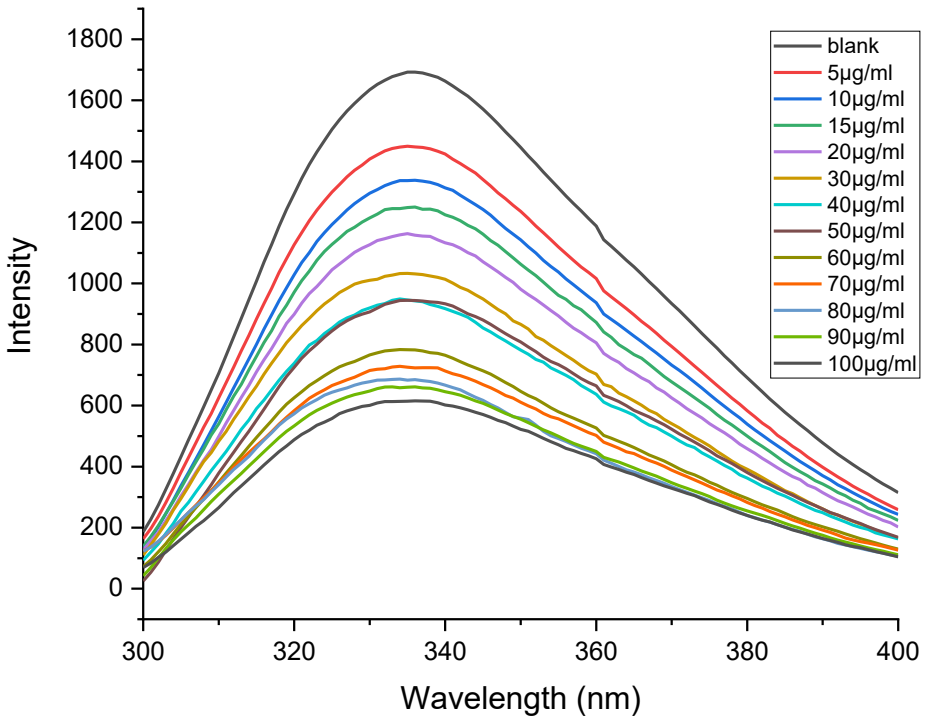

Graph 3.10: Fluorescence emission spectra of lysozyme (10 μg/ml) in the presence of bG.

From Graph 3.10, it can be observed that the fluorescence intensity of lysozyme gradually decreases with the increase of bG concentration, while no shift in the emission wavelength is observed. The decrease in the intensity probably suggests that bG interacts in a way that alters the local environment surrounding the Trp residues. However, the quenching effect of bG is lower than that of GO. When GO is used at a concentration of 50 μg/mL, the fluorescence intensity of lysozyme decreases at 20.7%, while when bG is used at a concentration of 100 μg/mL (2-fold), the residual fluorescence intensity of lysozyme is preserved at 36.3% (see Appendix Graphs C1 and C2, indicating that higher concentrations of this nanomaterials are needed to achieve similar quenching effect as GO.

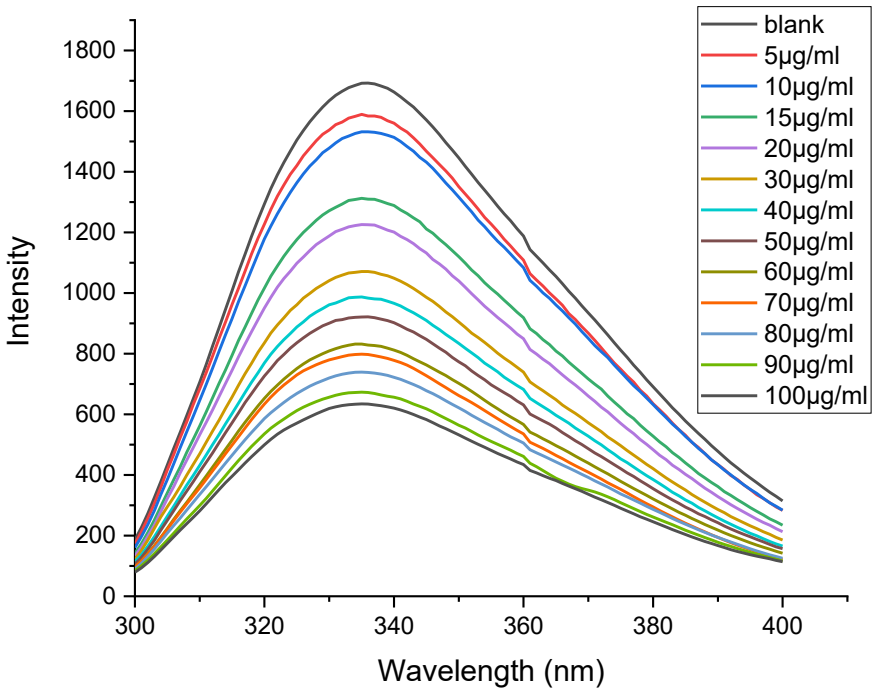

Graph 3.11. *Fluorescence emission spectra of lysozyme (10 μg/ml) in the presence of bG-MNPs.*

As seen from Graph 3.11, the increasing concentrations of bG-MNPs affect the fluorescence intensity of lysozyme. However, in this case too, the quenching effect of this nanomaterial is lower than that of GO. When GO is used at a concentration of 50 μg/mL, the fluorescence intensity of lysozyme decreases at 20.7%, while when bG-MNPs is used at a concentration of 100 μg/mL (2-fold), the residual fluorescence intensity of lysozyme is preserved at 37.5% (see Appendix, Graph C3). The quenching effect of bG-MNPs is similar to that of bG, indicating that the biologically exfoliated graphite preserves the tertiary structure of lysozyme to a greater extent than the chemically synthesized GO.

To deepen our understanding of the changes in the tertiary structure of lysozyme in the presence of the nanomaterials, the Stern–Volmer (K_{sv}) constants, which describe the quenching rate, were also determined, and they are presented in Graph 3.12. The Stern–Volmer equation relates the decrease in fluorescence intensity to the concentration of a collisional quencher, in our case, the nanomaterials, and is described by Equation (3):

$$F_0/F=1+Ksv[Q] \quad (3)$$

where F_0 and F are the fluorescence intensity in the absence and in the presence of the quenching agent, respectively, [Q] is the concentration of the quenching agent, and K_{sv} is the Stern–Volmer quenching constant (Gehlen, 2020).

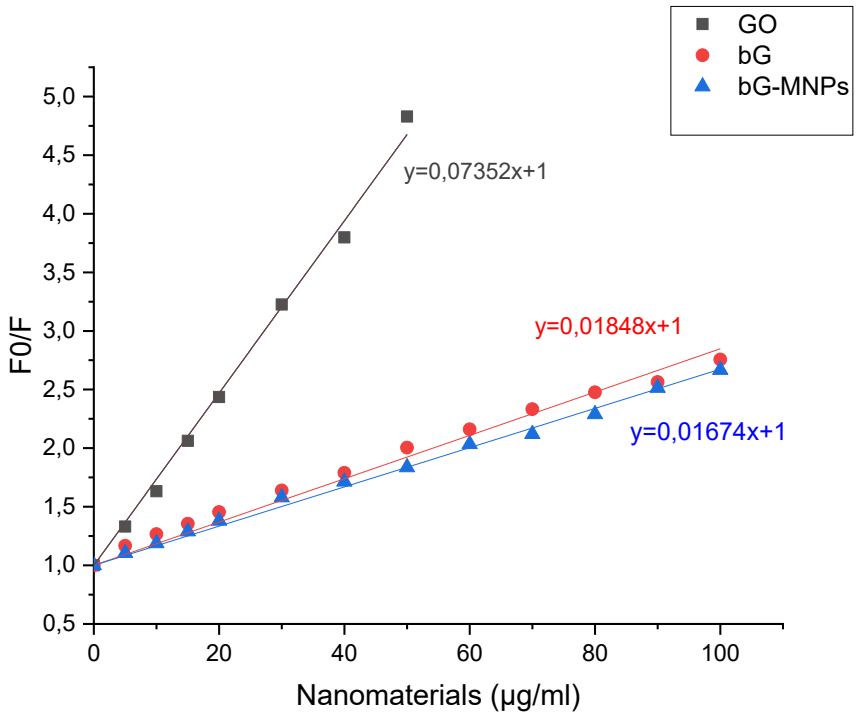

Graph 3.12. *Stern-Volmer curves of lysozyme in the presence of GO, bG, and bG-MNPs.*

The Stern–Volmer plot for lysozyme in the presence of all nanomaterials remained linear, indicating a single dominant quenching mechanism, most likely dynamic quenching. Dynamic quenching occurs when the excited fluorophore is deactivated through collisions with a quencher molecule, resulting in decreased fluorescence intensity and lifetime without forming a stable complex. In contrast, static quenching involves the formation of a non-fluorescent ground-state complex between the fluorophore and quencher, reducing fluorescence intensity but not affecting fluorescence lifetime. Thus, dynamic quenching is diffusion-dependent, while static quenching depends on complex formation (Lakowicz, 1999).

The K_{sv} of lysozyme in the presence of GO, bG, and bG-MNPs were calculated at 0.073, 0.018, and 0.017 µg/ml, respectively. The highest K_{sv} value in the presence of GO suggests that the space between the fluorophore and the quencher decreases, and the decreased K_{sv} for bG and bG-MNPs reflects weaker interactions and reduced quenching efficiency.

Finally, the Hill model equation is applied in protein fluorescence studies with nanomaterials to quantify binding affinity and cooperativity via quenching of intrinsic tryptophan fluorescence as nanomaterial concentration increases. The Hill model is described by Equation (4):

$$Q = (Q_{max} * C^n) / (K_d^n + C^n) \quad (4)$$

where C is the nanomaterial concentration, Q_{max} is the maximum bound proteins, n is the Hill coefficient, and K_d is the dissociation constant. The molecular dissociation constant, K_d, is a well-established parameter to quantify the affinity of protein-protein or other molecular interactions (Jiang et al., 2019). It represents the ligand concentration at which half of the binding sites are occupied. Lower K_d values indicate higher affinity, which means tighter binding, while higher K_d values indicate lower affinity, which means weaker binding (B. Yan & Bunch, 2025). Moreover, Hill coefficient (n) is a parameter used to measure the cooperativity of ligand binding to enzymes with multiple binding sites (Abeliovich, 2005). When n>1, there is positive cooperativity, which means binding of one molecule site increases the affinity for subsequent sites. When n<1, there is negative cooperativity, and consequently binding of one molecule site decreases the affinity for others (Yifrach, 2004). Last, in the cases where n=1, there is non-cooperative binding, meaning that ligand binding events occur independently without interaction between binding sites. In this case, the Hill's Model fitted curve follows a Michaelis-Menten-like behavior, and the apparent K_d represents the true binding constant.

The results of this analysis for lysozyme occurred from the fluorescence spectroscopy using Hill's Model equation and are presented in Table 3.4. The Hill's Model fitted curves are presented in Graphs D1-D3 in the Appendix.

Table 3.4. *The fluorescence apparent dissociation constant of lysozyme in the presence of nanomaterials.*

System	K_d (μg/mL)	n
Lysozyme-GO	14.392	1.074
Lysozyme-bG	69.769	0.761
Lysozyme-bG-MNPs	55.564	0.925

The K_d values indicate that lysozyme exhibits the strongest binding affinity towards GO, as shown by the lowest K_d value, while weaker interactions are observed for bG and bG–MNPs. The Hill coefficient of lysozyme-bG-MNPs is ≈1, indicating predominantly non-cooperative binding behavior. The slightly higher n value for lysozyme–GO suggests weak positive cooperativity, whereas lysozyme–bG shows mild negative cooperativity. These results suggest that GO provides a

more favorable surface for lysozyme adsorption compared to the other nanomaterials (Roy & Horovitz, 2022).

3.1.8.3. Circular Dichroism

Circular dichroism (CD) spectroscopy was used to assess the secondary structure and conformational stability of lysozyme. By monitoring its characteristic spectral features, CD provides insight into how the protein's α-helical content and overall fold respond to experimental conditions. The far-UV CD spectra of lysozyme were studied in the absence and presence of different concentrations of nanomaterials (5 and 25 μg/ml), as described in Section 2.2.9.3. The secondary structure of lysozyme in the presence of nanomaterials was analyzed using the K2D algorithm from Dicroweb. The results are presented in Graphs 3.13-3.15 and Tables 3.5-3.7.

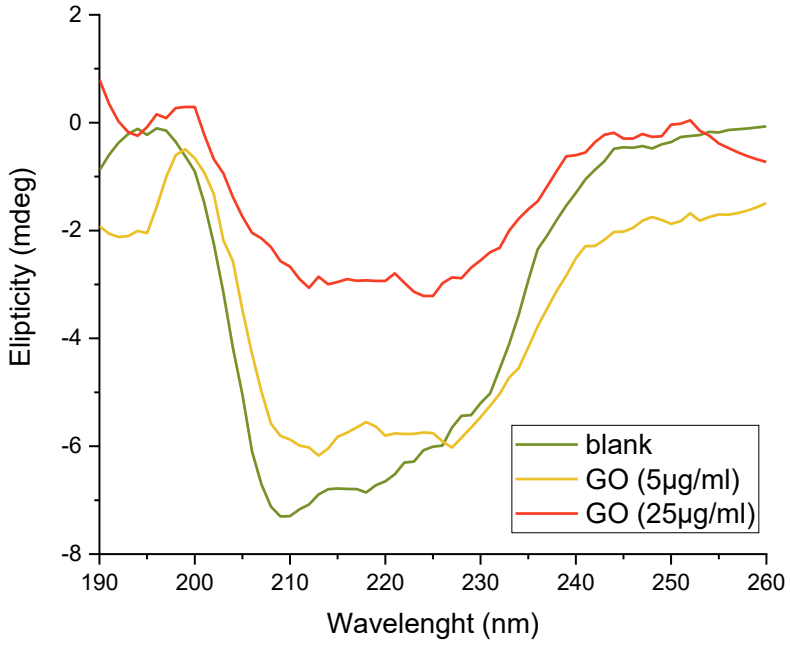

Graph 3.13. *CD spectra of Lysozyme (10 μg/ml) in the far-UV region, in the presence of GO.*

Table 3.5. *Secondary structure analysis of lysozyme in the presence of GO.*

System	a-helix	b-sheet	Random coil
Lysozyme	31	10	59
Lys- GO (5 μg/ml)	31	11	58
Lys- GO (25 μg/ml)	15	35	50

As observed from the results, the CD spectra of lysozyme in the presence of GO indicate a noticeable reduction in α-helical content, reflected by an increased intensity at 208 and 222 nm. At a low concentration of 5 μg/mL, no severe alterations are observed in the secondary structure of lysozyme. The effect of GO is more pronounced when the nanomaterial is used at a concentration of 25 μg/mL, where ~50% of the α-helical content of lysozyme is converted to a β-sheet structure. This unfolding aligns with literature reports showing that GO interacts with lysozyme and disrupts its native helical structure. Literature studies similarly describe that adsorption onto GO surfaces perturbs the native fold of lysozyme, promoting helix disruption and increased conformational flexibility (Bai et al., 2017). Also, the results agree with the fluorescence measurements discussed above.

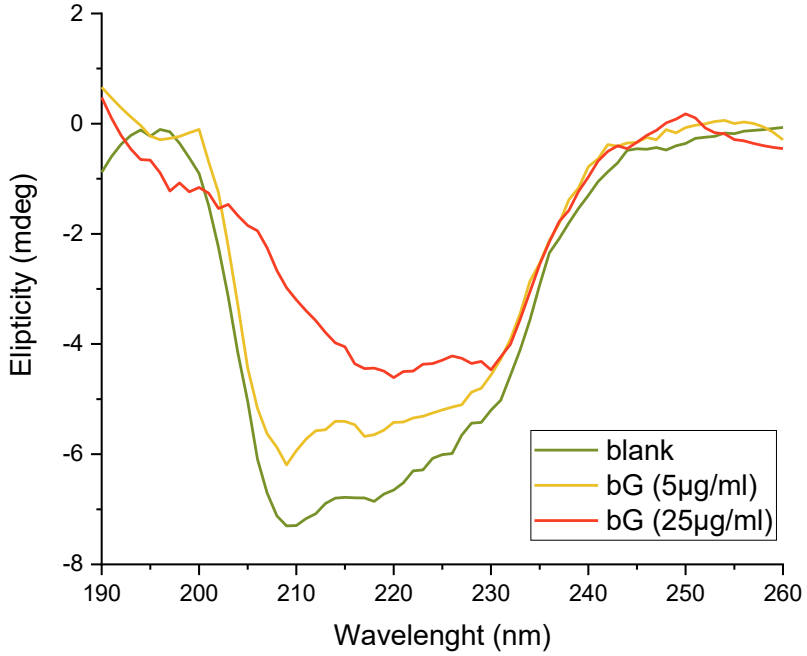

Graph 3.14. *CD spectra of lysozyme (10 μg/ml) in the far-UV region, in the presence of bG.*

Table 3.6. *Secondary structure analysis of lysozyme in the presence of bG.*

System	a-helix	b-sheet	Random coil
Lysozyme	31	10	59
Lys- bG (5 μg/ml)	30	12	58
Lys- bG (25 μg/ml)	24	22	54

The CD spectra of lysozyme in the presence of bG also show a reduction in α-helical content, but the effect is less intense than with GO. This milder structural disruption is anticipated, likely due to bG's green synthesis and greater biocompatibility. Thus, lysozyme undergoes only partial α-helix loss, suggesting that bG perturbs the native fold to a lesser extent than GO.

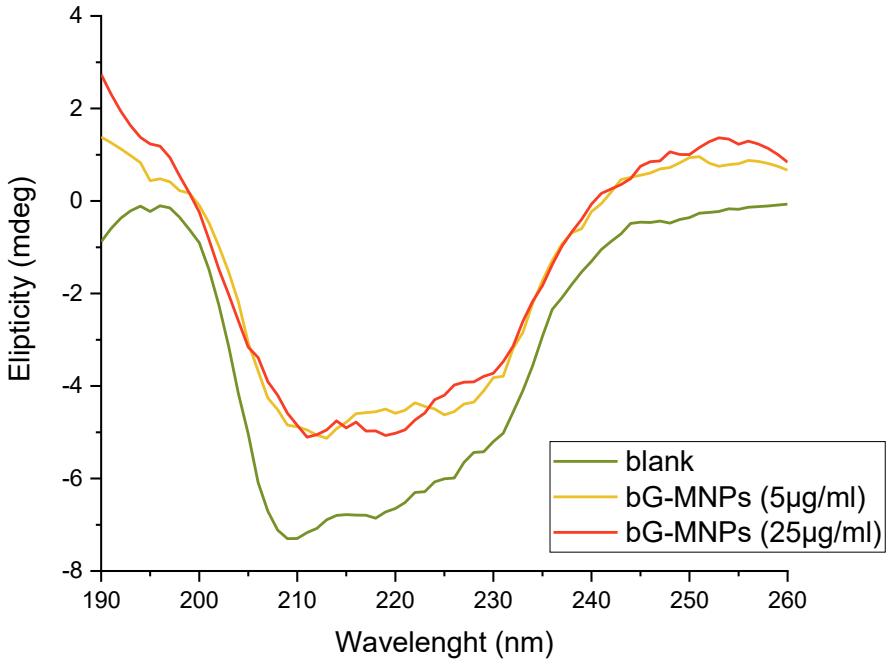

Graph 3.15. *CD spectra of lysozyme (10 µg/ml) in the far-UV region, in the presence of bG-MNPs.*

Table 3.7. *Secondary structure analysis of lysozyme in the presence of bG-MNPs.*

System	a-helix	b-sheet	Random coil
Free Lysozyme	31	10	59
Lys- bG-MNPs (5 µg/ml)	25	20	55
Lys- bG-MNPs (25 µg/ml)	25	20	55

The CD spectra of lysozyme in the presence of bG-MNPs show a slight loss of α-helical content. However, the loss of α-helix remains essentially unchanged for both concentrations of the nanomaterial. This suggests that lysozyme–nanoparticle interactions reach a structural effect plateau at low concentrations. These results agree with the fluorescence measures discussed above.

3.2. α-Amylase

3.2.1. Effect of the presence of nanomaterials on the activity of free α-amylase

The effect of nanomaterials on the activity of free α-amylase was studied as described in Section 2.2.5.3, for material concentrations ranging from 5 to 25 μg/ml. The nanomaterials used were graphene oxide (GO), biographene (bG), and biographene magnetic nanoparticles (bG-MNPs). The results are presented in Graph 3.16. In each case, 100% corresponds to the maximum activity exhibited by the enzyme in the absence of nanomaterials.

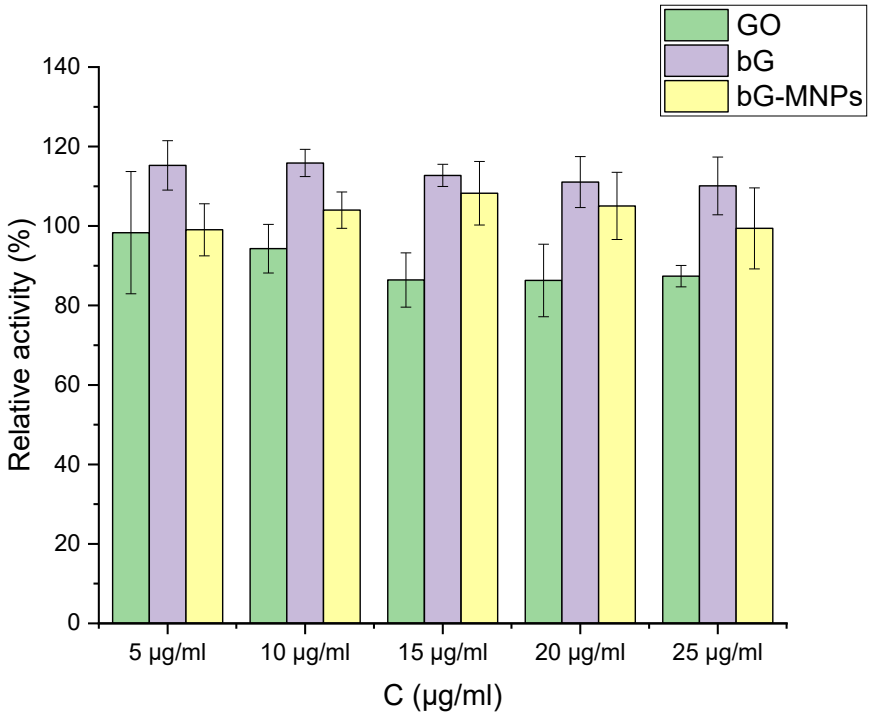

Graph 3.16. *Effect of the presence of nanomaterials on the activity of free α-amylase.*

According to Graph 3.16, α-amylase shows reduced activity in the presence of GO. This effect is dose-dependent; as the concentration of GO increases, the activity of α-amylases decreases. In the presence of bG, the enzyme exhibits higher activity than when the nanomaterial is absent. The biofunctionalization of graphene sheets with BSA seems to offer a beneficial advantage in the catalytic activity of the enzyme. Last, in the presence of bG-MNPs, the highest activity is observed when the concentration is 15 μg/ml, indicating that the presence of magnetic NPs on the graphitic surface enhances the enzyme activity. The effect of the nanomaterials on the activity of α-amylase is similar to that observed in the case of lysozyme, indicating that these nanomaterials present similar interactions with both hydrolytic enzymes.

3.2.2. α-Amylase immobilization efficiency on nanomaterials

The immobilization of α-amylase on the nanomaterials was achieved by physical adsorption, and in each case, the immobilization efficiency was calculated as described in Section 2.2.4. The results are presented in Table 3.8.

Table 3.8. *Immobilization efficiency of α-amylase on nanomaterials.*

Nanomaterial	Immobilization yield
GO	100.0 ± 0.1%
bG	76.8% ± 0.6%
bG -MNPs	79.3% ± 0.5%

As shown in Table 3.8, the immobilization yield of α-amylase on GO is 100%. In their work, Liu et al. (2023), refer that GO exhibits a remarkable higher adsorption capacity for α-amylase compared to other nanomaterials. This enhanced affinity can be attributed to multiple non-covalent interactions, including hydrophobic interactions, hydrogen bonding, van der Waals forces, and electrostatic attraction, arising from the amphiphilic nature of both GO and the enzyme. In addition, the aromatic groups of GO and within the amino acid residues of α-amylase may facilitate π–π stacking, further strengthening the adsorption process.

For bG and bG-MNPs, the immobilization yield is high. bG has been previously reported to be a potential carrier for enzyme immobilization. Alatzoglou et al. (2022) have demonstrated that glucose oxidase, horseradish peroxidase, and β-glucosidase can be effectively immobilized on bG, with immobilization yields reaching up to 98.5 %. Moreover, a similar magnetic bio-graphene has been recently applied for the co-immobilization of cellulase and β-glucosidase, exhibiting excellent characteristics as an immobilization matrix (Alatzoglou et al., 2025).

3.2.3. Determination of immobilized α-amylase activity

Having determined the immobilization yield of α-amylase, the specific enzymatic activity was subsequently calculated, as described in Section 2.2.5. The results are presented in Table 3.9.

Table 3.9. *Specific activity of free and immobilized α-amylase.*

System	Units/mg enzyme
Free α-amylase	486.41 ± 40.44
α-amylase-GO	5.60±0.36
α-amylase-bG	0.22 ±0.03
α-amylase-bG-MNPs	3.33±0.32

As observed from Table 3.9, the activity of immobilized α-amylase is particularly low compared to that of the free enzyme. As mentioned in the case of lysozyme, the interactions created during the immobilization of enzymes on nanomaterials through physical adsorption often lead to structural changes and a reduction of their catalytic activity (Gkantzou et al., 2021). In addition, enzyme immobilization may introduce mass transfer limitations, since substrates must diffuse from the bulk solution to the immobilized enzyme active sites, which can decrease the observed reaction rate and consequently the measured activity (Carballares et al., 2024). Furthermore, immobilization can restrict enzyme conformational flexibility or cause partial structural changes due to interactions between the enzyme and the support interactions, which may reduce catalytic activity (Datta et al., 2013b). Therefore, the lower specific activity observed for immobilized α-amylase is mainly due to normalization against the total biocatalyst mass, diffusion limitations, and structural constraints rather than a complete loss of enzymatic function. Similar results have been observed in the literature. For example, in the work of Mardani et al., (2018) and Ji et al., (2018), α-amylase was immobilized on chitosan-montmorillonite nanocomposite beads and cellulose nanocrystals, respectively. In both cases, the activity of the enzyme was reduced.

3.2.4. Reuse of immobilized α-amylase

The reusability of α-amylase was studied as described in Section 2.2.10.2. The results are presented in Graph 3.16. In each case, 100% corresponds to the maximum activity exhibited by the enzyme in the first reuse cycle.

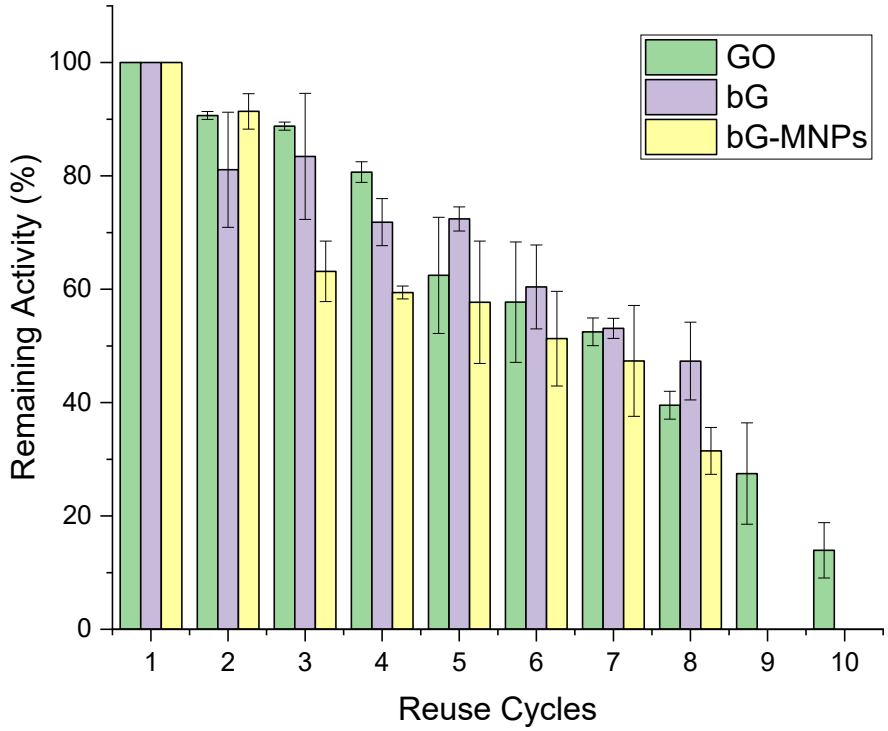

Graph 3.16. *The reuse cycles of immobilized α-amylase.*

As observed in Graph 3.16, the enzyme can be reused up to 10 cycles after being immobilized in GO and up to 8 cycles after being immobilized in bG and bG-MNPs. After the fifth cycle, the remaining enzyme activities of a-amylase immobilized in GO, bG, and bG-MNPs were 62.45%, 72.4%, and 57.69%, respectively. The gradual loss of enzyme activity could be either due to leakage from the support or to structural destabilization during the successive catalytic cycles. According to the literature, several studies have demonstrated that immobilizing α-amylase on various nanosupports enables efficient recovery and repeated use of the enzyme. In these studies, α-amylase has been immobilized on different types of MNPs and on Calcium-alginate beads. In all cases, the enzyme maintains satisfactory catalytic activity upon repeated use, for several cycles (Baskar et al., 2015; Dhavale et al., 2018; Naskar et al., 2024) . All these agree with the results presented in this work.

3.2.5. Spectroscopic techniques for determining the structure of α-amylase

3.2.5.1. UV-Vis Spectroscopy

The UV-Vis spectra of α-amylase were studied in the absence and in the presence of different concentrations of nanomaterials (5-40 μg/mL), as described in Section 2.2.9.1. The results are presented in Graphs 3.17-3.19.

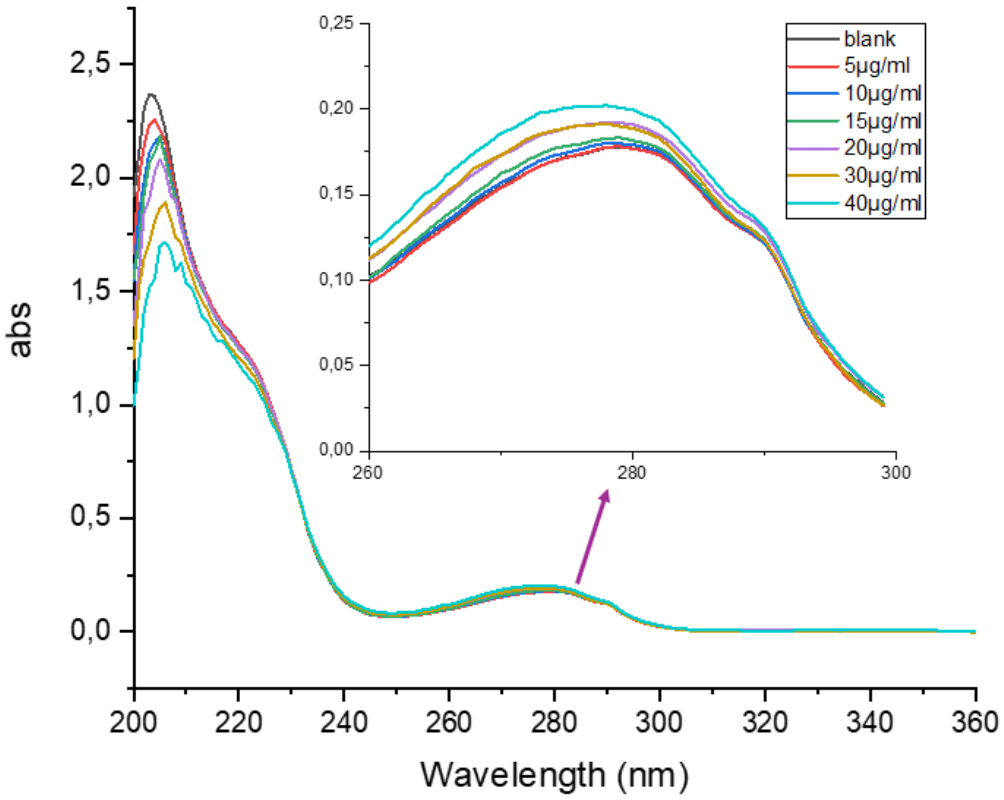

Graph 3.17. *UV-Vis spectra of α-amylase (C=100 μg/ml) in the presence of GO.*

As observed from Graph 3.17, the absorbance at 280 nm increases with the increase in GO concentration, as was also observed in the case of lysozyme. The most possible explanation is that the interactions between the enzyme and GO have altered the enzyme's structure, exposing the aromatic residues, and leading to an increase in peak absorption at 280nm. In their work, Liu et al. (2023), have also studied the interactions between GO and α-amylase using UV–Vis absorption spectroscopy. α-Amylase showed distinct absorption peaks at 205 nm and 280 nm, which correspond to the protein's backbone structure and the aromatic residues Tyr and Trp, respectively. As the GO concentration increased, the absorbance of α-amylase at 280 nm also increased.

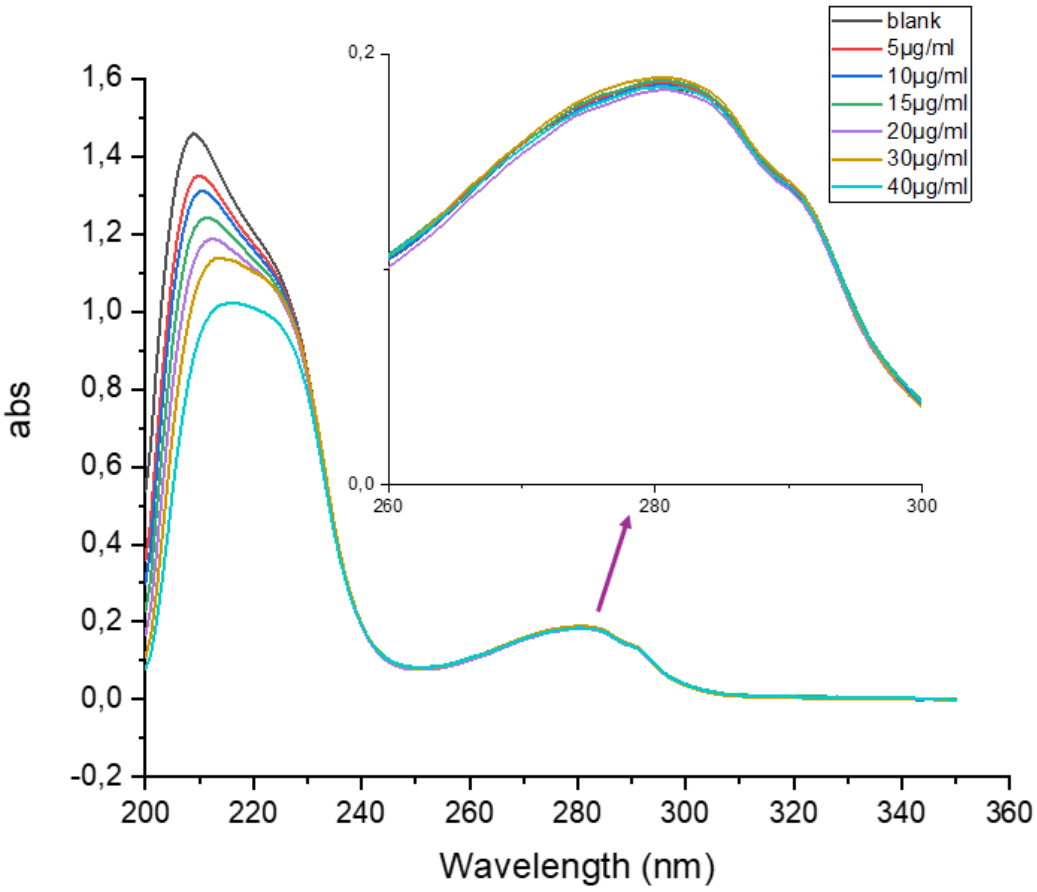

Graph 3.18. *UV-Vis spectra of α-amylase (C=100 μg/ml) in the presence of bG.*

As seen from Graph 3.18, bG did not affect the spectrum of α-amylase, indicating that this nanomaterial does not provoke significant alterations to the tertiary structure of the enzyme. In a similar study, the UV-Vis spectra of glucose oxidase did not present significant changes, even at high concentrations of bG, showing that the enzyme maintains its natural form (Alatzoglou et al., 2023).

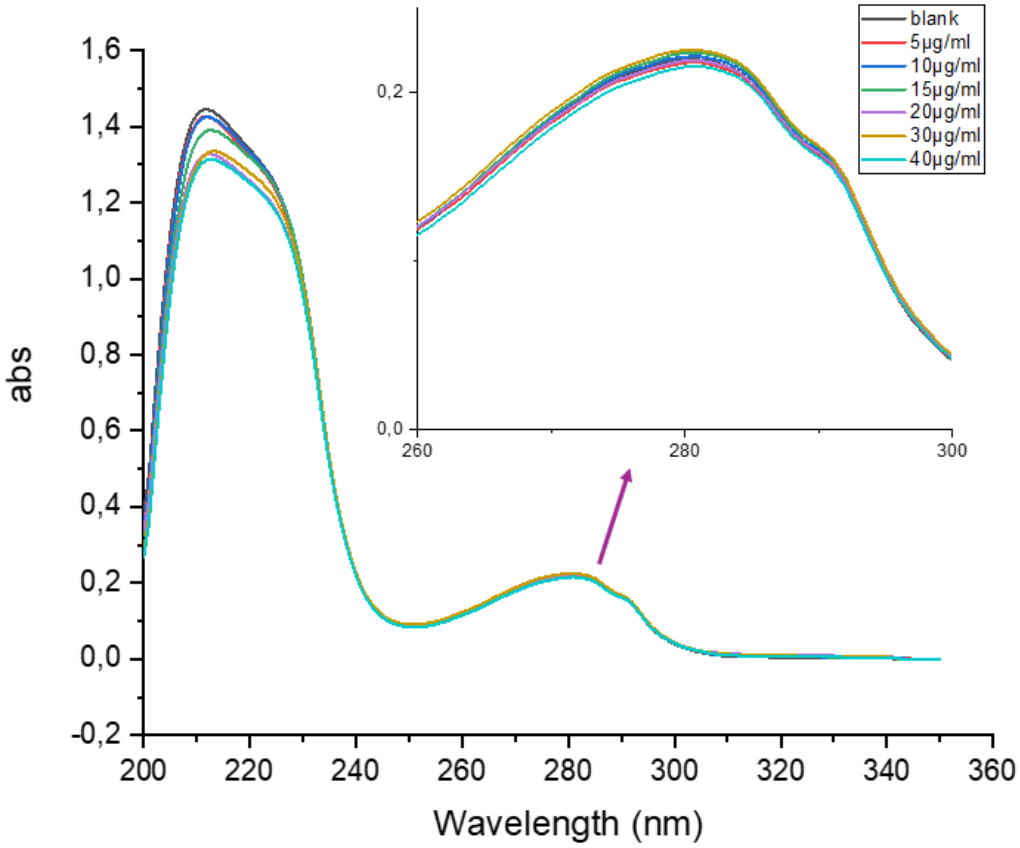

Graph 3.19: UV-Vis spectra of α-amylase (C=100 μg/ml) in the presence of bG-MNPs.

Similarly, in the case of bG-MNPs, non-significant alterations in the 280 nm absorption band are recorded, indicating that the nanomaterial does not affect the aromatic amino acids in the enzyme's structure.

3.2.5.2. Fluorescence spectroscopy

The Fluorescence of α-amylase was studied in the absence and presence of different concentrations of nanomaterials (2,5-100 μg/mL), as described in Section 2.2.9.2. The results are presented in graphs 3.20-3.22.

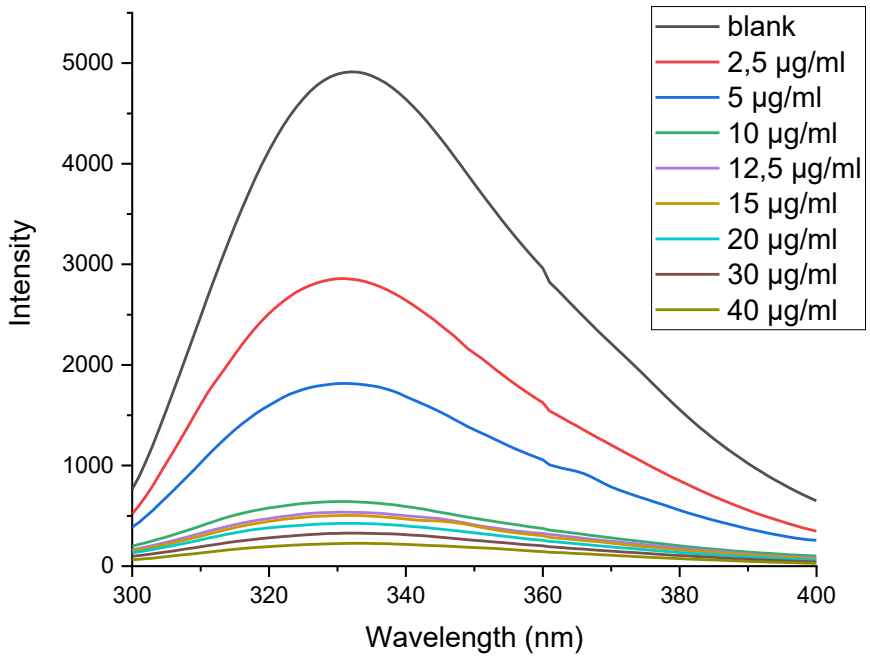

Graph 3.20. *Fluorescence emission spectra of α-amylase (10 μg/ml) in the presence of GO.*

The significant decrease in α-amylase fluorescence intensity in the presence of GO indicates strong interactions. As commented before for lysozyme, GO has been reported to strongly quench the intrinsic fluorescence of proteins containing tryptophan and tyrosine residues and is described as a universal quencher for such biomolecules. The quenching mechanism is mainly attributed to static quenching and Förster resonance energy transfer, with additional contributions from electrostatic and hydrophobic interactions between proteins and GO surfaces (S. Li et al., 2012). The large surface area of GO facilitates the adsorption of proteins, leading to enhanced fluorescence quenching (Kenry et al., 2016). Similar results have been observed by Liu et al., (2023), where α-amylase was immobilized on GO, and a decline in fluorescence intensity was observed, indicating that the intrinsic fluorescence of α-amylase was quenched by GO. It is worth noting that these results also agree with the reusability of α-amylase immobilized on GO. That complex achieved up to 10 cycles of reusability, in contrast with bG and bG-MNPs, indicating the stability of α-amylase after immobilization on GO

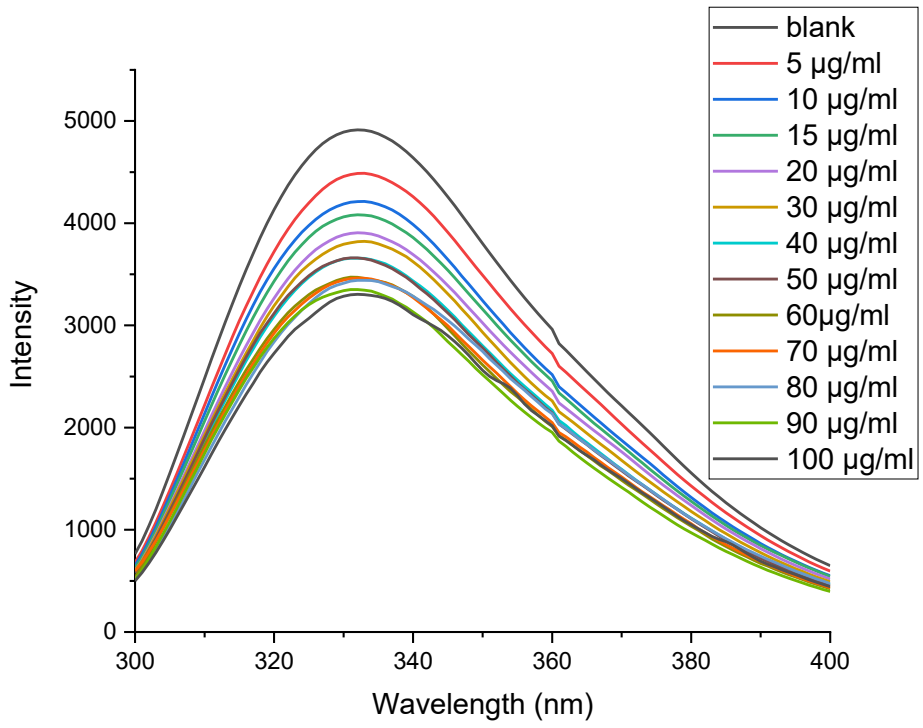

Graph 3.21. *Fluorescence emission spectra of α-amylase (10 μg/ml) in the presence of bG.*

In the case of bG, a-amylase shows less quenching, which means a smaller decrease in the intensity of the peak of the emission spectra. The quenching effect of bG is much lower than that of GO. When GO is used at a concentration of 40 μg/mL, the fluorescence intensity of α-amylase decreases at 20.7%, while when bG is used at a concentration of 100 μg/mL, the residual fluorescence intensity of α-amylase is preserved at 67.2% (see Appendix, Graphs E1 and E2). Similar observations have been reported for bG while interacting with glucose oxidase. The nanomaterials did not affect the emission spectra of glucose oxidase, indicating that the enzyme preserved its tertiary structure (Alatzoglou et al., 2023)

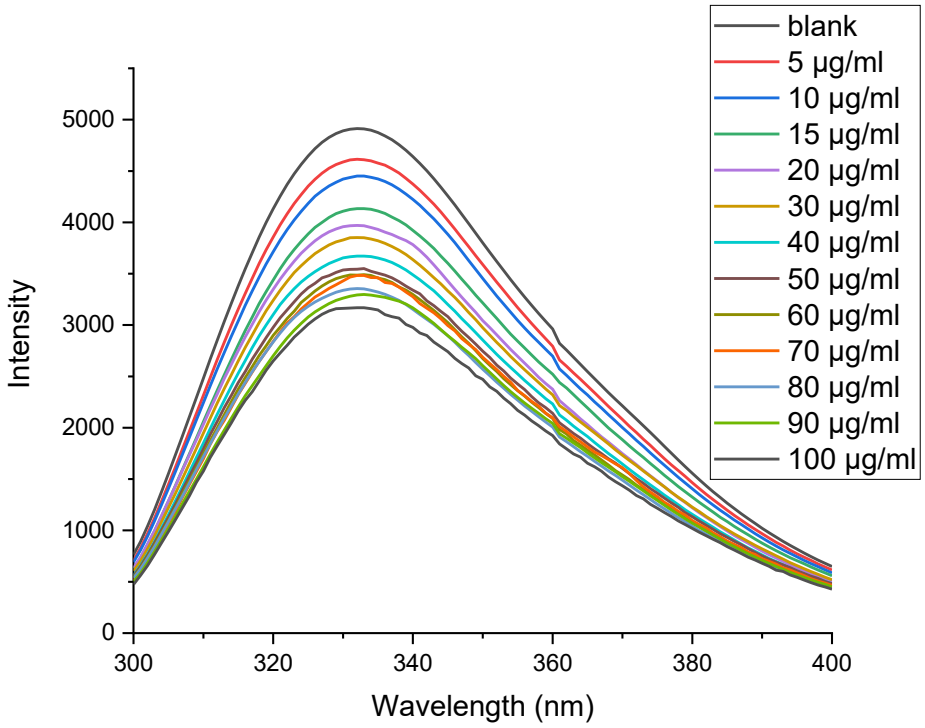

Graph 3.22. *Fluorescence emission spectra of α-amylase (10 µg/ml) in the presence of bG-MNPs.*

As observed from Graph 3.22, a-amylase shows similar quenching, as in the case of bG, which means a smaller decrease in the intensity of the peak of the emission spectra is observed in contrast to GO. Here, when bG-MNPs is used at a concentration of 100 µg/mL, the fluorescence intensity of α-amylase decreases at 64.5% (see Appendix, Graph E3). bG-MNPs is synthesized in a “green” way, which means that it has a lower oxidation degree and surface charge. Therefore, weaker electrostatic and hydrogen-bonding interactions with proteins are developed, resulting in lower quenching.

In the next step, the Stern–Volmer (K_{sv}) constants were also determined and are presented in Graph 3.23.

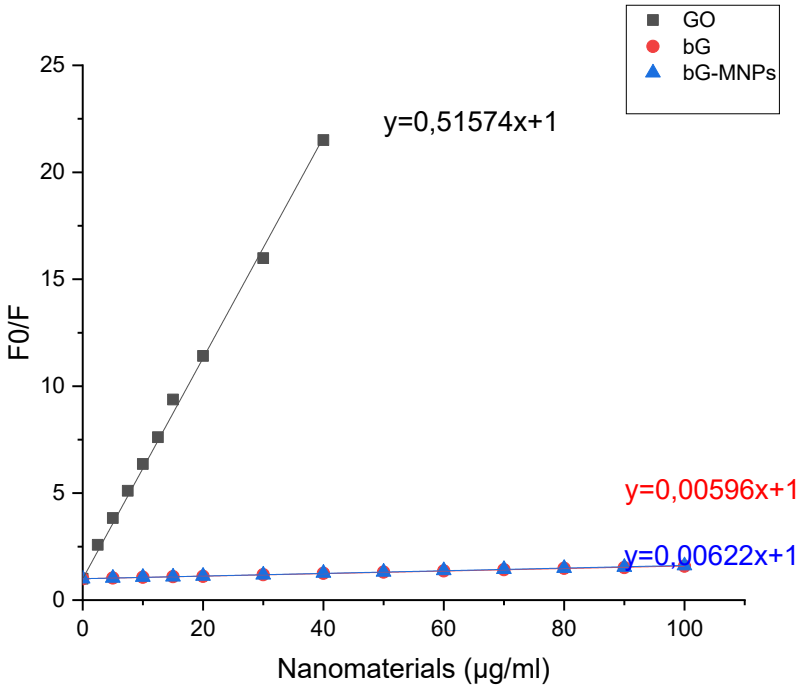

Graph 3.23. *Stern-Volmer curves of a-amylase in the presence of GO, bG, and bG-MNPs.*

The K_{sv} of a-amylase in the presence of GO, bG, and bG-MNPs were calculated at 0.515, 0.006, and 0.006 µg/ml, respectively. The significantly lower K_{sv} values observed for bG and bG-MNPs indicate a reduced quenching efficiency compared to GO. This behavior suggests weaker enzyme–nanomaterial interactions, possibly due to differences in surface chemistry and structural properties of the bG-based materials. The Stern–Volmer results obtained in this work are consistent with previous reports on α-amylase–GO interactions, indicating predominantly static fluorescence quenching due to complex formation between the enzyme and GO. This suggests similar binding mechanisms, likely governed by non-covalent interactions such as hydrogen bonding and van der Waals forces (Liu et al., 2023).

The molecular dissociation constant, K_d, and the Hill coefficient (n) were also calculated and are presented in Table 3.10. The Hill's Model fitted curves are presented in the Appendix (Graphs F1-F3).

Table 3.10. *The fluorescence apparent dissociation constant of α-amylase in the presence of nanomaterials*.

System	K_d (μg/mL)	n
α-amylase-GO	3.058	1.620
α-amylase-bG	27.286	0.773
α-amylase -bG-MNPs	29.155	1.011

The K_d values indicate that α-amylase shows the strongest binding affinity towards GO, as evidenced by the lowest K_d value, whereas significantly weaker interactions are observed for bG and bG–MNPs. The Hill coefficient for α-amylase–GO suggests positive cooperative binding, indicating that adsorption of α-amylase on GO may enhance subsequent binding events. In contrast, α-amylase–bG exhibited a Hill coefficient < 1 indicating mild negative cooperativity, while α-amylase–bG–MNPs showed an n value close to 1, suggesting nearly independent binding sites. Overall, these results imply that GO provides a highly favorable and cooperative adsorption surface for α-amylase, whereas the other nanomaterials exhibit weaker and less cooperative interactions.

3.2.5.3. Circular Dichroism

The far-UV CD spectra of a-amylase were studied in the absence and presence of different concentrations of nanomaterials (5 and 25 μg/ml, respectively), as described in paragraph 2.2.9.3. The results are presented in graphs 3.24-3.26 and tables 3.11-3.13.

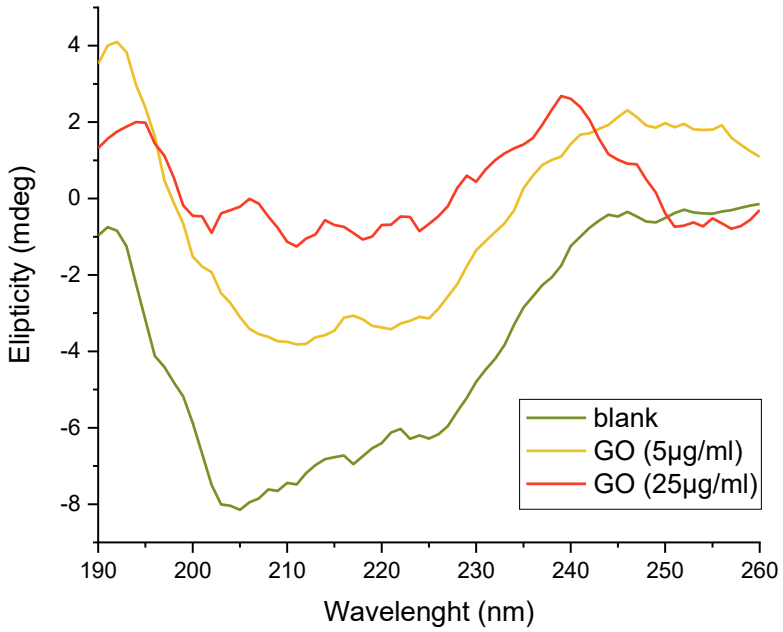

Graph 3.24. *CD spectra of a-amylase (10 µg/ml) in the presence of GO.*

Table 3.10. *Secondary structure analysis of α-amylase in the presence of GO.*

System	α-helix	β-sheet	Random coil
α-amylase	22	20	58
α-amylase - GO (5 µg/ml)	15	33	52
α-amylase - GO (25 µg/ml)	5	47	48

As seen in Graph 3.24, there are two negative peaks around 208 nm and 222 nm for α-amylase. These represent the n-π * and π-π * transitions of the peptide bond inside the α-helix (Rigos et al., 2003). As observed from Table 3.10, the α-helical structure of lysozyme converts into a β-sheet structure in the presence of GO, indicating significant conformational alterations. Similar results have been observed in the work of Liu et al., (2023), where GO induced extensive alterations in the secondary structure of α-amylase. The CD results are consistent with the fluorescence results.

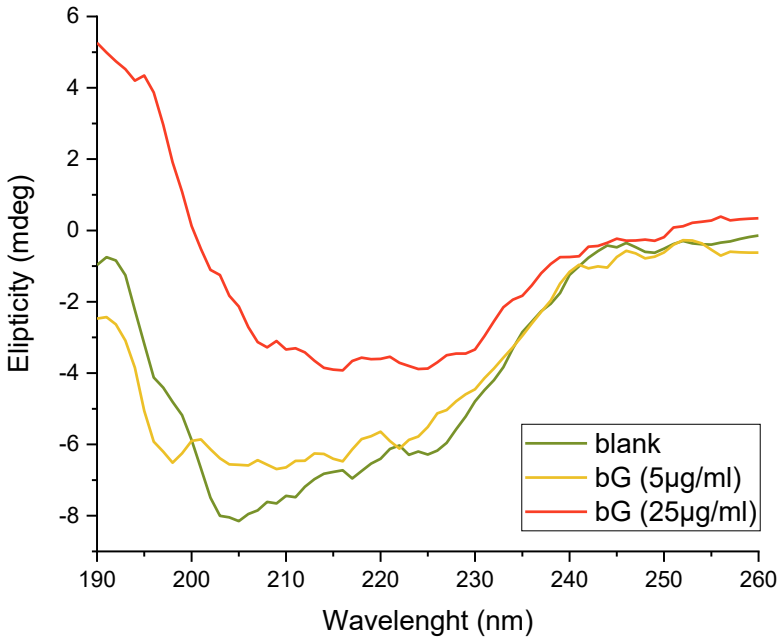

Graph 3.25. *CD spectra of a-amylase (10 μg/ml) in the presence of bG.*

Table 3.11. *Secondary structure analysis of α-amylase in the presence of bG.*

System	α-helix	β-sheet	Random coil
α-amylase	22	20	58
α-amylase - bG (5 μg/ml)	21	26	53
α-amylase - bG (25 μg/ml)	18	25	57

In the case of bG, no significant reduction of the α-helical structure is observed. The CD results are consistent with the fluorescence results, indicating that this nanomaterial does not affect the conformation of the protein molecule. Similarly, bG was found to preserve the secondary structure of glucose oxidase upon interactions (Alatzoglou et al., 2023).

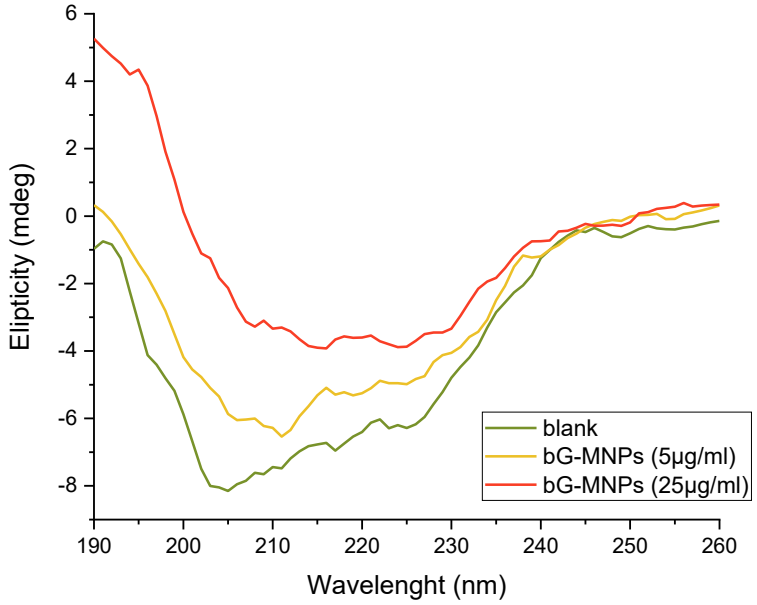

Graph 3.26. *CD spectra of a-amylase (10 µg/ml) in the presence of bG-MNPs.*

Table 3.12. *Secondary structure analysis of α-amylase in the presence ofbG-MNPs.*

System	α-helix	β-sheet	Random coil
α-amylase	22	20	58
α-amylase – bG-MNPs (5 µg/ml)	21	26	53
α-amylase – bG-MNPs (25 µg/ml)	17	27	56

In the case of bG-MNPs, only a slight reduction of the α-helical structure is observed, highlighting the protective effect of this nanomaterial towards the enzyme's secondary structure. The CD results are consistent with the fluorescence results, indicating that bG-MNPs can serve as an efficient support for preserving the enzyme's conformational integrity.

4. Conclusions

The present diploma thesis was conducted to study the relationship between the structure and function of enzymes when interacting with carbon-based nanomaterials. The enzymes investigated were lysozyme and α-amylase, while the nanomaterials examined were graphene oxide, biographene, and magnetic biographene. Graphene oxide is a widely studied material, ideal for enzyme immobilization, and was used as a reference material for comparison. Biographene and magnetic biographene are two promising nanomaterials produced through a green synthetic route based on protocols developed in the Biotechnology Laboratory.

Initially, the enzyme lysozyme was studied. At the preliminary stage, the effect of the nanomaterials on the free enzyme was investigated. Subsequently, the enzyme was immobilized on GO, bG, and bG-MNPs through physical adsorption. Then, the immobilization yield and enzymatic activity were determined, while the kinetic parameters (K_m and V_{max}) were also evaluated. Furthermore, the effects of pH and temperature on the activity of lysozyme were examined, as well as the thermal stability of immobilized lysozyme at 50 and 60 °C.

The results showed a high immobilization yield (~96%) and a decrease in enzymatic activity after immobilization (free lysozyme had ~20% higher specific activity in comparison with the immobilized). Next, the apparent K_m was higher for lysozyme immobilized on GO, the same when immobilized on bG, and lower when immobilized on bG-MNPs. The apparent V_{max} was reduced in all cases. Also, the optimum pH and temperature for immobilized lysozyme changed. Lastly, the thermal stability was similar to the free enzyme only in the case of bg.

The experimental procedure followed involved the structural study of lysozyme. Initially, UV–Vis spectroscopy was used to investigate the effect of the nanomaterials on lysozyme, specifically at a wavelength of 280 nm, which is characteristic of aromatic amino acids. A pronounced effect of graphene oxide was observed, along with a significant decrease in the intensity of the peak at 280 nm, in contrast to the milder effect and minimal reduction in peak intensity observed for bG and bG-MNPs.

Subsequently, fluorescence spectroscopy was employed to further investigate the interaction between lysozyme and the nanomaterials through the analysis of the emission spectra of lysozyme. In each case, the Stern–Volmer quenching constant (K_{sv}), the equilibrium dissociation constant (K_d), which quantifies the binding affinity, and the Hill coefficient (n), which represents the degree of cooperativity, were determined. The results indicate a higher quenching effect in the presence of GO. In contrast, the interactions between lysozyme and bG and bG-MNPs are milder.

Finally, circular dichroism spectra were recorded to determine the secondary structural characteristics of lysozyme, providing information on the percentage of α-helix, β-sheet, and random coil content, respectively. More specifically, a decrease in the α-helical content of lysozyme was observed, predominantly in the presence of GO. A smaller reduction in α-helix content was observed in the other two cases.

In the second part of the experimental procedure, a-amylase was studied. Firstly, the effect of nanomaterials on the free enzyme was investigated. Subsequently, the enzyme was immobilized on GO, bG, and bG-MNPs through physical adsorption. Then, the immobilization yield and enzymatic activity were determined, while the reusability of the enzyme was also studied.

The results showed a reduced activity in the presence of GO and slightly higher activity in the presence of the other two nanomaterials. Next, the immobilization yield was ~100% when α-amylase was immobilized on GO and ~±77% when immobilized on bG and bG-MNPs. As for the specific activity, a huge decrease was observed after immobilization. Lastly, α-amylase's reusability reached up to 10 cycles in case of GO and up to 8 cycles in the other two cases.

In the following steps, the same structural studies occurred. The UV-Vis spectroscopy showed increased intensity around 280 nm as the GO concentration increased, while no significant changes were observed in the presence of bG and bG-MNPs. The fluorescence also indicated very strong interactions between α-amylase and GO, while the quenching effect was milder for both bG and bG-MNPs. These results were also confirmed by the determination of K_{sv}, $K_{d,}$ and n. Lastly, the CD agrees with the UV-Vis and Fluorescence spectra. In the presence of GO, α-amylase loses most of the a-helical content (22% → 5%). For bG and bG-MNPs, no significant loss is observed.

Overall, the results of this thesis demonstrate that the physicochemical properties of carbon-based nanomaterials strongly influence enzyme structure and function, thereby affecting immobilization efficiency, catalytic activity, and stability. GO exhibited stronger interactions that induced significant structural alterations and reduced enzymatic performance, whereas bG and bG-MNPs preserved enzyme structure and activity to a greater extent. These findings highlight the potential of biographene-based nanomaterials as promising, green, and biocompatible platforms for enzyme immobilization and biotechnological applications.

APPENDIX

i. Michaelis-Menten Graphs

The following page presents the Graphs for the kinetic studies of free and immobilized lysozyme on Graphene Oxide, bio-Graphene, and Magnetic bio-Graphene.

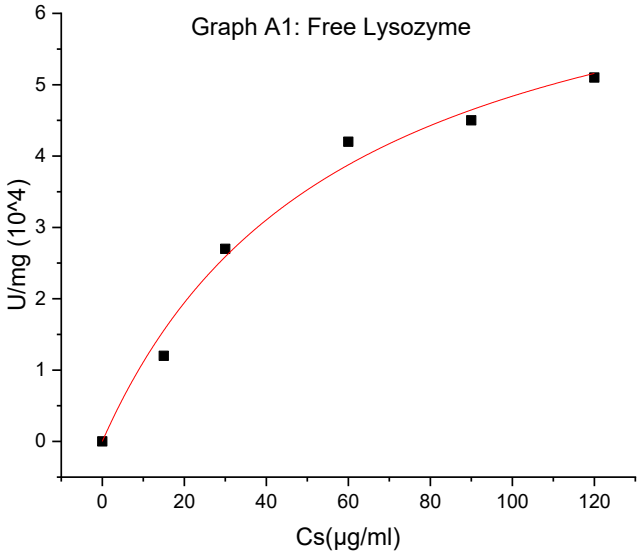

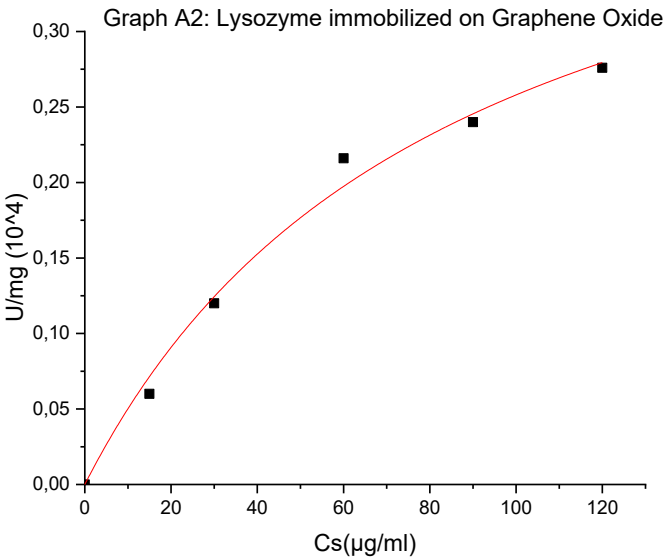

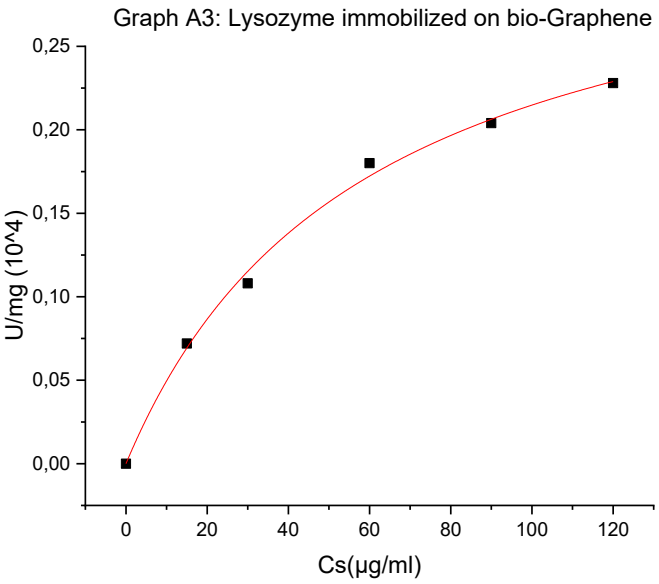

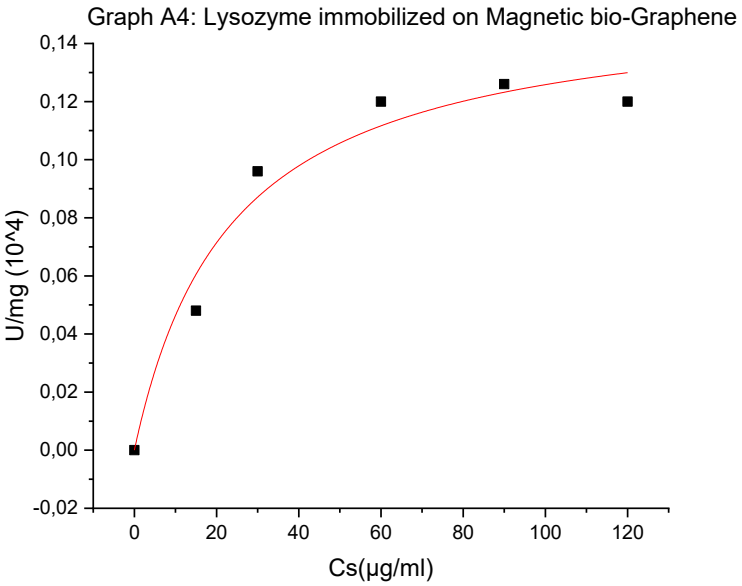

ii. Effect of temperature on the activity of free and immobilized lysozyme

Graph B1: Thermal activity of free lysozyme

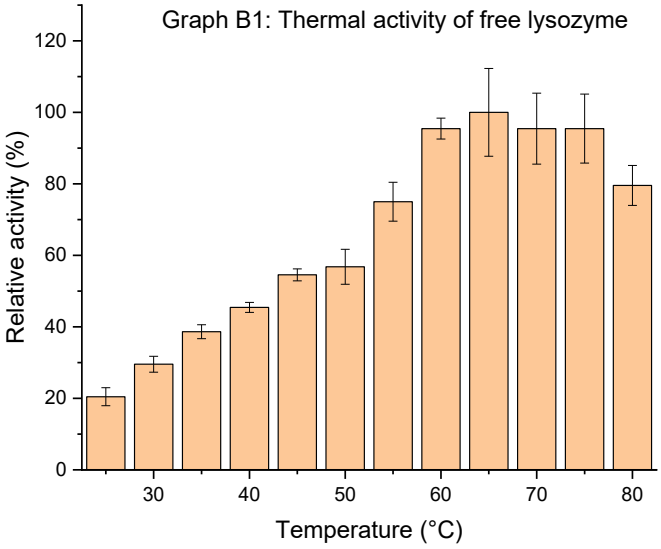

Graph B2: Thermal acivity of lysozyme immobilized on GO

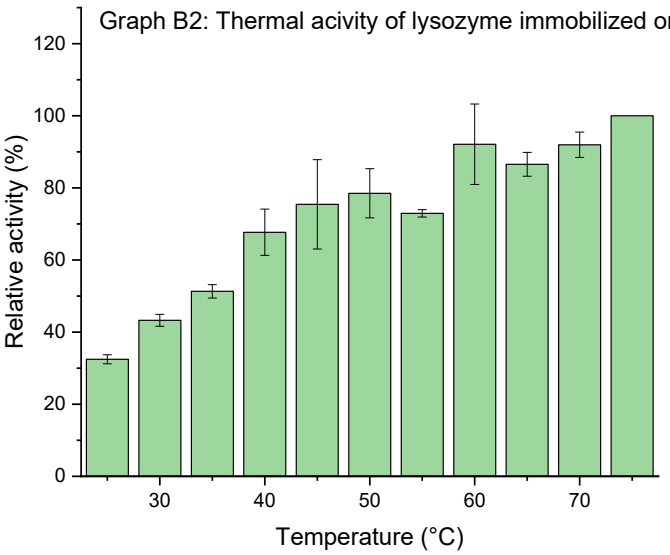

Graph B3: Thermal activity of lysozyme immobilized on bG

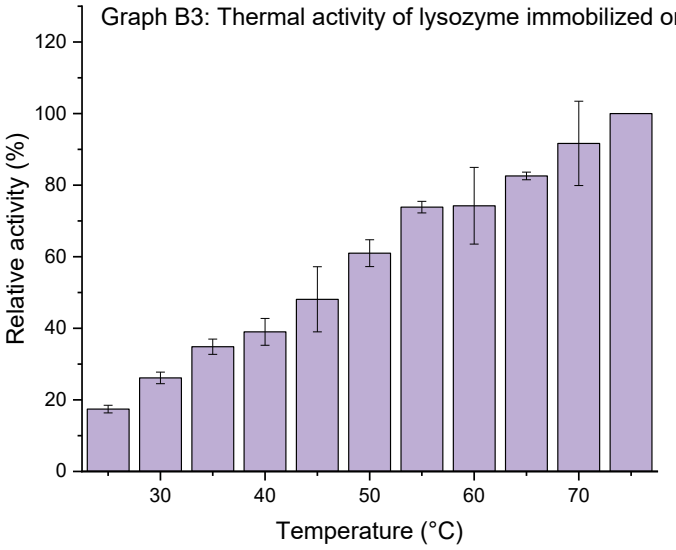

Graph B4: Thermal activity of lysozyme immobilized on bG-MNPs

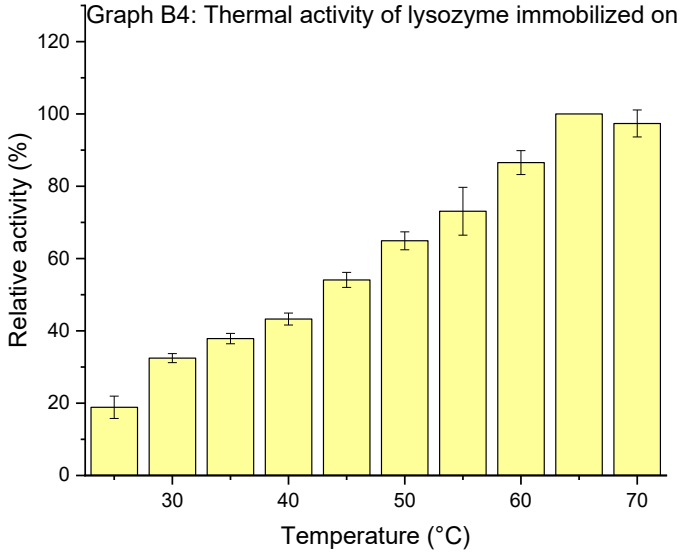

iii. Remaining Intensity of Lysozyme

The following Graphs present the remaining intensity of Lysozyme at 335 nm as it emerged from the Fluorescence data.

Graph C1: Remaining Intensity of Lysozyme in presence of GO

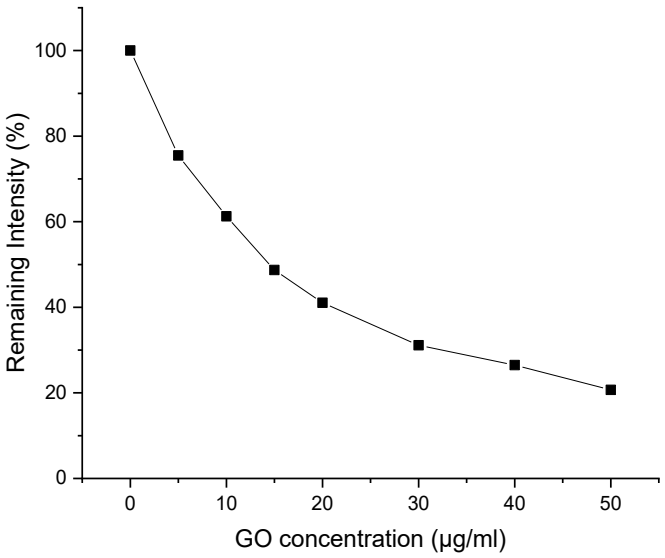

Graph C2: Remaining Intensity of Lysozyme in presence of bG

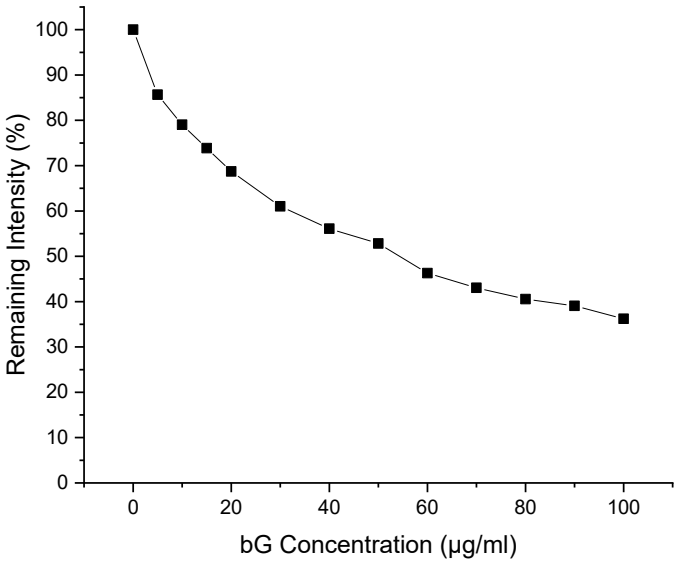

Graph C3: Remaining Intensity of Lysozyme in presence of bG-MNPs

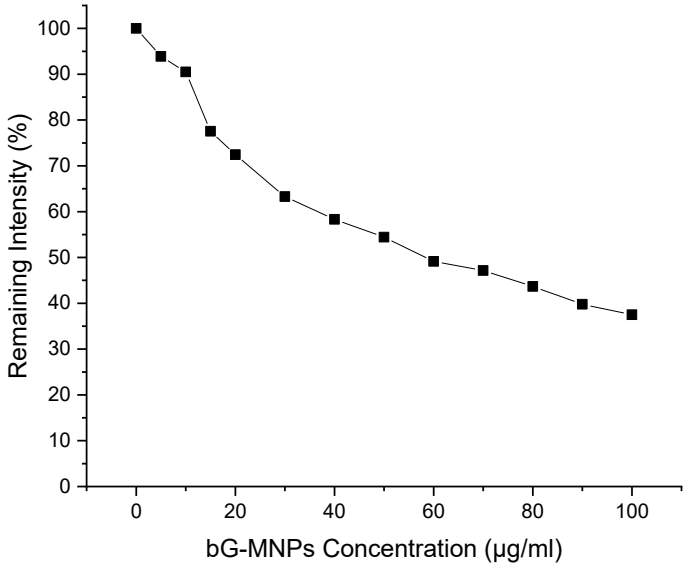

iv. Hill's Model Curves of Lysozyme

The following Graphs present the Hills model of Lysozyme and a-amylase as these emerged from the Fluorescence data and the analysis using Origin Pro 2018.

Graph D1: Hill's model fitted curve of lysozyme in presence of GO

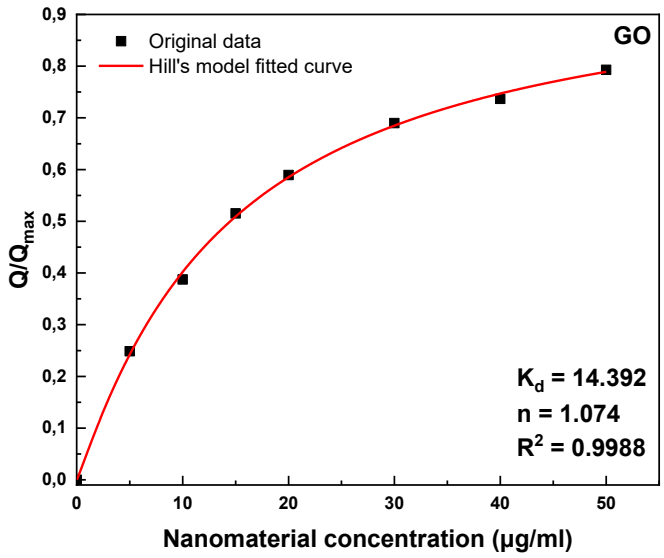

Graph D2: Hill's model fitted curve of lysozyme in presence of bG

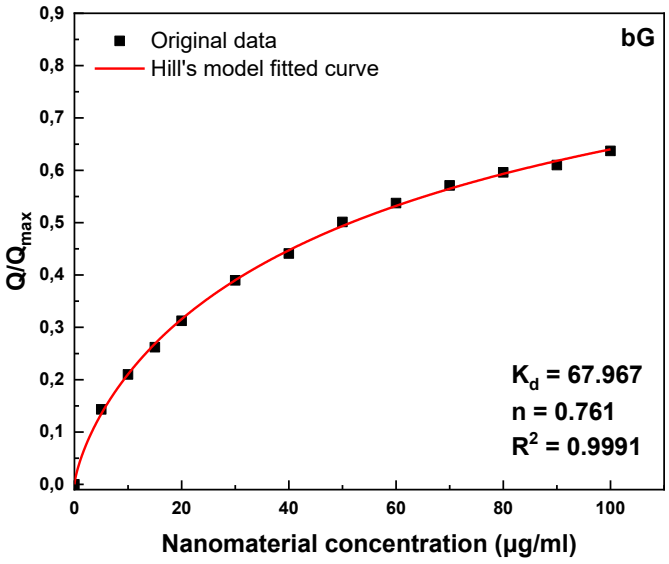

Graph D3: Hill's model fitted curve of lysozyme in presence of bG-MNPs

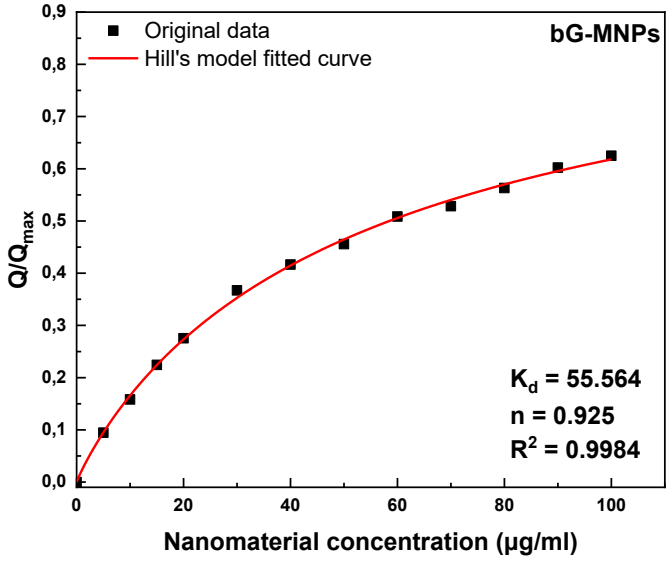

v. Remaining Intensity of α-amylase

The following Graphs present the remaining intensity of α-amylase at 332 nm as it emerged from the Fluorescence data.

Graph E1: Remaining Intensity of α-amylase in presence of GO

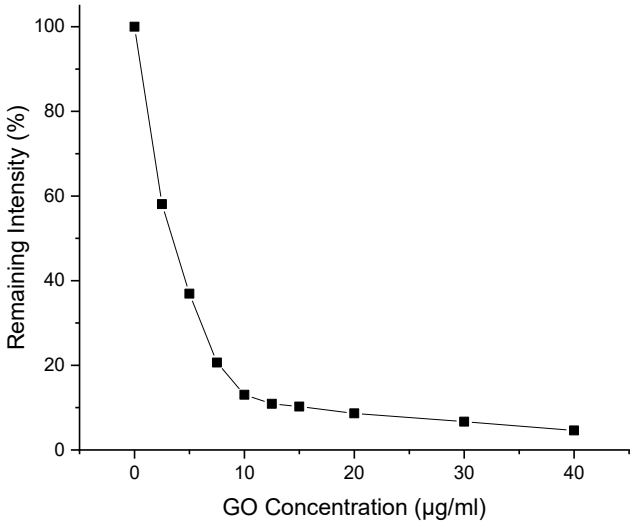

Graph E2: Remaining Intensity of α-amylase in presence of bG

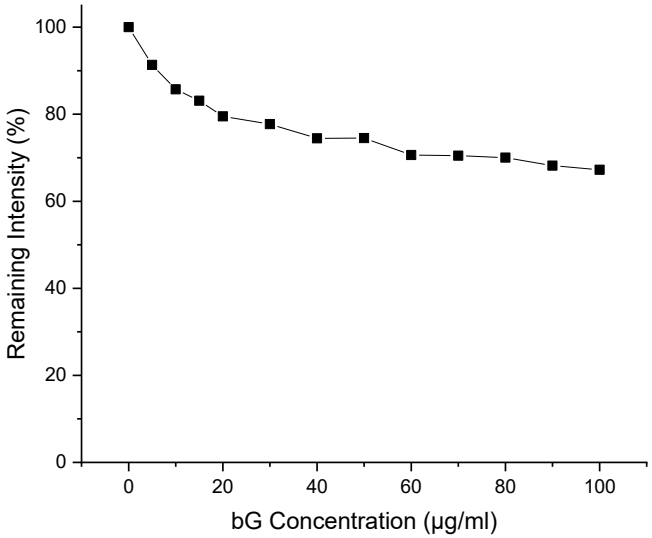

Graph E3: Remaining Intensity of α-amylase in presence of bG-MNPs

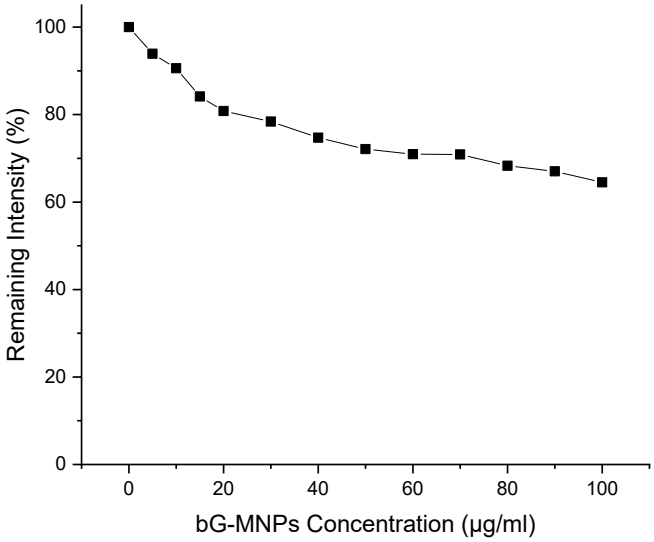

vi. Hill's Model Curves of α-amylase

Graph F1: Hill's model fitted curve of α-amylase in presence of GO

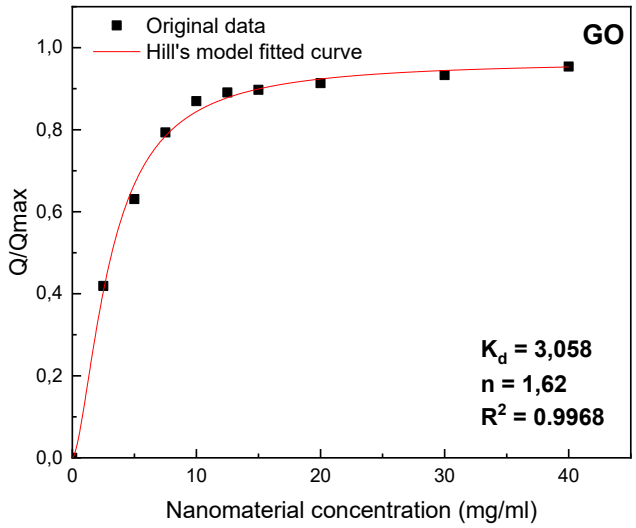

Graph F2: Hill's model fitted curve of α-amylase in presence of bG

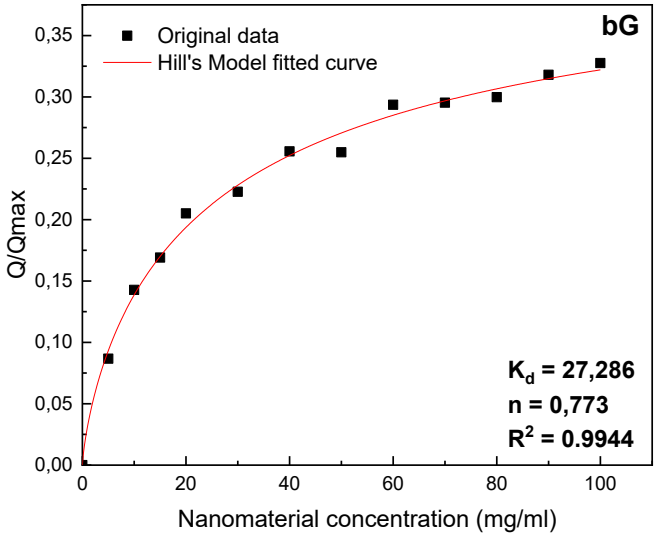

Graph F3: Hill's model fitted curve of α-amylase in presence of bG-MNPs

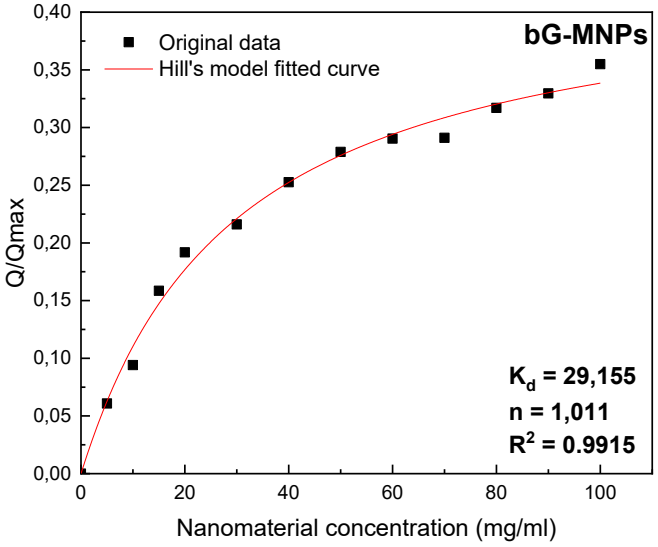

5. Bibliography

Abeliovich, H. (2005). An Empirical Extremum Principle for the Hill Coefficient in Ligand-Protein Interactions Showing Negative Cooperativity. *Biophysical Journal*, *89*(1), 76–79. https://doi.org/10.1529/biophysj.105.060194

Alatzoglou, C., Patila, M., Giannakopoulou, A., Spyrou, K., Yan, F., Li, W., Chalmpes, N., Polydera, A. C., Rudolf, P., Gournis, D., & Stamatis, H. (2022). Development of a Multi-Enzymatic Biocatalytic System through Immobilization on High Quality Few-Layer bio-Graphene. *Nanomaterials*, *13*(1), 127. https://doi.org/10.3390/nano13010127

Alatzoglou, C., Patila, M., Ziogas, P. G., Skonta, A., Politi, D., Spyrou, K., Kaloudi, A. S., Douvalis, A. P., Gournis, D. P., & Stamatis, H. (2025). Green synthesis of magnetic bio-Graphene nanohybrid for the immobilization of hydrolytic enzymes towards sustainable bioconversion of cellulose. *RSC Advances*, *15*(44), 37194–37208. https://doi.org/10.1039/D5RA06271C

Alatzoglou, C., Tzianni, E. I., Patila, M., Trachioti, M. G., Prodromidis, M. I., & Stamatis, H. (2023). Structure-Function Studies of Glucose Oxidase in the Presence of Carbon Nanotubes and Bio-Graphene for the Development of Electrochemical Glucose Biosensors. *Nanomaterials*, *14*(1), 85. https://doi.org/10.3390/nano14010085

Alcántara, A. R., Hernaiz, M.-J., & Sinisterra, J.-V. (2011). Biocatalyzed Production of Fine Chemicals. In *Comprehensive Biotechnology* (pp. 309–331). Elsevier. https://doi.org/10.1016/B978-0-08-088504-9.00225-7

Alexander Flemming. (1922). On a remarkable bacteriolytic element found in tissues and secretions. *Proceedings of the Royal Society of London. Series B, Containing Papers of a Biological Character*, *93*(653), 306–317. https://doi.org/10.1098/rspb.1922.0023

Ali, M. (2019). Chemical, structural and functional properties of whey proteins covalently modified with phytochemical compounds. *Journal of Food Measurement and Characterization*, *13*(4), 2970–2979. https://doi.org/10.1007/s11694-019-00217-1

Alqarni, L. S., Alghamdi, M. D., Alshahrani, A. A., & Nassar, A. M. (2022). Green Nanotechnology: Recent Research on Bioresource-Based Nanoparticle Synthesis and Applications. *Journal of Chemistry*, *2022*, 1–31. https://doi.org/10.1155/2022/4030999

Anastas, P. T., Rodriguez, A., de Winter, T. M., Coish, P., & Zimmerman, J. B. (2021). A review of immobilization techniques to improve the stability and bioactivity of lysozyme. *Green Chemistry Letters and Reviews*, *14*(2), 302–338. https://doi.org/10.1080/17518253.2021.1890840

Ashwini John, J., Samuel, M. S., & Selvarajan, E. (2023). Immobilized cellulase on Fe3O4/GO/CS nanocomposite as a magnetically recyclable catalyst for biofuel application. *Fuel*, *333*, 126364. https://doi.org/10.1016/j.fuel.2022.126364

Bai, Y., Ming, Z., Cao, Y., Feng, S., Yang, H., Chen, L., & Yang, S.-T. (2017a). Influence of graphene oxide and reduced graphene oxide on the activity and conformation of lysozyme. *Colloids and Surfaces B: Biointerfaces*, *154*, 96–103. https://doi.org/10.1016/j.colsurfb.2017.03.011

Bai, Y., Ming, Z., Cao, Y., Feng, S., Yang, H., Chen, L., & Yang, S.-T. (2017b). Influence of graphene oxide and reduced graphene oxide on the activity and conformation of lysozyme. *Colloids and Surfaces B: Biointerfaces*, *154*, 96–103. https://doi.org/10.1016/j.colsurfb.2017.03.011

Baskar, G., Afrin Banu, N., Helan Leuca, G., Gayathri, V., & Jeyashree, N. (2015). Magnetic immobilization and characterization of α-amylase as nanobiocatalyst for hydrolysis of sweet potato starch. *Biochemical Engineering Journal*, *102*, 18–23. https://doi.org/10.1016/j.bej.2015.02.020

Bera, S., Dhar, J., Dasgupta, R., Basu, G., Chakraborti, S., & Chakrabarti, P. (2018). Molecular features of interaction involving hen egg white lysozyme immobilized on graphene oxide and the effect on activity. *International Journal of Biological Macromolecules*, *120*, 2390–2398. https://doi.org/10.1016/j.ijbiomac.2018.09.007

Bergamo, A., & Sava, G. (2023). Pharmacological Modulation of Host Immunity with Hen Egg White Lysozyme (HEWL)—A Review. *Molecules*, *28*(13), 5027. https://doi.org/10.3390/molecules28135027

Berthomieu, C., & Hienerwadel, R. (2009). Fourier transform infrared (FTIR) spectroscopy. *Photosynthesis Research*, *101*(2–3), 157–170. https://doi.org/10.1007/s11120-009-9439-x

Bolibok, P., Wiśniewski, M., Roszek, K., & Terzyk, A. P. (2017). Controlling enzymatic activity by immobilization on graphene oxide. *The Science of Nature*, *104*(3–4), 36. https://doi.org/10.1007/s00114-017-1459-3

Bose Aswathy, T. I. K. G. and A. E. (2018). Fluorescence spectroscopy and its applications: A Review. *International Journal of Advances in Pharmaceutical Analysis*, *08*(01), 01–08.

Bradford, M. M. (1976). A rapid and sensitive method for the quantitation of microgram quantities of protein utilizing the principle of protein-dye binding. *Analytical Biochemistry*, *72*(1–2), 248–254. https://doi.org/10.1016/0003-2697(76)90527-3

Bumbrah, G. S., & Sharma, R. M. (2016). Raman spectroscopy – Basic principle, instrumentation and selected applications for the characterization of drugs of abuse. *Egyptian Journal of Forensic Sciences*, *6*(3), 209–215. https://doi.org/10.1016/j.ejfs.2015.06.001

Calik, P., & Ozdamar, T. (2001). Carbon sources affect metabolic capacities of Bacillus species for the production of industrial enzymes theoretical analyses for serine and neutral proteases and alpha-amylase. *Biochemical Engineering Journal*, *8*, 61–81.

Carballares, D., Abellanas-Perez, P., de Andrades, D., Polizeli, M. de L. T. de M., Rocha-Martin, J., & Fernandez-Lafuente, R. (2024). Reutilization of the Most Stable Coimmobilized Enzyme Using Glutaraldehyde Chemistry to Produce a New Combi-biocatalyst When the Coimmobilized Enzyme with a Lower Stability Is Inactivated. *ACS Sustainable Chemistry & Engineering*, *12*(17), 6564–6572. https://doi.org/10.1021/acssuschemeng.3c08231

Castro, A. M. De, Fragoso, A., Kachrimanidou, V., Koutinas, A. A., & Freire, D. M. G. (2018). Production of Proteases and Amylases and Their Application in Nutrient Medium. *Current Developments in Biotechnology and Bioengineering*, 185–210.

Celina Selvakumari, J., Nishanthi, S. T., Dhanalakshmi, J., Ahila, M., & Padiyan, D. P. (2020). Synthesis of graphene nanosheets using Camellia sinensis and its electrochemical behavior for energy storage application. *Materials Chemistry and Physics*, *239*, 122001. https://doi.org/10.1016/j.matchemphys.2019.122001

Cerón, A., Costa, S., Imbernon, R., de Queiroz, R., de Castro, J., Ferraz, H., Oliveira, R., & Costa, S. (2023). Study of stability, kinetic parameters and release of lysozyme immobilized on chitosan microspheres by crosslinking and covalent attachment for cotton fabric functionalization. *Process Biochemistry*, *128*, 116–125. https://doi.org/10.1016/j.procbio.2023.02.023

Chaves, O. A., Soares, B. A., Maciel, M. A. M., Sant'Anna, C. M. R., Netto-Ferreira, J. C., Cesarin-Sobrinho, D., & Ferreira, A. B. B. (2016). A Study of the Interaction Between *trans* -Dehydrocrotonin, a Bioactive Natural 19- *nor* -Clerodane, and Serum Albumin. *Journal of the Brazilian Chemical Society*. https://doi.org/10.5935/0103-5053.20160069

Chen, L.-L., Shi, W.-P., Yang, J.-J., Jiao, C.-L., & Wei, P.-F. (2024). Research advancements in the purification technology and application of hen egg white lysozyme. *Applied Food Research*, *4*(2), 100632. https://doi.org/10.1016/j.afres.2024.100632

Chung, C., Kim, Y.-K., Shin, D., Ryoo, S.-R., Hong, B. H., & Min, D.-H. (2013). Biomedical Applications of Graphene and Graphene Oxide. *Accounts of Chemical Research*, *46*(10), 2211–2224. https://doi.org/10.1021/ar300159f

Coleman, J. N. (2013). Liquid Exfoliation of Defect-Free Graphene. *Accounts of Chemical Research*, *46*(1), 14–22. https://doi.org/10.1021/ar300009f

Concu, R., & Cordeiro, M. N. D. S. (2019). Alignment-Free Method to Predict Enzyme Classes and Subclasses. *International Journal of Molecular Sciences*, *20*(21), 5389. https://doi.org/10.3390/ijms20215389

Cooper, D. R., D'Anjou, B., Ghattamaneni, N., Harack, B., Hilke, M., Horth, A., Majlis, N., Massicotte, M., Vandsburger, L., Whiteway, E., & Yu, V. (2012). Experimental Review of Graphene. *ISRN Condensed Matter Physics*, *2012*, 1–56. https://doi.org/10.5402/2012/501686

Corrêa, D., & Ramos, C. (2009). The use of circular dichroism spectroscopy to study protein folding , form and function. *African Journal of Biochemistry Research* , *3*, 164–173.

Couto, S. R., & Sanromán, M. Á. (2006). Application of solid-state fermentation to food industry—A review. *Journal of Food Engineering*, *76*(3), 291–302. https://doi.org/10.1016/j.jfoodeng.2005.05.022

Datta, S., Christena, L. R., & Rajaram, Y. R. S. (2013a). Enzyme immobilization: an overview on techniques and support materials. *3 Biotech*, *3*(1), 1–9. https://doi.org/10.1007/s13205-012-0071-7

Datta, S., Christena, L. R., & Rajaram, Y. R. S. (2013b). Enzyme immobilization: an overview on techniques and support materials. *3 Biotech*, *3*(1), 1–9. https://doi.org/10.1007/s13205-012-0071-7

de Souza, P. M., & de Oliveira Magalhães, P. (2010). Application of microbialα-amylase in industry: A review. . *Braz J Microbiology*, *41*, 850–861.

Dhaffouli, A. (2025). Eco-friendly nanomaterials synthesized greenly for electrochemical sensors and biosensors. *Microchemical Journal*, *217*, 115051. https://doi.org/10.1016/j.microc.2025.115051

Dhavale, R. P., Parit, S. B., Sahoo, S. C., Kollu, P., Patil, P. S., Patil, P. B., & Chougale, A. D. (2018). α -amylase immobilized on magnetic nanoparticles: reusable robust nano-biocatalyst for starch hydrolysis. *Materials Research Express*, *5*(7), 075403. https://doi.org/10.1088/2053-1591/aacef1

Dikshit, P., Kumar, J., Das, A., Sadhu, S., Sharma, S., Singh, S., Gupta, P., & Kim, B. (2021). Green Synthesis of Metallic Nanoparticles: Applications and Limitations. *Catalysts*, *11*(8), 902. https://doi.org/10.3390/catal11080902

dos Santos, M. S., Silva, J. M., Barbieri, M. B., Filho, S. A., & Backx, B. P. (2024). Bionanotechnology and its applications: The plurality of science is fundamental for the search for solutions. *Plant Nano Biology*, *7*, 100060. https://doi.org/10.1016/j.plana.2024.100060

ElMasry, G., Nagai, H., Moria, K., Nakazawa, N., Tsuta, M., Sugiyama, J., Okazaki, E., & Nakauchi, S. (2015). Freshness estimation of intact frozen fish using fluorescence spectroscopy and chemometrics of excitation–emission matrix. *Talanta*, *143*, 145–156. https://doi.org/10.1016/j.talanta.2015.05.031

Eskandar, K. (2025). Green biotech: innovations driving a sustainable future. *International Journal of Environmental Quality*, *68*, 28–36.

Farhan, M., Hasani, I. W., Khafaga, D. S. R., Ragab, W. M., Ahmed Kazi, R. N., Aatif, M., Muteeb, G., & Fahim, Y. A. (2025). Enzymes as Catalysts in Industrial Biocatalysis: Advances in Engineering, Applications, and Sustainable Integration. *Catalysts*, *15*(9), 891. https://doi.org/10.3390/catal15090891

Fasim, A., More, V. S., & More, S. S. (2021). Large-scale production of enzymes for biotechnology uses. *Current Opinion in Biotechnology*, *69*, 68–76. https://doi.org/10.1016/j.copbio.2020.12.002

Ferraboschi, P., Ciceri, S., & Grisenti, P. (2021). Applications of Lysozyme, an Innate Immune Defense Factor, as an Alternative Antibiotic. *Antibiotics*, *10*(12), 1534. https://doi.org/10.3390/antibiotics10121534

Gálvez-Iriqui, A. C., Plascencia-Jatomea, M., & Bautista-Baños, S. (2020). Lysozymes: characteristics, mechanism of action and technological applications on the control of pathogenic microorganisms. *Revista Mexicana de Fitopatología, Mexican Journal of Phytopathology*, *38*(3). https://doi.org/10.18781/R.MEX.FIT.2005-6

Gandhimathi R., V. S. , J. M. P. (2012). ANALYTICAL PROCESS OF DRUGS BY ULTRAVIOLET (UV) SPECTROSCOPY – A REVIEW. *International Journal of Pharmaceutical Research & Analysis*, *2*(2), 72–78.

Gehlen, M. H. (2020). The centenary of the Stern-Volmer equation of fluorescence quenching: From the single line plot to the SV quenching map. *Journal of Photochemistry and Photobiology C: Photochemistry Reviews*, *42*, 100338. https://doi.org/10.1016/j.jphotochemrev.2019.100338

Geim, A. K., & Novoselov, K. S. (2007). The rise of graphene. *Nature Materials*, *6*(3), 183–191. https://doi.org/10.1038/nmat1849

Ghosh, K., Rathi, S., & Arora, D. (2016). Fluorescence spectral studies on interaction of fluorescent probes with Bovine Serum Albumin (BSA). *Journal of Luminescence*, *175*, 135–140. https://doi.org/10.1016/j.jlumin.2016.01.029

Gkantzou, E., Chatzikonstantinou, A. V., Fotiadou, R., Giannakopoulou, A., Patila, M., & Stamatis, H. (2021). Trends in the development of innovative nanobiocatalysts and their application in biocatalytic transformations. *Biotechnology Advances*, *51*, 107738. https://doi.org/10.1016/j.biotechadv.2021.107738

Gladwin Alex, A., Kedir, A., & Gebrehiwet Tewele, T. (2022). Review on effects of graphene oxide on mechanical and microstructure of cement-based materials. *Construction and Building Materials*, *360*, 129609. https://doi.org/10.1016/j.conbuildmat.2022.129609

Gopinath, S. C. B., Anbu, P., Arshad, M. K. M., Lakshmipriya, T., Voon, C. H., Hashim, U., & Chinni, S. V. (2017). Biotechnological Processes in Microbial Amylase Production. *BioMed Research International*, *2017*, 1–9. https://doi.org/10.1155/2017/1272193

Govinda Verma, Dr. M. M. (2018). DEVELOPMENT AND OPTIMIZATION OF UV-VIS SPECTROSCOPY - A REVIEW. *World Journal of Pharmaceutical Research*, *7*(11), 1170–1180.

Greenfield, N. J. (2006). Using circular dichroism spectra to estimate protein secondary structure. *Nature Protocols*, *1*(6), 2876–2890. https://doi.org/10.1038/nprot.2006.202

Guardia, L., Fernández-Merino, M. J., Paredes, J. I., Solís-Fernández, P., Villar-Rodil, S., Martínez-Alonso, A., & Tascón, J. M. D. (2011). High-throughput production of pristine graphene in an aqueous dispersion assisted by non-ionic surfactants. *Carbon*, *49*(5), 1653–1662.

Gupta, A. K., & Gupta, M. (2005). Synthesis and surface engineering of iron oxide nanoparticles for biomedical applications. *Biomaterials*, *26*(18), 3995–4021. https://doi.org/10.1016/j.biomaterials.2004.10.012

Gupta, D., Boora, A., Thakur, A., & Gupta, T. K. (2023). Green and sustainable synthesis of nanomaterials: Recent advancements and limitations. *Environmental Research*, *231*, 116316. https://doi.org/10.1016/j.envres.2023.116316

Gupta, R., Gigras, P., Mohapatra, H., Goswami, V. K., & Chauhan, B. (2003). Microbial α-amylases: a biotechnological perspective. *Process Biochemistry*, *38*(11), 1599–1616. https://doi.org/10.1016/S0032-9592(03)00053-0

Gupta, V., Sengupta, M., Prakash, J., & Tripathy, B. C. (2017). An Introduction to Biotechnology. In *Basic and Applied Aspects of Biotechnology* (pp. 1–21). Springer Singapore. https://doi.org/10.1007/978-981-10-0875-7_1

Gutiérrez-Cruz, A., Ruiz-Hernández, A. R., Vega-Clemente, J. F., Luna-Gazcón, D. G., & Campos-Delgado, J. (2022). A review of top-down and bottom-up synthesis methods for the production of graphene, graphene oxide and reduced graphene oxide. *Journal of Materials Science*, *57*(31), 14543–14578. https://doi.org/10.1007/s10853-022-07514-z

Hansen, S. K., Jamali, B., & Hubbuch, J. (2013). Selective high throughput protein quantification based on UV absorption spectra. *Biotechnology and Bioengineering*, *110*(2), 448–460. https://doi.org/10.1002/bit.24712

Hermanová, S., Zarevúcká, M., Bouša, D., Pumera, M., & Sofer, Z. (2015). Graphene oxide immobilized enzymes show high thermal and solvent stability. *Nanoscale*, *7*(13), 5852–5858. https://doi.org/10.1039/C5NR00438A

Hmidet, N., Bayoudh, A., Berrin, J. G., Kanoun, S., Juge, N., & Nasri, M. (2008). Purification and biochemical characterization of a novel alpha-amylase from Bacillus licheniformis.NH1: cloning, nucleotide sequence and expression of amyN gene in Escherichia coli. . *Process Biochemistry*, *43*, 499–510.

Hossein Hosseinkhani. (2022). Nanobiotechnology. In *Biomedical Engineering* (pp. 209–254). Wiley. https://doi.org/10.1002/9783527826674.ch9

Ji, N., Liu, C., Li, M., Sun, Q., & Xiong, L. (2018). Interaction of cellulose nanocrystals and amylase: Its influence on enzyme activity and resistant starch content. *Food Chemistry*, *245*, 481–487. https://doi.org/10.1016/j.foodchem.2017.10.130

Jiang, L., Xiong, Z., Song, Y., Lu, Y., Chen, Y., Schultz, J. S., Li, J., & Liao, J. (2019). Protein–Protein Affinity Determination by Quantitative FRET Quenching. *Scientific Reports*, *9*(1), 2050. https://doi.org/10.1038/s41598-018-35535-9

Jun, B.-H. (2021). *Nanotechnology for Bioapplications* (B.-H. Jun, Ed.; Vol. 1309). Springer Singapore. https://doi.org/10.1007/978-981-33-6158-4

KAFARSKI, P. (2012). Rainbow code of Biotechnology. *CHEMIK*, *66*, 814–816.

Kaur, K., & Thombre, R. (2021). Nanobiotechnology: methods, applications, and future prospects. In *Nanobiotechnology* (pp. 1–20). Elsevier. https://doi.org/10.1016/B978-0-12-822878-4.00001-8

Kenry, K., Loh, K. P., & Lim, C. T. (2016). Molecular interactions of graphene oxide with human blood plasma proteins. *Nanoscale*, *8*(17), 9425–9441. https://doi.org/10.1039/C6NR01697A

Khan, I., Saeed, K., & Khan, I. (2019). Nanoparticles: Properties, applications and toxicities. *Arabian Journal of Chemistry*, *12*(7), 908–931. https://doi.org/10.1016/j.arabjc.2017.05.011

Khan, M. R. (2021). Immobilized enzymes: a comprehensive review. *Bulletin of the National Research Centre*, *45*(1), 207. https://doi.org/10.1186/s42269-021-00649-0

Khorshidian, N., Khanniri, E., Koushki, M. R., Sohrabvandi, S., & Yousefi, M. (2022). An Overview of Antimicrobial Activity of Lysozyme and Its Functionality in Cheese. *Frontiers in Nutrition*, *9*. https://doi.org/10.3389/fnut.2022.833618

KONSOULA, Z., & LIAKOPOULOUKYRIAKIDES, M. (2007). Co-production of α-amylase and β-galactosidase by Bacillus subtilis in complex organic substrates. *Bioresource Technology*, *98*(1), 150–157. https://doi.org/10.1016/j.biortech.2005.11.001

Kumar, C. V., & Pattammattel, A. (2016). Chapter Eleven - BioGraphene: Direct Exfoliation of Graphite in a Kitchen Blender for Enzymology Applications. In C. V. Kumar (Ed.),

Methods in Enzymology (Vol. 571, pp. 225–244). Academic Press. https://doi.org/10.1016/bs.mie.2016.03.009

Kundu, S., Aswal, V. K., & Kohlbrecher, J. (2016). Synergistic effect of temperature, protein and salt concentration on structures and interactions among lysozyme proteins. *Chemical Physics Letters*, *657*, 90–94. https://doi.org/10.1016/j.cplett.2016.05.066

Kurdyumov, A. S., Manuvera, V. A., Baskova, I. P., & Lazarev, V. N. (2015). A comparison of the enzymatic properties of three recombinant isoforms of thrombolytic and antibacterial protein—Destabilase-Lysozyme from medicinal leech. *BMC Biochemistry*, *16*(1), 27. https://doi.org/10.1186/s12858-015-0056-3

Lakowicz, J. R. (1999). *Principles of Fluorescence Spectroscopy*. Springer US. https://doi.org/10.1007/978-1-4757-3061-6

Laurent, S., Forge, D., Port, M., Roch, A., Robic, C., Vander Elst, L., & Muller, R. N. (2008). Magnetic Iron Oxide Nanoparticles: Synthesis, Stabilization, Vectorization, Physicochemical Characterizations, and Biological Applications. *Chemical Reviews*, *108*(6), 2064–2110. https://doi.org/10.1021/cr068445e

Lee, C., & Au-Duong, A. (2018). Enzyme Immobilization on Nanoparticles: Recent Applications. In *Emerging Areas in Bioengineering* (pp. 67–80). Wiley. https://doi.org/10.1002/9783527803293.ch4

Lesnierowski, G., & Kijowski, J. (2007). Lysozyme. In *Bioactive Egg Compounds* (pp. 33–42). Springer Berlin Heidelberg. https://doi.org/10.1007/978-3-540-37885-3_6

Leśnierowski, G., & Yang, T. (2021). Lysozyme and its modified forms: A critical appraisal of selected properties and potential. *Trends in Food Science & Technology*, *107*, 333–342. https://doi.org/10.1016/j.tifs.2020.11.004

Li, B., Hao, C., Liu, H., Yang, H., Zhong, K., Zhang, M., & Sun, R. (2022). Interaction of graphene oxide with lysozyme:Insights from conformational structure and surface charge investigations. *Spectrochimica Acta Part A: Molecular and Biomolecular Spectroscopy*, *264*, 120207. https://doi.org/10.1016/j.saa.2021.120207

Li, S., Aphale, A. N., Macwan, I. G., Patra, P. K., Gonzalez, W. G., Miksovska, J., & Leblanc, R. M. (2012). Graphene Oxide as a Quencher for Fluorescent Assay of Amino Acids, Peptides, and Proteins. *ACS Applied Materials & Interfaces*, *4*(12), 7069–7075. https://doi.org/10.1021/am302704a

Li, S., Mulloor, J. J., Wang, L., Ji, Y., Mulloor, C. J., Micic, M., Orbulescu, J., & Leblanc, R. M. (2014). Strong and Selective Adsorption of Lysozyme on Graphene Oxide. *ACS Applied Materials & Interfaces*, *6*(8), 5704–5712. https://doi.org/10.1021/am500254e

Li, W., Wen, H., Shi, Q., & Zheng, G. (2016). Study on immobilization of (+) γ-lactamase using a new type of epoxy graphene oxide carrier. *Process Biochemistry*, *51*(2), 270–276. https://doi.org/10.1016/j.procbio.2015.11.030

Liao, H., Chao, L., Xie, D., Zhu, X., Zhuang, Q., & Zhang, J. (2025). Application of fluorescence spectroscopy in meat analysis. *Journal of Food Composition and Analysis*, *143*, 107613. https://doi.org/10.1016/j.jfca.2025.107613

Liu, J.-F., Liu, H., Tan, B., Chen, Y.-H., & Yang, R.-J. (2012). Reversible immobilization of K. fragilis β-galactosidase onto magnetic polyethylenimine-grafted nanospheres for synthesis of galacto-oligosaccharide. *Journal of Molecular Catalysis B: Enzymatic*, *82*, 64–70. https://doi.org/10.1016/j.molcatb.2012.06.001

Liu, X., Sun, B., Xu, C., Zhang, T., Zhang, Y., & Zhu, L. (2023). Intrinsic mechanisms for the inhibition effect of graphene oxide on the catalysis activity of alpha amylase. *Journal of Hazardous Materials*, *453*, 131389. https://doi.org/10.1016/j.jhazmat.2023.131389

Losada-Garcia, N., Berenguer-Murcia, A., Cazorla-Amorós, D., & Palomo, J. M. (2019). *Green Exfoliation of Graphite Flakes to Efficiently Synthesize Biographene*. https://doi.org/10.26434/chemrxiv.8797871.v1

Machius, M., Declerck, N., Huber, R., & Wiegand, G. (1998). Activation of Bacillus licheniformis α-amylase through a disorder→order transition of the substrate-binding site mediated by a calcium–sodium–calcium metal triad. *Structure*, *6*(3), 281–292. https://doi.org/10.1016/S0969-2126(98)00032-X

Madurani, K. A., Suprapto, S., Machrita, N. I., Bahar, S. L., Illiya, W., & Kurniawan, F. (2020). Progress in Graphene Synthesis and its Application: History, Challenge and the Future Outlook for Research and Industry. *ECS Journal of Solid State Science and Technology*, *9*(9), 093013. https://doi.org/10.1149/2162-8777/abbb6f

Maldonado-Ruiz, K., Pedroza-Islas, R., & Pedraza-Segura, L. (2024). Blue Biotechnology: Marine Bacteria Bioproducts. *Microorganisms*, *12*(4), 697. https://doi.org/10.3390/microorganisms12040697

Mardani, T., Khiabani, M. S., Mokarram, R. R., & Hamishehkar, H. (2018). Immobilization of α-amylase on chitosan-montmorillonite nanocomposite beads. *International Journal of Biological Macromolecules*, *120*, 354–360. https://doi.org/10.1016/j.ijbiomac.2018.08.065

Masschalck, B., & Michiels, C. W. (2003). Antimicrobial Properties of Lysozyme in Relation to Foodborne Vegetative Bacteria. *Critical Reviews in Microbiology*, *29*(3), 191–214. https://doi.org/10.1080/713610448

McDonald, A. G., & Tipton, K. F. (2022). Parameter Reliability and Understanding Enzyme Function. *Molecules*, *27*(1), 263. https://doi.org/10.3390/molecules27010263

McDonald, A. G., & Tipton, K. F. (2023). Enzyme nomenclature and classification: the state of the art. *The FEBS Journal*, *290*(9), 2214–2231. https://doi.org/10.1111/febs.16274

Meersman, F., Atilgan, C., Miles, A. J., Bader, R., Shang, W., Matagne, A., Wallace, B. A., & Koch, M. H. J. (2010). Consistent Picture of the Reversible Thermal Unfolding of Hen Egg-White Lysozyme from Experiment and Molecular Dynamics. *Biophysical Journal*, *99*(7), 2255–2263. https://doi.org/10.1016/j.bpj.2010.07.060

Mehta, R. V. (2017). Synthesis of magnetic nanoparticles and their dispersions with special reference to applications in biomedicine and biotechnology. *Materials Science and Engineering: C*, *79*, 901–916. https://doi.org/10.1016/j.msec.2017.05.135

Miles, A. J., Janes, R. W., & Wallace, B. A. (2021). Tools and methods for circular dichroism spectroscopy of proteins: a tutorial review. *Chemical Society Reviews*, *50*(15), 8400–8413. https://doi.org/10.1039/D0CS00558D

Mobini-Dehkordi M., & Javan F. (2012). Application of alpha-amylase in biotechnology. *Journal of Biology and Today's World* , *1*(1), 39–50.

Mobini-Dehkordi M, & Javan F. (2012). Application of alpha-amylase in biotechnology. *Journal of Biology and Today's World* , *1*(1), 39–50.

Mohamed, M. A., Jaafar, J., Ismail, A. F., Othman, M. H. D., & Rahman, M. A. (2017). Fourier Transform Infrared (FTIR) Spectroscopy. In *Membrane Characterization* (pp. 3–29). Elsevier. https://doi.org/10.1016/B978-0-444-63776-5.00001-2

Monajati, M., Ariafar, N., Abedi, M., Borandeh, S., & Tamaddon, A. M. (2024). Immobilization of L-Asparaginase on biofunctionalized magnetic graphene oxide nanocomposite: A promising approach for Enhanced Stability and reusability. *Heliyon*, *10*(21), e40072. https://doi.org/10.1016/j.heliyon.2024.e40072

MOTTA, J. F. G., FREITAS, B. C. B. de, ALMEIDA, A. F. de, MARTINS, G. A. de S., & BORGES, S. V. (2023). Use of enzymes in the food industry: a review. *Food Science and Technology*, *43*. https://doi.org/10.1590/fst.106222

Movahedpour, A., Asadi, M., Khatami, S. H., Taheri-Anganeh, M., Adelipour, M., Shabaninejad, Z., Ahmadi, N., Irajie, C., & Mousavi, P. (2022). A brief overview on the application and sources of α-amylase and expression hosts properties in order to production of recombinant α-amylase. *Biotechnology and Applied Biochemistry*, *69*(2), 650–659. https://doi.org/10.1002/bab.2140

Muralikrishna, G., & Nirmala, M. (2005). Cereal α-amylases—an overview. *Carbohydrate Polymers*, *60*(2), 163–173. https://doi.org/10.1016/j.carbpol.2004.12.002

Naskar, P., Chakraborty, D., Mondal, A., Das, B., & Samanta, A. (2024). Immobilization of α-amylase in calcium alginate-gum odina (CA-GO) beads: An easily recoverable and reusable support. *International Journal of Biological Macromolecules*, *258*, 129062. https://doi.org/10.1016/j.ijbiomac.2023.129062

Nawaz, N., Wen, S., Wang, F., Nawaz, S., Raza, J., Iftikhar, M., & Usman, M. (2022). Lysozyme and Its Application as Antibacterial Agent in Food Industry. *Molecules*, *27*(19), 6305. https://doi.org/10.3390/molecules27196305

Oliveira, J. R. P., Tusset, A. M., Andrade, D. I., Balthazar, J. M., Pagani, R. N., & Lenzi, G. G. (2024). Action Plans Study: Principles of Green Chemistry, Sustainable Development, and Smart Cities. *Sustainability*, *16*(18), 8041. https://doi.org/10.3390/su16188041

Oliver, W. T., & Wells, J. E. (2015). Lysozyme as an alternative to growth promoting antibiotics in swine production. *Journal of Animal Science and Biotechnology*, *6*(1), 35. https://doi.org/10.1186/s40104-015-0034-z

Onyancha, R. B., Ukhurebor, K. E., Aigbe, U. O., Osibote, O. A., Kusuma, H. S., & Darmokoesoemo, H. (2022). A Methodical Review on Carbon-Based Nanomaterials in Energy-Related Applications. *Adsorption Science & Technology*, *2022*. https://doi.org/10.1155/2022/4438286

Pang, Y. X., Yew, M., Yan, Y., Khine, P., Filbert, A., Manickam, S., Foo, D. C. Y., Sharmin, N., Lester, E., Wu, T., & Pang, C. H. (2021). Application of supercritical fluid in the synthesis of graphene materials: a review. *Journal of Nanoparticle Research*, *23*(9), 204. https://doi.org/10.1007/s11051-021-05254-w

Papanikolaou, E., Simos, Y. V., Spyrou, K., Patila, M., Alatzoglou, C., Tsamis, K., Vezyraki, P., Stamatis, H., Gournis, D. P., Peschos, D., & Dounousi, E. (2023). Does Green Exfoliation of Graphene Produce More Biocompatible Structures? *Pharmaceutics*, *15*(3), 993. https://doi.org/10.3390/pharmaceutics15030993

Paredes, J. I., & Villar-Rodil, S. (2016). Biomolecule-assisted exfoliation and dispersion of graphene and other two-dimensional materials: a review of recent progress and applications. *Nanoscale*, *8*(34), 15389–15413. https://doi.org/10.1039/C6NR02039A

Pattammattel, A., & Kumar, C. V. (2015a). Kitchen Chemistry 101: Multigram Production of High Quality Biographene in a Blender with Edible Proteins. *Advanced Functional Materials*, *25*(45), 7088–7098. https://doi.org/10.1002/adfm.201503247

Pattammattel, A., & Kumar, C. V. (2015b). Kitchen Chemistry 101: Multigram Production of High Quality Biographene in a Blender with Edible Proteins. *Advanced Functional Materials*, *25*(45), 7088–7098. https://doi.org/10.1002/adfm.201503247

Paul, J. S., Gupta, N., Beliya, E., Tiwari, S., & Jadhav, S. K. (2021). Aspects and Recent Trends in Microbial α-Amylase: a Review. *Applied Biochemistry and Biotechnology*, *193*(8), 2649–2698. https://doi.org/10.1007/s12010-021-03546-4

Pinto, A. M., Gonçalves, I. C., & Magalhães, F. D. (2013). Graphene-based materials biocompatibility: A review. *Colloids and Surfaces B: Biointerfaces*, *111*, 188–202. https://doi.org/10.1016/j.colsurfb.2013.05.022

Popescu, R. C., Andronescu, E., & Vasile, B. S. (2019). Recent Advances in Magnetite Nanoparticle Functionalization for Nanomedicine. *Nanomaterials*, *9*(12), 1791. https://doi.org/10.3390/nano9121791

Porfirif, M. C., Milatich, E. J., Farruggia, B. M., & Romanini, D. (2016). Production of alpha-amylase from Aspergillus oryzae for several industrial applications in a single step. *Journal of Chromatography B*, *1022*, 87–92. https://doi.org/10.1016/j.jchromb.2016.04.015

Prakash, O., & Jaiswal, N. (2010). α-Amylase: An Ideal Representative of Thermostable Enzymes. *Applied Biochemistry and Biotechnology*, *160*(8), 2401–2414. https://doi.org/10.1007/s12010-009-8735-4

Rezaei, B., Yari, P., Sanders, S. M., Wang, H., Chugh, V. K., Liang, S., Mostufa, S., Xu, K., Wang, J., Gómez-Pastora, J., & Wu, K. (2024). Magnetic Nanoparticles: A Review on Synthesis, Characterization, Functionalization, and Biomedical Applications. *Small*, *20*(5). https://doi.org/10.1002/smll.202304848

Ricci, A., Cataldi, A., Zara, S., & Gallorini, M. (2022). Graphene-Oxide-Enriched Biomaterials: A Focus on Osteo and Chondroinductive Properties and Immunomodulation. *Materials*, *15*(6), 2229. https://doi.org/10.3390/ma15062229

Rigos, C. F., Santos, H. de L., Thedei, G., Ward, R. J., & Ciancaglini, P. (2003). Influence of enzyme conformational changes on catalytic activity investigated by circular dichroism spectroscopy. *Biochemistry and Molecular Biology Education*, *31*(5), 329–332. https://doi.org/10.1002/bmb.2003.494031050264

Roy, M., & Horovitz, A. (2022). Partitioning the Hill coefficient into contributions from ligand-promoted conformational changes and subunit heterogeneity. *Protein Science*, *31*(5). https://doi.org/10.1002/pro.4298

Sanchez, O., & Cardona, C. A. (2008). Trends in biotechnological production of fuel ethanol from different feedstocks. *Bioresour Technol*, *99*, 5270–5295.

Saurabh, S., & Sahoo, P. K. (2008). Lysozyme: an important defence molecule of fish innate immune system. *Aquaculture Research*, *39*(3), 223–239. https://doi.org/10.1111/j.1365-2109.2007.01883.x

Shareghi, B., Farhadian, S., Zamani, N., Salavati-Niasari, M., & Gholamrezaei, S. (2016). Stability and enzyme activity of lysozyme in the presence of Fe3O4 nanoparticles. *Monatshefte Für Chemie - Chemical Monthly*, *147*(2), 465–471. https://doi.org/10.1007/s00706-015-1520-x

Shareghi, B., Farhadian, S., Zamani, N., Salavati-Niasari, M., Moshtaghi, H., & Gholamrezaei, S. (2015). Investigation the activity and stability of lysozyme on presence of magnetic nanoparticles. *Journal of Industrial and Engineering Chemistry*, *21*, 862–867. https://doi.org/10.1016/j.jiec.2014.04.024

Sheldon, R. A., & Woodley, J. M. (2018). Role of Biocatalysis in Sustainable Chemistry. *Chemical Reviews*, *118*(2), 801–838. https://doi.org/10.1021/acs.chemrev.7b00203

Shin, M., Lim, J., Park, Y., Lee, J.-Y., Yoon, J., & Choi, J.-W. (2024). Carbon-based nanocomposites for biomedical applications. *RSC Advances*, *14*(10), 7142–7156. https://doi.org/10.1039/D3RA08946K

Shin, W.-K., Cho, J., Kannan, A. G., Lee, Y.-S., & Kim, D.-W. (2016). Cross-linked Composite Gel Polymer Electrolyte using Mesoporous Methacrylate-Functionalized SiO2 Nanoparticles for Lithium-Ion Polymer Batteries. *Scientific Reports*, *6*(1), 26332. https://doi.org/10.1038/srep26332

Shokoohizadeh, M. J., Karami, F., Mousavi, S. A., Khodarahmi, R., & Almasi, A. (2022). Immobilization of IMP-1 metallo-beta-lactamase: the promising approach for the removal of beta-lactam antibiotics. *Desalination and Water Treatment*, *253*, 248–255. https://doi.org/10.5004/dwt.2022.28308

Shukla, E., D. Bendre, A., & M. Gaikwad, S. (2022). *Hydrolases: The Most Diverse Class of Enzymes*. https://doi.org/10.5772/intechopen.102350

Silva Almeida, C., Simão Neto, F., da Silva Sousa, P., da Silva Aires, F. I., de Matos Filho, J. R., Gama Cavalcante, A. L., Sousa Junior, P. G. de, Melo, R. L. F., & S. dos Santos, J. C. (2024). Enhancing Lipase Immobilization via Physical Adsorption: Advancements in Stability, Reusability, and Industrial Applications for Sustainable Biotechnological Processes. *ACS Omega*, *9*(47), 46698–46732. https://doi.org/10.1021/acsomega.4c07088

Singh, R. V., Singh, B., Kumar, A., Sambyal, K., Karuppanan, K. K., & Lee, J.-K. (2025). Enzyme Immobilization on Nanomaterials and Their Applications. *Materials*, *18*(17), 4106. https://doi.org/10.3390/ma18174106

Sivaramakrishnan, S., Gangadharan, D., Nampoothiri, K. M., Soccol, K., & Pandey, A. (2006). a-Amylases from Microbial Sources- An overview on Recent Developments . *Food Technology and Biotechnology*, *44*(2).

Speranza, G. (2021). Carbon Nanomaterials: Synthesis, Functionalization and Sensing Applications. *Nanomaterials*, *11*(4), 967. https://doi.org/10.3390/nano11040967

Sundarram A. et al. (2014). α-Amylase Production and Applications: A Review. *Journal of Applied & Environmental Microbiology*, *2*(4), 166–175.

Tarahi, M., Kalita, P., Deka, H., Oladzadabbasabadi, N., Ghaderi, S., Tavassoli, M., & Roy, S. (2025). A comprehensive review of lysozyme applications in food packaging: Current trends, developments, and challenges. *Trends in Food Science & Technology*, *164*, 105267. https://doi.org/10.1016/j.tifs.2025.105267

Tawfik, D. S. (2014). Accuracy-rate tradeoffs: how do enzymes meet demands of selectivity and catalytic efficiency? *Current Opinion in Chemical Biology*, *21*, 73–80. https://doi.org/10.1016/j.cbpa.2014.05.008

Thomas, D.-G., De-Alwis, S., Gupta, S., Pecharsky, V. K., Mendivelso-Perez, D., Montazami, R., Smith, E. A., & Hashemi, N. N. (2021). Protein-assisted scalable mechanochemical exfoliation of few-layer biocompatible graphene nanosheets. *Royal Society Open Science*, *8*(3), rsos.200911. https://doi.org/10.1098/rsos.200911

Tintor, Đ., Ninković, K., Milošević, J., & Polović, N. Đ. (2024). Gaining insight into protein structure via ATR-FTIR spectroscopy. *Vibrational Spectroscopy*, *134*, 103726. https://doi.org/10.1016/j.vibspec.2024.103726

Tiwari, P., Ekal, N. S., Rudani, B. A., Bahadur, P., & Tiwari, S. (2023). Stabilization of lysozyme in aqueous dispersion of graphene oxide sheets. *Colloids and Surfaces B: Biointerfaces*, *225*, 113250. https://doi.org/10.1016/j.colsurfb.2023.113250

Tiwari SP et al. (2015). AMYLASES: AN OVERVIEW WITH SPECIAL REFERENCE TO ALPHA AMYLASE. *Journal of Global Biosciences* , *4*(1), 1886–1901.

Tom J. (2023). UV-Vis Spectroscopy: Principle, Strengths and Limitations and Applications. *Technology Networks* . https://www.technologynetworks.com/analysis/articles/uv-vis-spectroscopy-principle-strengths-and-limitations-and-applications-349865

Turoverov, K. K., & Kuznetsova, I. M. (1998). [Intrinsic UV-fluorescence of proteins as a tool for studying their dynamics]. *Tsitologiia*, *40*(8–9), 735–746.

van der Maarel, M. J. E. C., van der Veen, B., Uitdehaag, J. C. M., Leemhuis, H., & Dijkhuizen, L. (2002). Properties and applications of starch-converting enzymes of the α-amylase family. *Journal of Biotechnology*, *94*(2), 137–155. https://doi.org/10.1016/S0168-1656(01)00407-2

Wu, T., Jiang, Q., Wu, D., Hu, Y., Chen, S., Ding, T., Ye, X., Liu, D., & Chen, J. (2019). What is new in lysozyme research and its application in food industry? A review. *Food Chemistry*, *274*, 698–709. https://doi.org/10.1016/j.foodchem.2018.09.017

Wu, W., He, Q., & Jiang, C. (2008). Magnetic Iron Oxide Nanoparticles: Synthesis and Surface Functionalization Strategies. *Nanoscale Research Letters*, *3*(11), 397. https://doi.org/10.1007/s11671-008-9174-9

Yan, B., & Bunch, J. (2025). A straightforward method for measuring binding affinities of ligands to proteins of unknown concentration in biological tissues. *Chemical Science*, *16*(20), 8673–8681. https://doi.org/10.1039/D5SC02460A

Yan, Q.-L., Gozin, M., Zhao, F.-Q., Cohen, A., & Pang, S.-P. (2016). Highly energetic compositions based on functionalized carbon nanomaterials. *Nanoscale*, *8*(9), 4799–4851. https://doi.org/10.1039/C5NR07855E

Yang, T., & Yan, W. (2025). Strategies for enhancing the antibacterial efficacy of lysozyme and the resulting outcome. *International Journal of Biological Macromolecules*, *310*, 143137. https://doi.org/10.1016/j.ijbiomac.2025.143137

Yifrach, O. (2004). Hill Coefficient for Estimating the Magnitude of Cooperativity in Gating Transitions of Voltage-Dependent Ion Channels. *Biophysical Journal*, *87*(2), 822–830. https://doi.org/10.1529/biophysj.104.040410

Yu, D., Li, Z., Zhou, X., Wang, W., Wang, L., Liu, T., & Du, J. (2022). Study on the modification of magnetic graphene oxide and the effect of immobilized lipase. *International Journal of Biological Macromolecules*, *216*, 498–509. https://doi.org/10.1016/j.ijbiomac.2022.06.203

Zhang, Q., Zhao, Y., Yao, Y., Wu, N., Chen, S., Xu, L., & Tu, Y. (2024). Characteristics of hen egg white lysozyme, strategies to break through antibacterial limitation, and its application in food preservation: A review. *Food Research International*, *181*, 114114. https://doi.org/10.1016/j.foodres.2024.114114

Zhang, W., & Rhim, J.-W. (2022). Functional edible films/coatings integrated with lactoperoxidase and lysozyme and their application in food preservation. *Food Control*, *133*, 108670. https://doi.org/10.1016/j.foodcont.2021.108670

Zobel-Roos, S., Mouellef, M., Siemers, C., & Strube, J. (2017). Process Analytical Approach towards Quality Controlled Process Automation for the Downstream of Protein Mixtures by Inline Concentration Measurements Based on Ultraviolet/Visible Light (UV/VIS) Spectral Analysis. *Antibodies*, *6*(4), 24. https://doi.org/10.3390/antib6040024

Greek Bibliography

Κίντζιος Σ. (2016*). Νανοβιοτεχνολογία και Βιοαισθητήρες*. Εκδόσεις ΕΜΒΡΥΟ.

Πατήλα Μ., (2016). Διδακτορική διατριβή: *«Ανάπτυξη νέων βιοκαταλυτικών συστημάτων μέσω της ακινητοποίησης ενζύμων σε νανοδομικά υλικά».* Πανεπιστήμιο Ιωαννίνων.

Σταμάτης Χ., (2016*). Ενζυμική Βιοτεχνολογία με στοιχεία Νανοβιοτεχνολογίας.*

Πανεπιστήμιο Ιωαννίνων.

Κλώνης Ι. (2018) *Ενζυμική Βιοτεχνολογία*. Πανεπιστημιακές Εκδόσεις Κρήτης

Links

https://www.weacademia.com/my/biology/form-5/biology-f5-chapter-13/biology-f5-chapter-13-2

https://www.ebi.ac.uk/pdbe/articles/wonders-salivary-amylase